ENCYCLOPEDIA OF
AEROSPACE
ENGINEERING

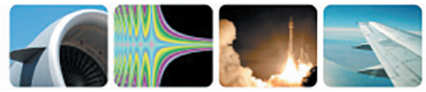

EDITORS-IN-CHIEF
RICHARD BLOCKLEY
WEI SHYY

UNMANNED AIRCRAFT SYSTEMS

EDITORS
ELLA ATKINS, ANÍBAL OLLERO, ANTONIOS TSOURDOS

WILEY

UNMANNED AIRCRAFT SYSTEMS

UNMANNED AIRCRAFT SYSTEMS

Unmanned Aircraft Systems Editors

Ella Atkins

Department of Aerospace Engineering, University of Michigan, Ann Arbor, MI, USA

Aníbal Ollero

Universidad de Sevilla and Scientific Advisory Department of the Center for Advanced Aerospace Technologies, Seville, Spain

Antonios Tsourdos

School of Aerospace, Transport & Manufacturing and Centre for Autonomous and Cyber-Physical Systems, Cranfield University, Cranfield, UK

Encyclopedia of Aerospace Engineering Editors-in-Chief

Richard Blockley

Aerospace Consultant, Cranfield University, Cranfield, UK
Former Head of Technical Programmes, BAE Systems, Farnborough, UK

Wei Shyy

Hong Kong University of Science and Technology, Hong Kong, P. R. China

WILEY

This edition first published 2016

Registered office
John Wiley & Sons Ltd, The Atrium, Southern Gate, Chichester, West Sussex, PO19 8SQ, United Kingdom

For details of our global editorial offices, for customer services and for information about how to apply for permission to reuse the copyright material in this book please see our website at www.wiley.com.

Library of Congress Cataloging-in-Publication Data is available for this title.

ISBN: 978-1-118-86645-0

A catalogue record for this book is available from the British Library.

Front cover: Drone image from John Lawson, Belhaven/Gettyimages

Typeset in 10.25/12.5pt TimesLTStd-Roman by Thomson Digital, Noida, India

1 2016

Contents

Contributors

Brandon R. Abel
International Center for Air Transportation, Massachusetts Institute of Technology, Cambridge, MA, USA

Domenico Accardo
University of Naples "Federico II", Napoli, Italy

José Joaquin Acevedo
Grupo de Robótica, Visión y Control, Universidad de Sevilla, Seville, Spain

Florian-Michael Adolf
German Aerospace Center (DLR), Department of Unmanned Aircraft, Institute of Flight Systems, Braunschweig, Germany

Jessica Alvarenga
Ritchie School of Engineering and Computer Science, DU Unmanned Research Institute, University of Denver, Denver, CO, USA

Brian M. Argrow
Department of Aerospace Engineering Sciences, Research and Engineering Center for Unmanned Vehicles, University of Colorado Boulder, Boulder, CO, USA

Begoña C. Arrue
Grupo de Robótica, Visión y Control, Universidad de Sevilla, Seville, Spain

Ella M. Atkins
Department of Aerospace Engineering, University of Michigan, Ann Arbor, MI, USA

Randal W. Beard
Department of Electrical and Computer Engineering, Brigham Young University, Provo, UT, USA

Yunfeng Cao
College of Astronautics, Nanjing University of Aeronautics and Astronautics, Nanjing, China

Jesús Capitán
Grupo de Robótica, Visión y Control, Universidad de Sevilla, Seville, Spain

Philip B. Charlesworth
Airbus Group Innovations, Newport, UK

Wen-Hua Chen
Department of Aeronautical and Automotive Engineering, Loughborough University, Loughborough, UK

Yang Quan Chen
School of Engineering, University of California, Merced, CA, USA

Matthew Coombes
Department of Aeronautical and Automotive Engineering, Loughborough University, Loughborough, UK

Mary L. Cummings
Humans and Autonomy Laboratory, Duke University, Durham, NC, USA

Dan DeLaurentis
School of Aeronautics and Astronautics, Purdue University, West Lafayette, IN, USA

Pedro F.A. Di Donato
Department of Aerospace Engineering, University of Michigan, Ann Arbor, MI, USA and National Civil Aviation Agency–Brazil (ANAC), São, José dos Campos, Brazil

Haibin Duan
School of Automation Science and Electrical Engineering, Beihang University, Beijing, P.R. China

John T. Economou
Centre for Defence Engineering, Defence Academy of the United Kingdom, Cranfield University, Swindon, UK

Gary J. Ellingson
Mechanical Engineering Department, Brigham Young University, Provo, UT, USA

Paul G. Fahlstrom
United States Army Materiel Command, Huntsville, AL, USA

Farhan A. Faruqi
Information Processing and Human Sciences Group, Combat and Mission Systems, WCSD, Defence Science and Technology Organisation, Edinburgh, South Australia

Giancarmine Fasano
University of Naples "Federico II", Napoli, Italy

Karen Feigh
Cognitive Engineering Center, Georgia Tech, Atlanta, GA, USA

C.E. "Noah" Flood
CAVU Global LLC, Purcellville, VA, USA

Michael S. Francis
United Technologies Research Center, East Hartford, CT, USA

Seng Keat Gan
Australian Centre for Field Robotics, The University of Sydney, Sydney, Australia

Alessandro Gardi
RMIT University, Melbourne, Australia

Thomas J. Gleason
Gleason Research Associates, Inc., Columbia, MD, USA

R. John Hansman
International Center for Air Transportation, Massachusetts Institute of Technology, Cambridge, MA, USA

Inseok Hwang
School of Aeronautics and Astronautics, Purdue University, West Lafayette, IN, USA

Mario Innocenti
Munitions Directorate, Eglin Air Force Base, Air Force Research Laboratory, FL, USA

Pantelis Isaiah
Faculty of Aerospace Engineering, The Technion—Israel Institute of Technology, Haifa, Israel

Stéphane Kemkemian
Thales Airborne Systems, Elancourt, France

Seungkeun Kim
Department of Aerospace Engineering, Chungnam National University, Daejeon, Republic of Korea

Trevor Kistan
RMIT University, Melbourne, Australia and THALES Australia, Melbourne, Australia

Daniel P. Koch
Mechanical Engineering Department, Brigham Young University, Provo, UT, USA

Cheolhyeon Kwon
School of Aeronautics and Astronautics, Purdue University, West Lafayette, IN, USA

Jack W. Langelaan
Department of Aerospace Engineering, The Pennsylvania State University, University Park, PA, USA

Nicolas Léchevin
Department of Mechanical and Industrial Engineering, Concordia University, Montreal, Quéebec, Canada

Christopher W. Lum
William E. Boeing Department of Aeronautics & Astronautics, University of Washington, Seattle, WA, USA

Douglas M. Marshall
TrueNorth Consulting LLC, Grand Forks, ND, USA and De Paul University College of Law, Chicago, IL, USA

David W. Matolak
Department of Electrical Engineering, University of South Carolina, Columbia, SC, USA

Iván Maza
Grupo de Robótica, Visión y Control, Universidad de Sevilla, Seville, Spain

Timothy W. McLain
Mechanical Engineering Department, Brigham Young University, Provo, UT, USA

Luis Merino
Grupo de Robótica, Visión y Control, Universidad Pablo de Olavide, Seville, Spain

Antonio Moccia
University of Naples "Federico II", Napoli, Italy

Linas Mockus
School of Aeronautics and Astronautics, Purdue University, West Lafayette, IN, USA

Eric Mueller
NASA, Moffett Field, CA, USA

Myriam Nouvel
Thales Airborne Systems, Elancourt, France

Paul W. Nyholm
Mechanical Engineering Department, Brigham Young University, Provo, UT, USA

Hyondong Oh
Department of Aeronautical and Automotive Engineering, Loughborough University, Loughborough, UK

Aníbal Ollero
Universidad de Sevilla and Scientific Advisory Department of the Center for Advanced Aerospace Technologies, Seville, Spain

Martina Orefice
Air Transport Sustainability Department, CIRA Italian Aerospace Research Center, Capua, Italy

Charles H. Patchett
School of Engineering, University of Liverpool, Liverpool, UK

Lorenzo Pollini
Department of Information Engineering, University of Pisa, Pisa, Italy

Amy Pritchett
Cognitive Engineering Center, Georgia Tech, Atlanta, GA, USA

Camille A. Rabbath
Department of Mechanical and Industrial Engineering, Concordia University, Montreal, Quéebec, Canada

Matthew R. Rabe
International Center for Air Transportation, Massachusetts Institute of Technology, Cambridge, MA, USA

Subramanian Ramasamy
RMIT University, Melbourne, Australia

Francisco J. Ramos
UAS Ground Segment Department, Airbus Defence & Space, Getafe, Spain

James M. Rankin
Avionics Engineering Center, School of Electrical Engineering and Computer Science, Russ College of Engineering and Technology, Ohio University, Athens, OH, USA

Keith A. Rigby
BAE Systems, Warton Aerodrome, Preston, UK

Matthew J. Rutherford
Ritchie School of Engineering and Computer Science, DU Unmanned Research Institute, University of Denver, Denver, CO, USA

Roberto Sabatini
RMIT University, Melbourne, Australia

Daniel P. Salvano
Aviation Consultant, Safety, Certification and CNS Systems, Haymarket, VA, USA

A. Savvaris
Centre for Cyberphysical Systems, Institute for Aerospace Sciences, Cranfield University, Cranfield, UK

Corey J. Schumacher
711 HPW/RH, Wright-Patterson AFB, Ohio, OH, USA

Pau Segui-Gasco
Centre for Autonomous and Cyber-Physical Systems, SATM, Cranfield University, Cranfield, UK

Madhavan Shanmugavel
School of Engineering, Monash University Malaysia, Selangor, Malaysia

Tal Shima
Faculty of Aerospace Engineering, The Technion—Israel Institute of Technology, Haifa, Israel

Hyo-Sang Shin
Centre for Autonomous and Cyber-Physical Systems, SATM, Cranfield University, Cranfield, UK

Brandon J. Stark
School of Engineering, University of California, Merced, CA, USA

Chun-Yi Su
Department of Mechanical and Industrial Engineering, Concordia University, Montreal, Quéebec, Canada

Salah Sukkarieh
Australian Centre for Field Robotics, The University of Sydney, Sydney, Australia

Shigeru Sunada
Department of Aerospace Engineering, Osaka Prefecture University, Osaka, Japan

Hiroshi Tokutake
Department of Aerospace Engineering, Osaka Prefecture University, Osaka, Japan

Christoph Torens
German Aerospace Center (DLR), Department of Unmanned Aircraft, Institute of Flight Systems, Braunschweig, Germany

Giulia Torrano
Air Transport Sustainability Department, CIRA Italian Aerospace Research Center, Capua, Italy

Antonios Tsourdos
School of Aerospace, Transport & Manufacturing and Centre for Autonomous and Cyber-Physical Systems, Cranfield University, Cranfield, UK

Dai A. Tsukada
William E. Boeing Department of Aeronautics & Astronautics, University of Washington, Seattle, WA, USA

Joseph J. Vacek
Department of Aviation, University of North Dakota, Grand Forks, ND, USA

Kimon P. Valavanis
Ritchie School of Engineering and Computer Science, DU Unmanned Research Institute, University of Denver, Denver, CO, USA

Antidio Viguria
Center for Advanced Aerospace Technologies (CATEC), Seville, Spain

Vittorio Di Vito
Air Transport Sustainability Department, CIRA Italian Aerospace Research Center, Capua, Italy

Nikolaos I. Vitzilaios
Ritchie School of Engineering and Computer Science, DU Unmanned Research Institute, University of Denver, Denver, CO, USA

David O. Wheeler
Department of Electrical and Computer Engineering, Brigham Young University, Provo, UT, USA

Brian White
Centre for Autonomous Systems and Cyber-Physical Systems, Cranfield University, Cranfield, UK

Zhe Xu
Australian Centre for Field Robotics, The University of Sydney, Sydney, Australia

Oleg A. Yakimenko
Graduate School of Engineering and Applied Science, Naval Postgraduate School, Monterey, CA, USA

Andy Yu
School of Aeronautics and Astronautics, Purdue University, West Lafayette, IN, USA

Greg L. Zacharias
Charles River Analytics, Cambridge, MA, USA

Foreword

The *Encyclopedia of Aerospace Engineering*, first published in 2010, represents a singular attempt to capture the aerospace community's ever-expanding collective body of knowledge into an easy-to-use, cohesive, universal reference framework.

The past few years have marked rapid growth in aerospace systems and technology – as new and innovative designs and applications come to the fore, new ways of thinking about old challenges emerge, and as existing technology and systems have continued to evolve in new and exciting directions. This growth has been especially dynamic in the field of unmanned aircraft systems (UAS).

No longer solely the tools of the military, UAS have experienced a cost and capability revolution, performing important missions across many fields – agricultural sensing, infrastructure inspection, scientific research, and logistics – with significant implications for the research and development enterprise. The new complementary technologies involving intelligent systems are continually changing how we think about the capabilities and applications of UAS technology and how it will continue to transform our lives.

The absence of the human payload and its associated systems has inspired and delivered remarkable innovations in our industry. Yet unmanned systems still face extraordinary challenges to deliver comparable situational awareness to the operator, and we are all aware of the potential threats to safety and security associated with the widespread availability and increasing affordability of small-scale, remotely piloted aircraft. To address these challenges and to leverage these associated innovations fully, we need ongoing access to information. We therefore welcome this addition to the *Encyclopedia of Aerospace Engineering* as both timely and comprehensive, covering a remarkable range of UAS issues from platform technology, autonomy, security, and fail-safe systems through to integration with manned aviation and the regulatory and legal regimes – all critical pieces of knowledge if we are to continue developing the UAS enterprise to its fullest potential.

The year 2016 marks both the 150th anniversary of the Royal Aeronautical Society (RAeS) and the 85th anniversary of the American Institute of Aeronautics and Astronautics (AIAA). With a combined membership of more than 50,000 aerospace professionals, our two organizations celebrate these milestones and our members' never-ending quest for knowledge and solutions not just to the problems and challenges of today but also of the next impossible thing. It is our members who evolve UAS technology to even greater capabilities and uses than that exist today.

Aerospace make the world safer, more connected, more accessible, and more prosperous. We hope that the addition of this volume to the *Encyclopedia* continues this trend and is as professionally valuable and influential to its readers – and the industry – as were the preceding volumes.

As we write, there is perhaps no issue more timely in aviation than unmanned aircraft systems. That is why it is our pleasure to jointly commend to you this new contribution to the aerospace engineering body of knowledge.

Mr. James Maser
President, American Institute of Aeronautics and Astronautics
and
Vice President, Operations Program Management,
Pratt & Whitney, East Hartford, CT, USA
and
Dr. Chris Atkin
President, Royal Aeronautical Society
and
Professor of Aeronautical Engineering,
City University London, UK

Preface

The Wiley *Encyclopedia of Aerospace Engineering* offers the aerospace and robotics communities a series of accessible chapters covering all disciplines of the Aerospace field. While the Encyclopedia is regularly updated to ensure currency, the editors also decided to pursue new key volumes in important and emerging Aerospace areas. This volume covers the technology, operations, and policy challenges associated with both small and large unmanned aircraft systems (UAS).

Small UAS operating at low altitudes are rapidly proliferating for uses ranging from hobby to surveillance and package delivery. Configurations range from traditional fixed-wing aircraft to the popular multirotor helicopter or multicopter offering unprecedented maneuverability. Plastic and composite materials, low-cost manufacturing processes, and capable embedded sensors and processors support both the fully piloted and fully autonomous flight. Motors powered by lithium–polymer batteries are mass-produced at low cost, yet further improvements in onboard energy storage and power requirements are essential to increase small UAS range and endurance. This UAS volume provides essential background in UAS configurations and subsystem design with respect to aerodynamic, structural, propulsion, and power system considerations as well as avionics, communication, sensing, control, and planning functions.

Because traditional manned aircraft have always relied upon the onboard pilot or crew to assimilate information and make safety-critical decisions, UAS necessarily introduce a number of new challenges in control, communication, and information management. What sensing and control strategies are effective for the spectrum of UAS configurations and missions, and what level of decisional autonomy is required or even desired? How do remote operators maintain situational awareness, how can the ground–air link be ensured secure and reliable, and what protocols are appropriate in lost link situations? How will UAS sense and avoid each other and manned aircraft? What functions should be implemented onboard and which in the ground station? Small UAS may be beneficially organized in multiagent teams to simplify mission coordination and handling in the National Airspace System (NAS), the National Air Traffic Services (NATS), and other air traffic control systems. The chapters in this volume covers the spectrum of sensors, guidance, navigation, and control algorithms, and mission-level decision-making algorithms offering UAS the ability to autonomously execute mission plans and effectively coordinate actions with other UAS. Remaining challenges in ensuring secure, safe, reliable, and robust UAS operation are also discussed.

The number of UAS operations per day is expected to quickly exceed the number of manned operations. Furthermore, these operations will routinely occupy the low-altitude airspace not commonly used for manned aircraft today. Small maneuverable UAS can be launched and recovered from almost any site and flown in cluttered areas. These factors introduce a variety of new concerns related to airspace access and policy, privacy, and social/legal issues. What restrictions should be placed on UAS operations based on overflown rural to urban property as well as airspace class? How can policy and law balance the desire to capitalize on new UAS capabilities while respecting privacy concerns and ensure acceptable levels of risk exposure to overflown people and property? This UAS volume offers chapters on UAS airspace access requirements and associated policy issues. These chapters outline capabilities and needs for standards and processes enabling UAS safety certification and security. As camera-equipped UAS operate "just over our backyards," new privacy and airspace ownership and control issues have emerged that are still under discussion. Chapters in this volume also outline privacy, social, and legal issues in the context of legal precedent and emerging community concerns.

As is evident from the diverse technology, operations, and policy content in this volume, UAS are truly "multidisciplinary systems" that offer exciting new mission capabilities but that also challenge traditional aviation assumptions regarding operational norms and personnel roles. UAS are motivating us to rethink information handling while truly offering everyone low-cost access to the sky.

Ella Atkins
Department of Aerospace Engineering,
University of Michigan, Ann Arbor, MI, USA

Aníbal Ollero
Universidad de Sevilla and Scientific Advisory
Department of the Center for Advanced Aerospace
Technologies, Seville, Spain

Antonios Tsourdos
School of Aerospace, Transport & Manufacturing and
Centre for Autonomous and Cyber-Physical Systems,
Cranfield University, Cranfield, UK

PART 1
Introductory

Chapter 1
UAS Uses, Capabilities, Grand Challenges

Michael S. Francis
United Technologies Research Center, East Hartford, CT, USA

1 INTRODUCTION

Unmanned aircraft have existed for almost as long as the human quest to achieve manned flight. Early unmanned heavier-than-air gliders, built by such notables as George Cayley and Otto Lilienthal, were used to pioneer the technologies required of early manned aircraft. With the powered variants that followed, the twentieth century is littered with a rich history of unmanned aircraft that were created to support an ever-increasing number of missions and applications, many driven by military needs and opportunities (Holder, 2001; Keane and Carr, 2013; Newcome, 2004). The last several decades have witnessed an even more explosive increase in unmanned aircraft of all shapes and sizes, including an increasingly large number intended for civil and commercial applications. Despite this long history, the unmanned aircraft revolution is arguably still in its infancy. To better understand this assertion, it is helpful to review the technological origins of these systems.

Unmanned Aircraft Systems. Edited by Ella Atkins, Aníbal Ollero, Antonios Tsourdos, Richard Blockley and Wei Shyy.
 ISBN: 978-1-118-86645-0.

The technological roots of the heavier-than-air, manned aircraft are firmly implanted in the industrial age. But these machines evolved considerably over their first century of existence due, in part, to the infusion of technologies that would eventually underpin the information age. Electronics, solid state devices, microprocessors, data storage, and sensors of many types would find their way into aviation systems at virtually all levels of system architecture and operation. Later, the advent of digital communications technology and introduction of the satellite-based global positioning system (GPS) added vital elements that would further enable practical, low-cost, remote operation of these platforms.

The dramatic increases in information technology over the last several decades, coupled with concomitant decreases in the size and cost of enabling electronics, would help usher in the era of affordable unmanned air systems, or UAS, that we know today. The levels of innovation and discovery that have spurred recent growth in UAS capabilities can be expected to continue. With no abatement to Moore's law in sight and new fundamental advances such as quantum computing forecast for the not-too-distant future, the information revolution is showing few signs of slowing down. From a technology perspective, UAS can be viewed as a bellwether "marriage" of the industrial age and the information revolution.

Despite the push from this high-power technology "engine" and the enthusiasm of its many proponents, UAS capability has not yet seen widespread acceptance and adoption, tempered by a number of factors that can be associated with societal "inertia." These include cultural and regulatory inhibitions, legal precedents, and infrastructure constraints. And while these factors have impacted other industries and markets, their effects appear to be especially prominent for this disruptive entrant to the aviation arena.

2 USES – MISSIONS AND APPLICATIONS

2.1 Early evolution

It is not surprising that development progress in unmanned aircraft was slow during the first half of the twentieth century when the technology of electronics was in its infancy and modern digital systems were essentially nonexistent. Their early operational adaptation significantly lagged that of their manned counterparts. The first entrants were experimental and supported high-risk research and development activities aimed primarily at establishing the feasibility of manned flight. The first unmanned operational designs were intended for military applications, serving as aerial targets or actual weapons.

Perhaps the first invention to have major impact on the viability of unmanned aircraft was the multi-axis gyroscope, introduced by Elmer Sperry almost a decade after the Wright brothers first flew. Sperry's invention has been cited by some as the single most significant enabler for unmanned aviation as we know it today (Newcome, 2004). Despite this important advance, early unmanned aircraft lacked the level of navigational precision necessary to reliably accomplish military objectives. Perhaps the greatest limitation for these early systems was the lack of "intelligence" required to accomplish complex missions in challenging and uncertain combat environments. Not only did these vehicles lack an onboard pilot, but also the technologies necessary for providing access to adequate *remote* intelligence (operators) did not yet exist. As a result, the operational footprint remained limited, with a focus largely on launch-and-leave concepts that were best suited to weapons and other expendable system applications. The Kettering "Bug" and Sperry–Curtiss aerial torpedo (circa 1916–1917) and the World War II vintage German V1 "buzz bomb" are examples of this trend from different eras. Over much of the twentieth century, unmanned platforms continued to serve in these roles, as end-of-life aircraft were converted to aerial targets, and high-tech cruise missile designs further expanded the arsenal of expendable, one-way platforms. It was much later that the term *unmanned air vehicle*, or UAV for short, would be employed to differentiate the reusable platforms from the expendable variants.

The first widespread use of reusable unmanned aircraft in an operational environment came during the course of the Vietnam War. The Ryan *Firebee*, originally developed for aerial target applications, was adapted to serve as an information-gathering platform in what we would call today an intelligence, surveillance, and reconnaissance – or ISR role. Launched from a large mother ship, often a C-130 transport, the Ryan AQM-34 "Lightning Bug" was configured to perform a preprogrammed mission over a scripted route followed by a parachute recovery into friendly territory. It was a true unmanned air system, by today's definition (Keane and Carr, 2013). In contrast to the high-speed, turbojet-powered Firebees developed in the United States, the Israelis introduced the first low-speed, real-time surveillance UAVs during the 1973 Yom Kippur war. In both cases, these systems were introduced to achieve specific tactical objectives and retained during the conflict solely for those purposes.

Radio frequency communications technology necessary to achieve remote unmanned aircraft operation was explored and tested as early as the eve of World War I, but deemed impractical. The idea was reintroduced on the eve of World War II with some success. But the concept of remotely operated "drones," as they had then come to be called, never found a niche for a role in the broader conflict. It was a subsequent key technology development, the introduction of inexpensive solid-state radios in the 1950s that "kick started" the era of modern radio-controlled aircraft in the United States. Now familiar to present day hobbyists, this was also the first introduction of remotely operated aircraft technology to a larger non-military marketplace.

It was not until the introduction of modern, compact, high-performance computer technology that the contemporary UAV became attractive enough to its user community to earn a permanent place in the defense inventory. In the 1980s, the Defense Advanced Research Projects Agency, or DARPA, began developing a new class of low-cost, long-endurance unmanned aircraft that could be employed in a variety of ISR missions. The agency's preoccupation with information technology and its role in the broader information revolution at that time helped motivate adoption of the UAV as an ideal "test case." As these systems matured and gained recognition, they were embraced by a variety of government customers including the intelligence agencies and the military departments.

2.2 Dull, dirty, and dangerous

The first Gulf War provided the first large-scale operational opportunity to test unmanned air systems in a realistic military environment. A number of them, such as the Predator medium-altitude long-endurance (MALE) UAV, gained notoriety for their ability to provide persistent, real-time streaming video imagery to remote operational command posts, including the Pentagon, during the actual course of operations. At the time, this capability was viewed as a game changer in modern warfare.

UAVs in a variety of sizes with similar capabilities emerged to support the allied war-fighting enterprise at virtually all levels of command. From the portable, hand-launched, locally controlled Raven peeking over-the-hill for a small Marine Corps squad to the medium-altitude, wide area-surveillance Predator – operated remotely by a continental US-based ground crew, these systems gained broad acceptance by their user communities. These systems have been proliferated in large numbers as a result of the conflicts in Iraq and Afghanistan. The introduction of the even more capable Global Hawk increased operational altitudes to beyond 60 000 ft and endurance timelines to in excess of 24 h. A variety of intermediate-sized unmanned aircraft such as the Shadow and Scan Eagle Tactical UAVs, among others, were also introduced to further expand battlefield ISR to other echelons of command to a level never before seen in combat.

The Reaper, a weaponized variant of the Predator UAV, provided a unique capability never before seen in armed conflict. Combining persistent surveillance and precision targeting with near instantaneous lethal response, these platforms served as ultimate “standoff snipers,” demonstrating an unprecedented level of precision engagement coupled with minimal collateral damage. Despite these unique capabilities, combat UAS have struggled to gain acceptance across the broader military community.

2.3 Emergence of civil and commercial applications

Arguably, the first highly visible civil (government-sponsored, nonmilitary) applications of modern UAS were in the pursuit of scientific understanding. In the mid-to-late 1990s, the US National Aeronautics and Space Administration (NASA) funded a number of then fledgling UAS developers to demonstrate very high altitude, long-endurance civil UAS under its Environmental Research and Sensor Technology (ERAST) program. ERAST was focused on developing capabilities for probing the upper atmosphere and providing the opportunity for *in-situ* measurements and remote-sensing resolution that space-based sensors could not achieve. Aircraft such as Aurora Flight Sciences’ Pegasus and Aerovironment’s pioneering solar-powered HELIOS, among others, were developed and flown as part of that effort. In recent years, UAS have also been employed for studying a variety of atmospheric phenomena ranging from hurricanes to super cell thunderstorms and incipient tornadoes (Figures 1 and 2) (Elston *et al*., 2011).

Figure 1. HELIOS unmanned air vehicle.

While UAS have become a staple in modern warfare, their application to nonmilitary missions has risen dramatically in just the past few years. And despite the rich operational history of several now well-known UAS models over the past two decades of conflict, it is a new generation of platforms and technology that have captured the public’s attention and interest.

Attempts to develop the so-called micro air vehicle (McMichael and Francis, 1997) reach back to the mid-1990s. But the recent, rapid ascendance and public embrace of these systems has been facilitated by the emergence of a number of new key technology elements that do not have their roots in defense technology. These include:

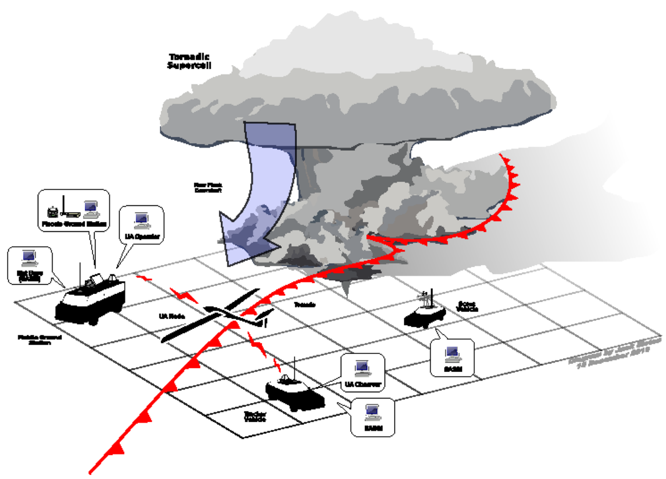

Figure 2. Operational architecture for tornadic supercell region penetration and assessment during Vortex II campaign. (Reproduced with permission from Wiley, 2011. © Wiley.) (Courtesy J. Elston and B. Argrow, University of Colorado.)

- small, inexpensive, inherently stable, operator-friendly "quad-rotor" air vehicles;
- low cost, compact imaging video sensors; and
- low cost, portable control stations equipped with digital wireless radio connectivity and intuitive digital operator interface.

These small and compact systems have underpinned the explosion in interest in UAS applications. The inherent stability and straightforward control of the signature multirotor platforms enable novice operators to easily control or manage their aircraft trajectories within line of sight. Public interest in social media, coupled with the fascination for flight and the low-cost entry to own and operate these systems have put them in high demand for commercial and recreational users. From realtors trying to carve out a new approach to selling property to infrastructure managers wanting to inspect otherwise inaccessible areas to a host of video enthusiasts simply trying to capture a "new perspective," small UAS have created both interest and controversy across the public domain. But while the small, easy-to-operate low-end platforms have played a significant role in increasing public interest in UAS, they do not possess the range, endurance, speed, or payload capacity of their larger, fixed-wing counterparts. A diverse array of these larger vehicles stands ready to further expand the spectrum of mission and applications.

In a recent publication addressing the civil and commercial marketplace, the Association of Unmanned Vehicle Systems International (AUVSI) highlighted a diverse range of applications; encompassing wildfire mapping; agricultural monitoring; disaster management; telecommunications; thermal infrared power line surveys; law enforcement; weather monitoring; aerial imaging/mapping; television news coverage; sporting events; moviemaking; environmental monitoring; oil and gas exploration; and freight transport (Jenkins and Vasigh, 2013). That report also predicts precision agriculture and public safety to be the two most impactful areas of commercial/civil use in the United States over the coming decade. Many of these projected applications exploit the remote sensing legacy of contemporary UAS, so successfully demonstrated by earlier military systems. This array of ISR-like applications has also been energized by the proliferation of very low cost, miniature commercial imaging sensors that have flooded the cell phone and tablet computer markets. But UAS can also be expected to be employed in an array of other uses, including the transport of cargo as an example.

Like the sensor–shooter combination demonstrated by the Reaper UAS, the on-platform integration of sensors with other payload elements affords an opportunity for further expansion of missions and applications. As an example, the combination of multispectral imaging with real-time nutrient/pesticide dispensing can potentially take "precision agriculture" to another level. Similarly, real-time infrared imaging with concurrent fire suppressant application could greatly improve the ability to mitigate incipient wildfires. Although the remote sensing capability adds great value by itself, the ability to integrate it with a timely response/action mechanism greatly increases the utility of the resultant system and a host of its applications.

3 EMERGING CAPABILITIES AND A LOOK AHEAD

Today's UAS, even the small inexpensive variety, possess attributes that would be the envy of their early radio-controlled predecessors. New capabilities that improve operational versatility seem to emerge on a regular basis. Auto takeoff, autoland, and waypoint navigation, coupled with highly stable and controllable air vehicle designs, are now commonplace even in the emerging commercial marketplace.

And while information age by-products have added significant new enabling capabilities, they have also spurred new developments on the industrial age side of the equation. For example, the search for more effective and efficient propulsion methodologies, new structural constructs, and new materials may be more extensively exploited in the unmanned systems community than the traditional manned aircraft segment.

3.1 Expanding the design space and operational envelope

The elimination of human presence on board the air vehicle affords an opportunity to introduce new attributes and mission capabilities to the aircraft, and, to some extent, redefine flight as we know it. To better understand this opportunity, it is useful to examine the benefits and constraints of the traditional onboard human presence (pilot, crew, and passengers).

In the early days of manned flight, the pilot performed all the functions necessary to control and manage the aircraft. The achievement of meaningful mission objectives under complex circumstances without the aid of an onboard human was virtually unfathomable. The pilot's eyes and ears were primary sensors, hands and feet served as primary effectors, and the human brain was the integrated flight and mission computer responsible for everything from basic maneuver execution to comprehensive mission management. In addition to direct sensing, the pilot was responsible for data interpretation and information synthesis related to all aspects of aircraft operation. Today, many of these requirements are allocated to automated systems, allowing the pilot and crew to focus on top-level supervisory tasks.

In contrast, the accommodation of human presence on board the aircraft has proven an ever more daunting and resource consuming task, as aircraft operate in domains far more demanding and complex compared to that experienced by the early aviation pioneers. The addition of pressurized systems with oxygen has become indispensable for high-altitude long-range operations. Other constraints imposed by the human anatomy have limited the way flight is prosecuted (e.g., coordinated bank to turn) and has significant impact in the design and configuration of the aircraft. The need for specific orientation with respect to the gravity vector has limited the way vertical takeoff or landing (VTOL) flight is achieved and has significant impact on the design of those aircraft.

Onboard human presence impacts flight vehicle design in many ways. It constrains platform acceleration in all axes, and limits vehicle endurance. The human factor has impacted the approach to reliability and safety from both design and operational perspectives. The need to maintain human functionality and performance within the volume and weight constrained confines of the cockpit has necessitated extensive and often costly training and proficiency regimens for the aircrew community. Onboard human presence has also invoked the addition of unique infrastructure, and diversely ranging from specialized training simulators to search, rescue, and other support capabilities that come into play in the event of aircraft mishaps. The on-aircraft interface between human and machine has become quite complex, encompassing everything from integrated control effectors, and complex displays to power-consuming environmental systems that enable crew comfort and survival during flight at all achievable altitudes and airspeeds.

While today's unmanned aircraft take full advantage of their capability for remote operation, few designs fully exploit the absence of human presence. This potential to enlarge the air vehicle design and operational envelopes is significant. A number of attributes that could be more fully advantaged in that regard include the following:

(a) Northrop Grumman *Global Hawk*

(b) General Atomics *Predator B*

Figure 3. Long-endurance aircraft examples.

- *Extreme Endurance:* This ability of a platform to stay aloft for periods that well exceed normal crew limitations has been demonstrated to a large extent in current operational systems. The attribute is a key performance driver for ISR mission systems such as those depicted here. 24-h endurance capabilities are commonplace for larger platforms and are rapidly becoming possible for their smaller, tactical-size counterparts. Designers are currently focused on week-long operation, with some experimental systems attempting even longer durations. Future missions such as aerial cell-phone relay and Internet distribution platforms will benefit greatly from these capabilities (Figure 3).
- *Small Size/Scale:* The ability to build and operate aircraft incapable of physically accommodating an adult human presence has already been realized. Small UAS (sUAS), such as the AAI Shadow UAS, have proliferated in military missions for over a decade and performed admirably in a variety of tactical roles. They are enablers for a variety of civil and commercial applications ranging from highway/bridge infrastructure inspection to precision agriculture. Even smaller variants, so-called "micro air vehicles" have begun to appear in real operational roles, although the very smallest, such as the Aerovironment Hummingbird is still in the experimental stage. With linear dimensions not exceeding 15 cm in any axis, they may prove extremely useful in highly confined spaces, such as building or even pipe interiors. With further miniaturization, they may even prove useful in internal bio-medical applications – exploring the interior of the human anatomy (Figure 4).
- *Extreme Maneuvering Capability:* Unmanned platforms are, in principal, capable of sustaining accelerations and

(a) Textron-AAI *Shadow UAV*

(b) Aerovironment *Hummingbird* Micro Air Vehicle

Figure 4. Small UAVs. (Courtesy AeroVironment, Inc.)

forces limited only by structural considerations, operating well beyond the tolerance of any human pilot. Turning accelerations up to approximately 30 g's – the limit where modern turbojet engines begin to experience "out-of-round" geometric distortion, might be possible without the introduction of other new technology. Such capabilities could revolutionize modern air combat, even with the introduction of more agile air-to-air weapons. Structural morphing capability, such as that depicted in this DARPA concept could be exploited to increase maneuver accelerations in future unmanned combat aircraft (Figure 5).

- *Arbitrary Orientation:* Unlike manned aircraft, the physical orientation of an unmanned air vehicle in any phase of flight need never be dictated by human physiology limitations. In theory, it can be completely arbitrary, limited only by physics-of-flight considerations and mission needs. An example illustrating the potential utility of this attribute is found in the tail-sitter concept, whose roots go back to the early 1950s in a then-impractical manned design (Chana and Coleman, 1996; Taylor and Michael, 1977). A modern UAS variant (the Sikorsky VTOL X-Plane) is an aircraft designed to pioneer the prospect of runway independent launch and recovery while achieving fixed wing-competitive cruise speeds. This class of aircraft has the potential to revolutionize high-priority transport – enabling, for example, the retrieval of cargo from a ship at sea and its rapid transport to even remote, unimproved areas without the need for a runway or any other form of terrestrial transportation in the process (Figure 6).
- *Unique Configurations:* Unmanned aircraft designers have already provided numerous examples of unconventional configurations ill suited to manned flight. Contemporary vehicle control technology has enabled innovative designs that capture the best of fixed and rotary wing designs in a relatively simple mechanical package. The lack of need for a conventional cockpit coupled with other attributes mentioned above can result in novel shapes and configurations more germane to niche missions or unique flight environments. Examples of these include the 1998-vintage Cypher UAV and an as yet untested dual-free wing concept capable of morphing from the biplane configuration (shown), operating at near zero-speed hover conditions, to a tandem-winged, tailless orientation that could fly at extremely high speeds because of its low aerodynamic drag (Figure 7).
- *Unconventional Launch and Recovery:* Novel approaches for launching and recovering UAS have increased significantly, especially for smaller air vehicles. Assisted rail launch capability and net or tether recovery techniques

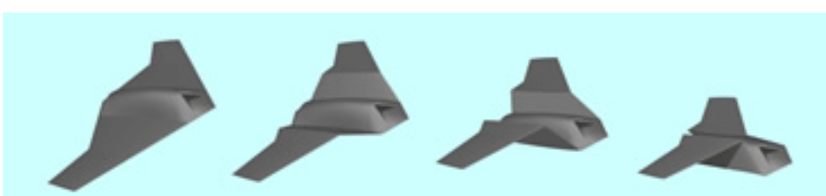

Figure 5. Extreme maneuvering may be enabled by morphing structure. (Reprinted with permission from Defense Advanced Research Projects Agency. Approved for Public Release, distribution unlimited.)

Figure 6. Arbitrary orientation – example: the Sikorsky VTOL X-Plane Concept. (Reproduced with permission from Chris Van-Buiten, 2016. © Sikorsky Innovations.)

(a) Cypher UAV

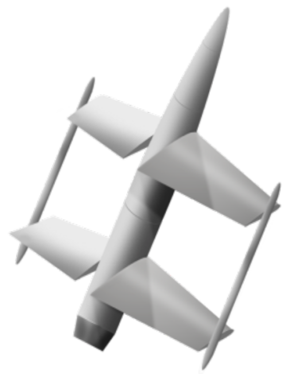

(b) Dual Free Wing UAV Concept

Figure 7. Unique configurations.

are employed on operational aircraft such as the Insitu Scan Eagle. Larger systems may find similar opportunities as in the depicted shipboard concept where a high-performance, unmanned UCAV is tube-launched like a cruise missile and later recovered shipside, following a near vertical, high angle-of-attack approach. An articulating, conforming porous arresting structure is configured to match the aircraft's approach orientation. The concept eliminates the need for conventional, often heavy landing gear, improving the vehicle's range-payload performance. More broadly, the concept reduces the need for conventional aircraft carrier operations, while simultaneously providing airpower projection capabilities to other surface ship types. Future novel launch and recovery techniques may well enable UAS operations in otherwise impractical civil and commercial environments as well (Figure 8).

- *Attritability:* The notion of an "attritable" (limited life, yet reusable) vehicle design is unrealistic for manned aircraft, but the capability could become a practical option for a number of unmanned vehicle applications. This airplane equivalent of a reusable but otherwise throw-away styrofoam cup could fill a gap between the long-life, fatigue-limited manned aircraft designs and the single-use missile/projectile configurations in common use today. The very first DARPA UCAV platform concept depicted here invoked that capability. During peacetime, manned combat aircraft can spend in excess of 90% of their flight hours for aircrew training and proficiency. For UAS, there is no "seat-of-the-pants" benefit to flying these aircraft during training missions unless operational synergies with close proximity manned aircraft are also sought. For all applications that require highly intermittent flight operations or those that involve lengthy downtime periods, limited life aircraft designs could offer significant life-cycle cost advantages. Missions such as *in situ* sensing of toxic or radiation clouds, where the vehicle may have to be disposed following a mission, as well as other missions into dangerous environmental conditions, such as extreme weather or other threats may be ideal for attritable aircraft. However, cost savings derived from attritable designs are likely limited, since these aircraft must possess the necessary levels of safety and reliability to conduct missions in shared common airspace (Figure 9).

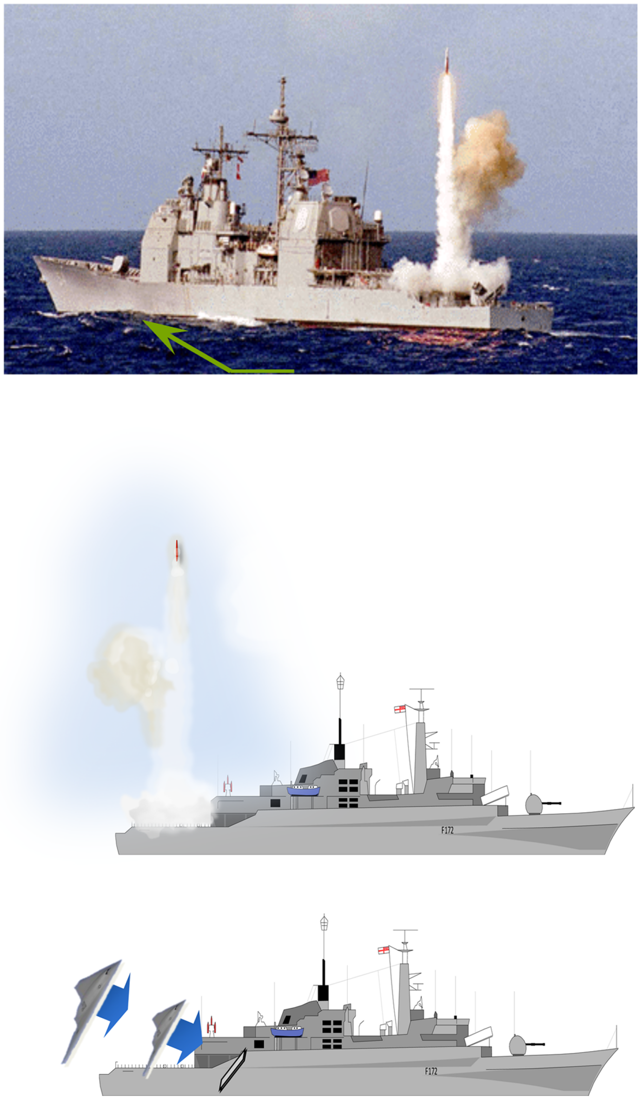

Figure 8. Novel shipboard launch and recovery of high-performance UAV.

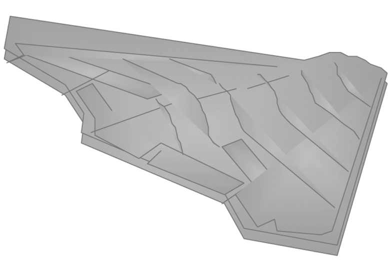

Figure 9. "Attritable" aircraft concept icon – DARPA's Unmanned Tactical Aircraft.

3.2 Autonomy

Automation has already contributed to a number of operational improvements for UAS by providing more time flexibility for the remote human crew to assess and act on information as the mission unfolds. The continued advance of modern computing power is opening the door to even higher levels of autonomous operation, where the human element is fully relieved of many minor decisions and becomes essentially supervisory in nature.

Fully autonomous flight remains an elusive objective for UAS proponents and will likely remain so for the foreseeable future. The leap from today's automation to tomorrow's autonomy is not a small step. An automated system is constrained to operate within prespecified bounds, with anticipated and preprogrammed alternatives available in the event of non-nominal circumstances. Most automation today is centered on basic, prescriptive flight functions, such as, for example, vehicle control (e.g., fly-by-wire control) or navigational route execution (so-called waypoint navigation). These advances have greatly improved the ability for the remote crew to interact intermittently in controlling the aircraft. However, much remains to be done in this domain. For example, many systems today limit UAS operation to one vehicle by one operator. Studies have been conducted to illustrate the possibility of managing multiple aircraft with a single human operator, if the level of supervisory interaction is high enough (Ruff, Narayanan, and Draper, 2002). For the latter to occur, the level of autonomy at the vehicle and system levels must increase dramatically.

Increasing the level of autonomy of an unmanned air system requires more than adding functionality in the form of new tasks or increasing task levels. A truly autonomous system would be capable of identifying and assessing a broad range of mission-level conditions and then adapting, as needed, to accomplish necessary tasks as the mission unfolds. It would be capable of brokering solutions that account for multiple objectives and circumstances that may have impact on the aircraft in its mission over several time scales (epochs) simultaneously. For example, an aircraft may be faced with a short-term requirement to avoid an unexpected obstacle, while coping with a potential threat just over the horizon, and while also facing a change to its overall mission endgame objective. A capable *autonomous mission manager* must cope with all of these circumstances simultaneously, while projecting an acceptable solution and executing successful outcomes throughout the mission timeline. The system would be capable of dealing with a broad range of variables, ranging from traditional well-defined physical parameters to less objective conditions, such as evolving environmental changes or even less predictable threats, such as those imposed by a human adversary.

The metric that best separates an autonomous system from a highly automated one is the ability to cope with the unknown – the condition or situation which was not considered in the system's "in-the-box" design. The ability to manage these kinds of contingencies will define the level of autonomy in future UAS. These future autonomous systems must be capable of learning from their experience, for it is that trait and the ability to adapt as a result that enables this behavior in the first place. Coping with the statistical probabilities associated with the operational environment, and adapting to conditions in a manner that will improve performance, mission success, safety, or other desired objectives are key behaviors that the autonomous system must master.

Robotics and artificial intelligence remain hot topics with seemingly limitless applications – from biomedical devices to driverless cars and unmanned air systems to domestic robots that can do the family laundry. Many of the challenges associated with advancing this disciplinary arena for the broader robotics community are well documented (Hager *et al*., 2015).

4 GRAND CHALLENGES AHEAD

Despite the tremendous potential of unmanned air systems across a range of economically beneficial and compelling applications, the obstacles to their successful introduction and implementation are significant. UAS today face a number of constraints that technology alone cannot overcome. Many are rooted in competing legacy systems and methods, as well as in institutional, regulatory, and cultural precedents that minimally assure a lengthy transition to an acceptable, productive future state. As a result, economic limitations for these systems are no longer centered on the cost of hardware and software. The fundamental inhibitions to ownership and operation can be found in the lack of acceptable regulatory infrastructure to guide their operations, combined with institutional conservatism in dealing with companion liability, insurability, legal issues, along with the concomitant consequences of negative public perceptions.

The "Grand Challenges" are those that require a coordinated, integrated approach to collectively address all these issues, technical and otherwise, in a manner that will enable UAS of all types to reach their full potential.

4.1 Access to the airspace

Today, limited access to the airspace is the dominant barrier to the realization of the full economic potential that can be derived from UAS capabilities. Most of today's operational requirements that regulate UAS operations in the common airspace are rooted in the regulatory precedents set by and for manned systems over decades with an evolved operational paradigm centered on pilot capabilities and behavior. In the manned aircraft, the pilot is omnipresent – assumed able to assess in-flight circumstances from a cockpit perspective and react to them virtually instantaneously. This is not the case with the modern UAS.

An array of real-world constraints and limitations is responsible for this dichotomy. These include wireless connectivity issues, including communications latency; environmental factors; and human frailties that can become exaggerated in the quest to provide the continuous human presence. The latter set ranges from situation awareness limitations imposed by the finite number and types of sensor and information sources to fundamental limits to human attention spans. More subtle factors associated with human cognition may also play a role. These constraints can be less significant in some operational circumstances, for example, short-duration flights within visual line of sight between the aircraft operator in reasonably good weather conditions. The problem can become acute in long-range beyond-line-of-sight operations, especially in adverse weather and/or in airspace crowded by aircraft or other physical obstacles. The need for UAS to project a continuous "crew presence" – able to respond with no delay, replete with a fault-free wireless connection between platform and remote crew simultaneously – represents its most demanding requirement and its greatest vulnerability.

In keeping with the slow evolution of manned flight prevalent over the last half-century, these rules have been slow to change despite the emergence of new or improved technologies designed to enhance reliability and safety. To the impatient drone entrepreneur, progress in integrating these systems into the common airspace appears glacial across much of the breadth of the international landscape.

Larger UAS must compete to share already crowded airspace with the manned platforms that have set the precedent and expectations for flight safety. Small UAS, in contrast, are pioneering access to a new region of airspace largely unfamiliar to both pilots and regulators. This low-altitude, obstacle-rich environment, ranging from below approximately 150 m down to the "blades of grass" adjacent to the earth's surface, presents a variety of challenges to remote operations. These include people – often transiting near vehicle flight routes, personal property adjacent to and along those routes, and other hazards, including nearby trees, buildings, and other obstacles.

The most difficult situations will likely involve operations in urban canyons, where traditional navigation sources like

GPS are intermittent or unavailable. The most demanding of these environments have rarely, if ever been encountered by larger manned aircraft. They present a new set of challenges for the regulatory communities and the public, as well. Ironically, it is this most complex set of environments that the smallest, least capable platforms and systems (size, weight, and power) have chosen to invade.

4.2 The quest for *trust*

The arguably greatest challenge and impediment to UAS acceptance and mission proliferation lies in gaining *trust* in the behavior of these technologically advanced systems. This need extends to the manned aircraft-dominated user community, an outdated and often incompatible regulatory system needed to support and promote their operation, and most importantly, a skeptical public.

Although UAS technologies have made significant strides over the past several decades, their vulnerabilities are well known to most. A century of manned aviation evolution has set high expectations for safety and reliability yet to be matched by the unmanned community. Growing prospects for cyber-physical security threats in recent years have added to public skepticism. Along with growing concerns over the illicit use of UAS and their prospects for violating individual privacy, resistance to their broad introduction has been significant (Tam, 2011; Watts, Ambrosia, and Hinkley, 2012). Many of these concerns are directed at the system users, and especially at their intent and integrity. They are likely to be resolved through a combination of properly defined regulatory constraints, coupled with adequate education of potential users and the public as well.

A more immediate concern that has long-term implications over the continued evolution of UAS revolves around the issue of trust in *intelligent software*. This turns out to be a problem for manned and unmanned systems alike. And it has its roots in a long evolved methodology for developing trust in physical systems.

Traditional rigorous hard science-based evaluation methods created to assure developer, user, and even public confidence in engineering products such as airplanes are not likely to prove adequate for the certification of future intelligent unmanned air systems. And software is the culprit. As software-based approaches and processes have proliferated within the aviation ecosystem, their collective verification, validation, and certification (VV&C) has proven to be perhaps the most significant factor to date to impact aircraft affordability. Current VV&C techniques based on, for example, FAA-referenced DO-178 B/C and comparable standards continue to consume an ever-increasing proportion of aircraft development budgets. Prospects for their application to future advanced unmanned air systems could prove even less successful.

The incompatibility of today's software and systems VV&C regulations with future, more fully autonomous systems represents a major obstacle to the advance toward more capable UAS. As is the case with hardware, software verification and validation techniques rest heavily on a testing philosophy that is comprehensive and a companion methodology that is thorough. In hardware, scientific laws and principles underpinned by years of research have been used to derive the transfer functions that relate input stimuli to quantifiable output expectations, with predictable error limits. This is not the case for software. The substitute for the elusive transfer function has been exhaustive testing of every logic path that exists within the man-made code. As software has become more capable and complex, this testing process has become more imposing and costly, in many cases pressing on the limits of system affordability. The basic construct, which served so well in gaining engineering confidence in the early days of software definition and development, has become a significant burden in the near-explosive advance of the information revolution.

The software test philosophy has affected all current generation aeronautical systems, due to the sheer complexity associated with the large number of system interactions that the software must reflect. Recently, suggestions to redefine the verification and validation (V&V) processes based on methodologies that rely on model-based design and formal methods have provided some near-term hope for reductions in testing. But these tools today have limited to no utility and supporting the development of *intelligent software*.

The intelligent software that will enable true autonomous functionality will be capable of adaptation to emerging mission and environmental conditions, potentially exhibiting attributes such as emergent behavior and other nondeterministic features. These are systems capable of learning in the course of operations and applying that knowledge to future situations. Current bottoms-up methods for software evaluation based on or that assume inherent determinism are incompatible with these intelligent systems. The fundamental issue that must be resolved is not only related to the current approach to VV&C, but also to the very attributes and characteristics that must define the *intelligent software* itself.

It is interesting to contrast the methodology employed to develop trust in human-authored software (today's VV&C procedures) with the seemingly much simpler and quite different process used to certify true *human software*, that is, the pilot. That latter interaction between pilot and examiner is usually a relatively brief encounter, involves mostly high-level logic associated with complex mission-based scenarios, invokes the desire for flexible, acceptable outcomes, and takes place in the domain language of flight, as opposed to some foreign language (i.e., software code) unfamiliar to the principals. The dialog between student and certifier is less about precision than it is about decisions and judgment. And it explores the learning acquired by the student as the mission unfolds, along with the behavior it evokes. Future *intelligent software* may need to possess some of the same traits to permit a very different approach to VV&C from what we know it to be today.

4.3 Integration

Ultimately, the development of a methodology that addresses the certification of and trust in an integrated *man–machine system*, where both elements are considered together in achieving acceptable operational results, is essential. The traditional methodology of dealing with the machine and human operator separately made sense in the industrial age where *all* system intelligence was provided by the human, and the exclusively hardware-based machine was solely the product of hard science-based engineering. That is certainly no longer the case for even today's modern systems, and the distinction will continue to blur as more and more of the intelligence resides in and is endemic to the machine.

The nature of the interaction with human supervisory operators will begin to evolve based on our understanding of *human–machine intelligence* integration. A system that optimizes this interaction in a manner so that the integrated system performance well exceeds that of the independent "sum of its parts" will likely prove to be a significant challenge for some time to come.

5 SUMMARY

Despite a century plus of slow evolution, the unmanned air systems revolution is technologically still in its infancy. Continuing advances in computing power will enable ever more capable systems – exploiting enhanced logic and sensing to achieve more versatile platforms that enable new and diverse missions with an economic leverage as good as any to emanate from the revolution in robotic systems. The integrated regulatory, legal, social, and cultural landscape poses the greatest array of impediments to this advance, but an ever-increasing and compelling array of capabilities and applications appears to have the edge in shaping the future of this upstart niche in aviation and aerospace.

REFERENCES

Chana, W. and Coleman, J. (1996) World's First VTOL Airplane Convair/Navy XFY-1 Pogo, SAE Technical Paper 962288. doi: 10.4271/962288.

Elston, J.S., Roadman, J., Stachura, M., Argrow, B., Houston, A., and Frew, E. (2011) The tempest unmanned aircraft system for *in situ* observations of tornadic supercells: design and VORTEX2 flight results. *J. Field Robot.*, 28(4), 461–483.

Hager, G.D., Rus, D., Kumar, V., and Christensen, H. (2015) *Toward a Science of Autonomy for Physical Systems*, Computing Community Consortium, Ver. 1.

Holder, B. (2001) *Unmanned Air Vehicles – An Illustrated Study of UAVs*, Schiffer Publishing Ltd, Atglen, Pennsylvania.

Jenkins, D. and Vasigh, B. (2013) *The Economic Impact of Unmanned Aircraft Systems Integration in the United States*, Association of Unmanned Vehicle Systems International (AUVSI), Alexandria, Virginia.

Keane, J.F. and Carr, S.S. (2013) *A Brief History of Early Unmanned Aircraft*. Johns Hopkins Applied Physics Laboratory Technical Digest, 32(3), 558–571.

McMichael, J. and Francis, M. (1997) The micro air vehicle – toward a new dimension in flight, *Unmanned Systems*, vol. 15, Association of Unmanned Vehicle Systems International (AUVSI), Alexandria, Virginia, 10–17.

Newcome, L.R. (2004) *Unmanned Aviation – A Brief History of Unmanned Air Vehicles*, American Institute of Aeronautics and Astronautics (AIAA), Reston, Virginia.

Ruff, H.A., Narayanan, S., and Draper, M.H. (2002) Human interaction with levels of automation and decision-aid fidelity in the supervisory control of multiple simulated unmanned air vehicles. *Presence – Teleoperators and Virtual Environments*, vol. 11, MIT Press, Cambridge, UK, 335–351.

Tam, A. (2011) Public perception of unmanned aerial vehicles, *Aviation Technology Graduate Student Publications*. Paper 3, Purdue University e-Publications, 2011, Available at http://docs.lib.purdue.edu/atgrads/3.

Taylor, J.W. and Michael, J.H. (1977) *Jane's Pocket Book of Research and Experimental Aircraft*, Collier Books, New York.

Watts, A.C., Ambrosia, V.G., and Hinkley, E.A. (2012) Unmanned aircraft systems in remote sensing and scientific research: classification and considerations of use. *Remote Sensing*, 4(6), 1671–1692.

PART 2
Missions

Chapter 2

Remote Sensing Methodology for Unmanned Aerial Systems

Brandon J. Stark and Yang Quan Chen
School of Engineering, University of California, Merced, CA, USA

1 INTRODUCTION

Unmanned aerial systems (UASs) have rapidly developed into a promising tool for remote sensing applications across a wide range of disciplines, from archeology to wildlife conservation. They can be designed and customized to fulfill a spectrum of characteristics and capabilities, such as low-altitude flying, long endurance, high maneuverability, and automated flight controls. But the UAS is simply the platform from which the target data are acquired. Unfortunately, with the multitude of UASs and combinations of sensing equipment, it can be a daunting challenge to determine the correct or cost-effective solution. The development of a thorough project methodology is an effective tool for addressing this challenge.

Section 2 of this chapter provides a guide to developing an effective methodology for UAS-based applications. Section 3 identifies several core attributes across three major types of remote sensing applications to guide the development of a methodology and influence equipment choices. Finally, in Section 4, imaging equipment attributes are discussed to provide guidance in their selection. While there are a multitude of different types of UASs and sensors, the chapter will utilize small UASs (<55 lb) and optical-based remote sensing as an example, although the overarching message is applicable for any UAS and sensing technique.

2 UAS REMOTE SENSING METHODOLOGY

It is far too easy for an application or project to be proposed with a UAS without a clear concept of the necessary methodology to address the problem. While public interest has fostered technological innovation, literature has been sparse of general methodology approaches for the unique challenges of UASs. Instead, UAS research is saturated with specific application with specialized workflows and methodologies unique for the immediate application. It has become necessary to promote methodology for the development of new applications and mature UASs.

An important challenge for the UAS project developers is to translate layman statements such as “Let’s use a drone to improve land management practices” into “Let’s use a remote sensing platform carrying radiometrically calibrated optical imagers in the visible and near-infrared (NIR) spectra for the bare ground classification of a 10 square mile area with a desired optical resolution to discern the endemic

Unmanned Aircraft Systems. Edited by Ella Atkins, Aníbal Ollero, Antonios Tsourdos, Richard Blockley and Wei Shyy.
 ISBN: 978-1-118-86645-0.

population of Meadowfoam (*Limnanthes alba*).” The first statement is a wishful goal; the second introduces the methodology necessary to ensure a successful application and that the initial development and equipment purchases will lead to an effective solution.

An effective methodology defines the end goal, the activity, the implementation of the activity, the measurement of progress, and the success of the project. It provides a guideline for solving the targeted problem with specific tasks, components, and metrics. An incomplete or poorly defined project methodology can lead to development delays, spiraling costs, purchases of incorrect equipment, or complete project failure. In practice, many project developers find it useful to formulate a project methodology in terms of a series of questions such as the following (as adapted from Bhatta (2013)):

- What is the purpose of the project?
- What is the stated goal of the project?
- Is the goal quantitative or qualitative?
- Does this project utilize the scientific method or the technological method?
- What objects or events are the desired outcomes related to?
- Are there specific relationships found within the object or event of interest that can be utilized or must be taken into consideration?
- What data are necessary to address the problem?
- How should the data be collected?
- What procedures should be used to analyze the data?
- Are there available models/procedures sufficient to analyze the data?
- Does it require developing new models/procedures?
- What efforts must be undertaken to ensure the validity and reliability of the project?
- What ethical issues need to be addressed?

Addressing the questions above and/or other clarifying questions about the proposed project is designed to help form connections between goal and implementation and identify specific methods that will enable the successful completion of the application or the project.

The first step in any project is to understand the goal with the intended purpose of narrowing down the language to actionable items. Simple classifications such as separating the goal between quantitative goals and qualitative goals are often useful in this regard. This step often requires a thorough understanding of the desired goal that may not always align with the wording of the stated goal. For example, a project with a purpose of “improving crop yield” utilizes language that implies a qualitative goal, but in practice would require quantitative goals such as “improve yield by 5%,” which implies accurate measurements to be achievable.

The method or body of techniques of the project is another example of a way to provide guidance to the development of an effective methodology. For UAS remote sensing applications, the scientific method and the technological or engineering method are the most common. Whereas the scientific method strives to advance knowledge, the technological method addresses specific problems or issues. If the scientific method is about *knowing*, then the technological method is about *applying* (Bhatta, 2013). The two methods may overlap at times and utilize similar approaches and equipment, but the differences play a role in the development of a UAS remote sensing methodology.

The scientific method can be described as a set of techniques based on empirical and measurable evidence with principles of reasoning and inquiry to arrive at new knowledge. It is a cycle of observations, refining hypotheses, and testing, until a thoroughly vetted understanding can be presented as knowledge. Environmental research UAS applications typically fall under this category and assume that the technical capability of the UAS-based remote sensing is sufficient. In contrast, the technological method is an application of research, directed at a specific target goal or a desired state. In this approach, the enabling technical capability is the target end goal. Validation and testing become methods to measure progress rather than part of the implementation. In some projects, both methods may be employed, such as answering a scientific inquiry while developing the underlying technical capability. Clarifying the goals and the methods of the project can help put realistic targets and progress metrics within the context of the project end goals, and prevent cost-control problems from inadequate detail planning.

Examining the relationships of the desired objects and events of the goal is another aspect of forming a methodology. Keeping track of strong correlations and dependencies can be valuable. In some cases, the target goal, for example, “measuring chlorophyll content,” might show a positive correlation with a reflectance ratio calculation known as normalized difference vegetation index (NDVI; Jones and Vaughan, 2010). Thus, utilizing NDVI might be an effective method. However, a thorough methodology may identify that NDVI also shows a strong correlation with a leaf area index (Jones and Vaughan, 2010), which may complicate the desired goal measurements if the influences of the two correlations cannot be separated.

Understanding the goals and ways that the desired data can be collected provides some guidance for equipment, software, and workflow requirements, but selecting the right pieces can still be a significant challenge. There are a wide variety of platforms, sensor packages, software solutions at an equally wide range of costs, and capabilities already commercially offered, but even still many researchers and developers end up implementing their own custom solutions (Stark, Smith, and Chen, 2013). This application-centric approach, choosing equipment based on the specific requirements of the application, is common, given the narrow and specialized applications proposed. However, this drives up costs and delays projects when incorrect equipment is purchased or developed.

Once the project's data goal is selected, the data must be collected. Data collection strategies vary significantly based on equipment, although there are plenty of examples of the use of modified equipment (Chabot and Bird, 2012; Jang and Kim, 2008; Jensen, Baumann, and Chen, 2008). However, one of the major challenges for remote sensing applications of UASs is the lack of standardized processing procedures. As many developers and researchers have discovered, specialized workflows are often necessary to process their data. Unfortunately, this poses problems in addressing whether or not the results of the project were valid and reliable. It is not an uncommon problem however, especially for remote sensing operations where different data generating processes can create data that may not be comparable with other sources (Trishchenko, Cihlar, and Li, 2002). Sections 3 and 4 provide guidance on selecting what type of data should be collected and how to collect it.

Ethical and legal issues are significant topics that require addressing with an effective methodology. The current legal environment, especially in the United States, is particularly challenging to traverse. However, it is important that UAS applications are developed with the legal restrictions and limitations in mind and understand how they may affect the data collection process and feasibility of the proposed goal. A challenge may arise from addressing privacy concerns. A common technique is to employ a "Privacy by Design" approach (Cavoukian, 2009), incorporating privacy considerations into the technology and methodology that addresses it at all stages: data collection, data management, data dissemination.

3 CORE CONCEPTS IN UAS REMOTE SENSING APPLICATIONS

In the following section, several core concepts are identified to provide guidance in the selection of the necessary data requirements and its influence on UAS and sensor selection. While there are many unique solutions in UAS remote sensing applications, there are some common equipment and workflow implementations that are useful to refer to when analyzing the data goal for a proposed project.

UAS remote sensing applications can be grouped by data goals into three major categories: detection or counting applications, identification or localization applications, and analysis applications. Detection or counting applications are focused on detecting or counting targets. Unlike the other types of applications, the data in these applications are in the form of contrasts, such as person versus not-person. Identification or localization applications are focused at understanding the contextual information associated with a target. Rather than looking for a herd of cattle, the size and location of the herd is vital to the application. Analysis applications require further investigation of the data and contextual information to create calibrated and meaningful or actionable information, although these applications can be very complex to establish. In general, the increasing complexity of the application is proportional to the costs, both in time and money.

3.1 Detection/Counting Applications

The detection or counting of targets is a common and valuable wide-area monitoring UAS application. Conceptually, the goal of such applications is simple: to find the existence of the desired target. The significant challenge is to determine the optimal way to separate the target from the rest of the scene, either of which could be static or moving. The target is the primary goal, thus the accuracy of the separation or classification is paramount to success rather than the accuracy of the image or other measurements. The separation or classification of the target can be accomplished in any variety of ways by focusing on finding specific characteristics such as color, texture, or shapes that are unique for the target. Additional contextual information, such as location, time of day, or *a priori* knowledge, may also be valuable for improving the accuracy, and could require the use of data fusion techniques or statistical modeling to reduce errors. However, in contrast to the accuracy requirement of the detection, the collection of the characteristic or contextual information is reliant on precision or the repeatability or reproducibility of the collection of the information. This is an important distinction to make because it may affect equipment choice. For example, if the goal is to find hogs on property (Hirsch, 2013), a thermal camera is an effective tool, but the temperature measurement of the hog is not of value, only the contrast of hot and cold. A lower cost precise thermal imager may be utilized rather than a more expensive accurate thermal imager.

Identifying the characteristics or contextual information necessary for detection influences equipment selection. Many characteristics such as texture and shape often require a high spatial resolution to discern small features. Contextual information, such as location, size, and depth, can be inferred from motion determined from images with a high temporal resolution such as individual frames in a video. Automated low-level control found in many cameras and video systems such as color balance, autofocus, aperture, and shutter speed control can be effective at maintaining the visibility of the image for characteristics to be discerned.

The time sensitiveness of the application also plays a role in the equipment selection, more so in detection and counting applications than the others (Doherty and Rudol, 2007). Often an immediate reaction is desired at the detection of a target, such as returning home or changing search patterns. This level of visual feedback into the system often requires real or near real-time communication and systems with a high frame rate are best suited (Peschel and Murphy, 2013). The desire to have an independently operated imaging system often requires the same level of visual feedback as well. For these reasons, video systems are more common for detection and counting applications where immediate visual feedback is prioritized over image quality and resolution.

The processing of the data can be automated or manually done with a human operator. Automated machine vision algorithms have been utilized and demonstrated widely, although human operator monitoring are commonplace. Search and rescue operations, especially, are staffed with human operators due to scene complexity and ease of implementation (Woods *et al.*, 2004).

However, there are specific challenges to detect and counting applications. For automated machine vision systems, the data processing increases significantly with image resolution, but too low of a resolution limits the ability to discern details such as texture. Human operators who monitor real-time video also have a number of challenges, as documented by studies on human factors for search and rescue operations with teleoperated robotics (Murphy, 2004). Operator fatigue and sensory overloads are common issues that lead to decreased detection and counting accuracy (Freed, Harris, and Shafto, 2004). Long operations may be limited by UAS platform capabilities, proper selection of the desired platform is another key for success (Stark, Smith, and Chen, 2013). In addition, the data bandwidth of the video system is often much greater than the rate of detection, leading to a significant amount of wasteful redundant data. From that challenge, it is important to recognize the value of optimal path planning and optimal sensing strategies (Chao and Chen, 2012).

3.2 Identification/Localization Applications

In many situations, the characteristic or contextual information of a target is a part of the data goal. This transforms the application into an identification or localization application, where instead of asking "is it there*?* " the question is "what is it*?* " Characteristic or contextual information commonly includes location and surroundings, but may also include size, time, color, or texture. These attributes often require a higher spatial resolving capability of imagery, though not necessarily always a faster temporal resolution. The addition of this information enables the classification or identification of a number of items such as plants, animals, vehicles, or sustained damage. However, the challenge of classification introduces the need for repeatability and consistency from image to image.

A wide variety of sensor equipment can be utilized for identification or localization applications. Video systems can be utilized effectively as described in firefighting efforts (Ambrosia *et al.*, 2003; Hinkley and Zajkowski, 2011). Digital cameras can often provide a higher resolution and many are affordable solutions where real time is not necessary. Other specialized equipment such as thermal imagers, multispectral imagers, or hyperspectral imagers are also effective equipment though are often a costly investment. Remote sensing applications may also utilize nonimaging sensors for air quality measurements and the inclusion of localization data enables the creation of detailed spatial maps.

Whereas some detection applications can be accomplished without specialized equipment, identification and localization applications often require contextual information to be stored during image collection and additional processing to fully utilize it. UAS payloads may employ camera systems with embedded Global Positioning Systems (GPSs) to record image locations. Photogrammetry software such as Pix4D (Pix4D SA, www.pix4d.com) and Ensomosiac UAV (MosaicMill Inc., www.mosaicmill.com) are commonly a part of the workflow.

The tracking of moving targets is another common UAS application that combines the challenge of object identification and localization (Ren and Beard, 2004). Challenges such as multiobject tracking may require the use of real-time data downlinks or significant onboard computing power. As with detection and identification applications, the use of auxiliary processing and data fusion algorithms may be useful for improving results at the expense of cost and complexity.

3.3 Analysis Applications

Analysis applications are typically complex and require significant development and a strong methodology. While identification applications ask "what is it?" analysis applications are designed around the question "what does it mean?" In essence, they are designed for the purpose of transforming remote sensing data into meaningful or actionable intelligence. The counting application will return with the information that there are 12 trees in the grove. The identification application will return with the location and size of each tree. The analysis application will generate the data to make estimations on the health of the trees and how much fruit will be produced.

In analysis applications, often the data produced is not the image, but rather a 2D map of the optical sensor measurements. As such, sensor calibration, radiative transfer models, ground control points, and bias corrections are standard elements of the analysis application workflow in an effort to relate sensor measurements to physical features. Commercially available point and shoot digital cameras may not always be well suited for these applications as they typically lack the ability to record sensor measurements. Multispectral cameras and hyperspectral imagers are commonly implemented and have demonstrated effectiveness in agricultural applications such as crop monitoring (Berni *et al.*, 2009) and environmental applications such as invasive weed monitoring (Rasmussen *et al.*, 2013).

The value of calibrated imaging equipment can be interpreted in the spectral reflectance of grass, dry grass, and brown sandy loam (Figure 1) (Baldridge *et al.*, 2009). Live vegetation, including grass, has a distinctive pattern of spectral reflectance or the amount of light that is reflected. Vegetation typically appears green to the human eye because it reflects more light in the green spectrum (0.53–0.58 μm) than red or blue. Most vegetation is also highly reflective in the near-infrared spectrum that is in the range of 0.7–1.0 μm, beyond what the human eye can see. An imaging system that can measure the reflectance of an object at multiple wavelengths would be able to very clearly determine the difference between grass and dry grass, which has a different spectral signature as depicted in Figure 1. However, if a sensor was uncalibrated and suffered from an unknown bias, the different materials may be separated, but not identified. The following section examines this issue in more detail.

4 UAS IMAGING EQUIPMENT

The development of an effective UAS remote sensing methodology requires knowledge of various equipment available and their capabilities. Rather than focusing on specific technological metrics, the following discussion focuses on the common qualities of selected imaging equipment types. Without specifying existing imaging resolutions or shutter speeds, it is still valuable to examine the different defining

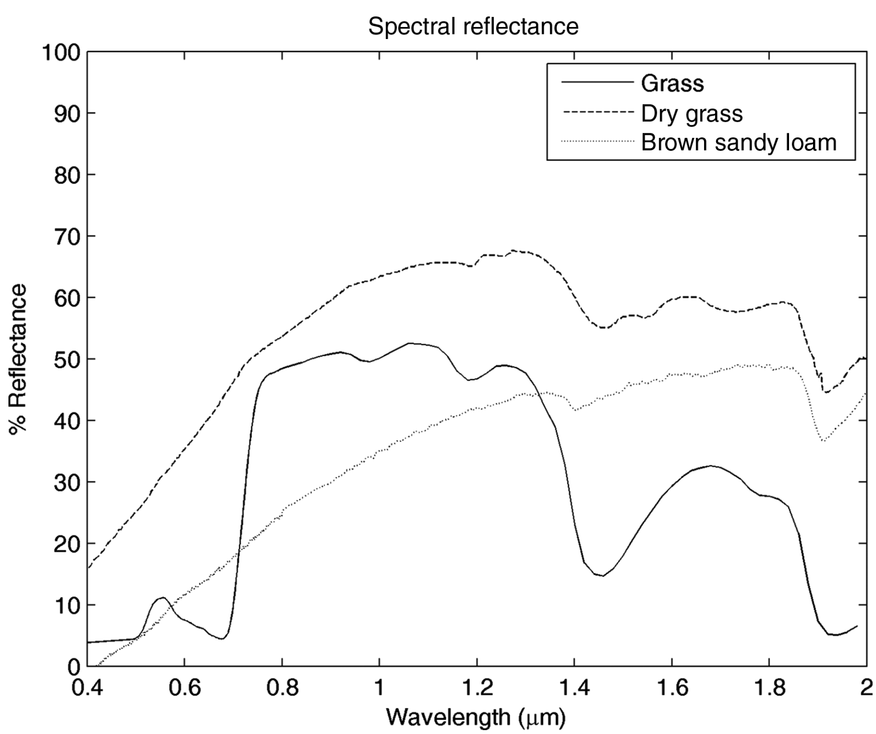

Figure 1. Spectral reflectance of grass, dry grass, and brown sandy loam (Baldridge *et al.*, 2009).

aspects and how they dictate the remote sensing workflows and best practices. The following section examines common UAS payloads such as video systems, digital cameras, and calibrated digital imagers with a discussion of the implementation strategies and methodology development. Additional equipment, such as thermal imagers, have been found to be significantly useful (Stark, Smith, and Chen, 2014), but are outside the scope of this section.

4.1 Video Systems

Video systems can be a simple payload to integrate into a UAS. It can be as simple as affixing a small HD video recorder to the UAS but also as advanced as a remotely operated gimbaled video system with real-time communication and control. The wide range in capabilities does enable project developers the ability to decide on the best system, balancing performance and cost with functionality.

Image quality and resolution vary significantly with quality and price, although, in general, they are not at the same level as digital cameras. However, the key aspect of video systems is the high frame rate rather than optical quality. For human viewers of live or recorded video, the implied motion visible from the rapid progression of frames provides significant contextual information such as movement direction, relative size and orientation of visible objects, and object depth that are difficult to discern from still imagery at lower frame rates.

With machine vision algorithms and automated processing, the high frame rate enables superior object tracking and coverage area with faster moving vehicles. The use of a controllable gimbal system provides improved situational awareness for human operators (Peschel and Murphy, 2013), a valuable capability for search and rescue operations, although at the cost of added complexity. While video systems typically have a lower image resolution than digital cameras, the use of a narrow field of view lens or a controllable zoom lens can enable a similar high spatial resolution at the tradeoff of a smaller viewing area.

Implementation of video systems into a project workflow is straightforward. Typically, they do not require preflight calibration or image correction as the information goal is to obtain visual references of objects or of characteristic information. Setting up ground control points can be utilized for postprocessing georeferencing. Depending on the desired autonomy, video processing can be done onboard or on the ground, though typically the computer power is greater on the ground.

4.2 Digital Cameras

Digital cameras are effective for many UAS operations that require high spatial resolution but do not require immediate visual feedback or a high frame rate. Many cameras, even those that are commercially available, have advanced automated features such as automatic focus, color balance, white balance, and image stabilization that ensure excellent pictures are generated. Overall, digital cameras provide excellent resolution for quantitative measurements of many characteristics such as small features and object texture, making them ideal for identification or localization applications. The additional contextual information, such as known ground control points or recording the position the picture was taken in, can enable accurate spatial measurements as well. With a sufficient coverage, a mosaic can be generated from the set of pictures over the targeted area (Figure 2). Combined with the contextual information, this enables high-resolution georectified orthophotos that can be used for applications such as mapping fire damage (Hinkley and Zajkowski, 2011) and rangeland management (Laliberte *et al.*, 2010). In the example orthophoto, the discoloration of soil is apparent in the area surrounding the water tower located on the right side of the orthophoto, which was caused by sediment leakage.

The pictures generated can also be used with a photogrammetry technique of generating 3D surface models from aerial images (Figure 3). Utilizing sufficiently overlapping pictures, image points from a structure-from-motion (SfM) algorithm are matched together to generate pixel depths and stitched together to form a digital surface model. These digital surface models have been presented as both accurate

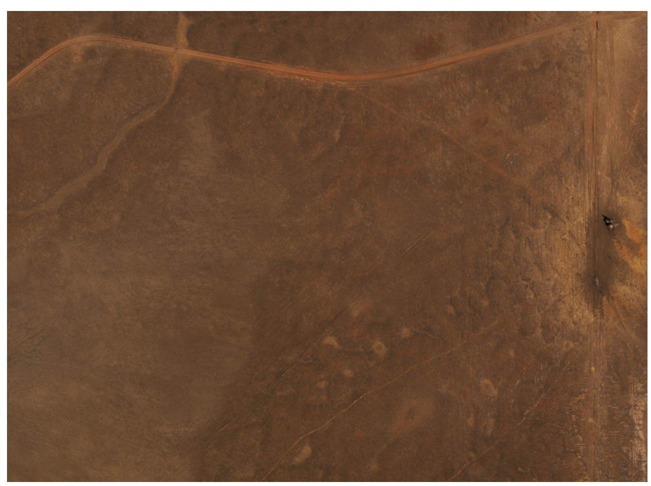

Figure 2. Example orthophoto.

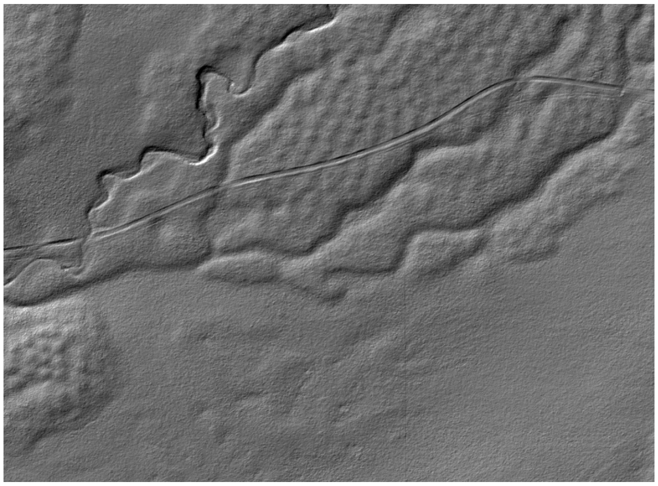

Figure 3. Example digital surface model (hillshaded for clarity).

and precise (Rock, Ries, and Udelhoven, 2011) enough to be utilized for applications such as modeling river topology (Javernick, Brasington, and Caruso, 2014) and mapping ice flows (Whitehead, Moorman, and Hugenholtz, 2013). In Figure 3, the digital surface model depicts the abundance of sediment mounds that characterize the formation of the seasonal vernal pools in the Merced Vernal Pool and Grassland Reserve.

While digital cameras have a number of advantages, they are less suited for applications where immediate responses or quantitative spectral measurements are needed. The automated features that enable high-quality pictures obscure accurate reflectance radiation measurements by dynamically adjusting color, light, and introducing artifacts through lossy compression.

4.3 Calibrated Digital Imagers

Quantifiable spectral measurements are a powerful analytical tool and the basis for most satellite remote sensing applications. While satellites suffer from low spatial resolution, low temporal resolution, and atmospheric interference, UASs can be utilized to counter these issues.

Calibrated systems are designed to provide accurate radiometric measurements, typically of the radiation emanating from the surface (Jones and Vaughan, 2010). Rather than looking at images in terms of colors, images are comprised of the intensity of energy received at particular wavelengths. Whereas a red object may appear slightly pink or orange depending on the time of day, camera orientation, or camera settings, a calibrated system is designed to isolate only the reflectance of an object and provide a consistent measurement across multiple settings and viewings.

4.3.1 Digital cameras as calibrated imagers

Digital cameras can be utilized as radiometrically calibrated imagers, although additional procedures are required for calibration. In Figure 4, an example workflow for using digital cameras as calibrated digital imagers is depicted. Field data collection is often a necessity for most workflows for radiometric calibration. Camera identification is also a process done prior to the flight operation, although this may not be necessarily prior to each flight. Lens calibration calibrates for the optical qualities. Flat-field calibration provides for adjustments from nonuniform image collection (vignetting, nonlinear response, and dead pixels). Spectral sensitivity enables radiometric data to be collected for spectral signature matching, which often requires ground control points and spectral control points. The data processing workflow includes the integration of metadata for spatial processing and raw band separation to adjust for band-to-band registration.

Digital cameras can also be modified to measure reflectance at the near-infrared spectrum. The CMOS- and CCD-based imaging sensors used for commercial cameras are also sensitive to the NIR spectrum, although normally NIR blocking filters are installed for regular pictures. Removal of this filter restores the NIR sensitivity, although it can be mixed with the red light spectrum. The installation of a NIR pass filter such as Hoya R72 (Hoya Filters, hoyafilters.com) blocks out the red spectrum to enable NIR measurements. Other solutions utilize a red notch filter, blocking only visible red while allowing visible blue and green and NIR (LDP LLC, www.maxmax.com). On some cameras, the blue channel is also marginally sensitive for NIR. In those cases, it is possible to install a blue notch filter. This has the intended effect of blocking the visible blue wavelengths on the blue channel while still allowing the NIR wavelengths to be measured on the blue channel.

4.3.2 Multispectral and hyperspectral imagers

Imaging equipment that specialize in measuring the reflected radiation at specific wavelengths are either considered multispectral or hyperspectral imagers. Multispectral imagers are typically only a handful of selected wavelengths, while hyperspectral generate upward of 60 channels of selected wavelengths, typically at much narrower bands than multispectral.

Advances in technology have led to the feasibility of the use of multispectral imagers such as those developed by Tetracam (Tetracam Inc., www.tetracam.com) and

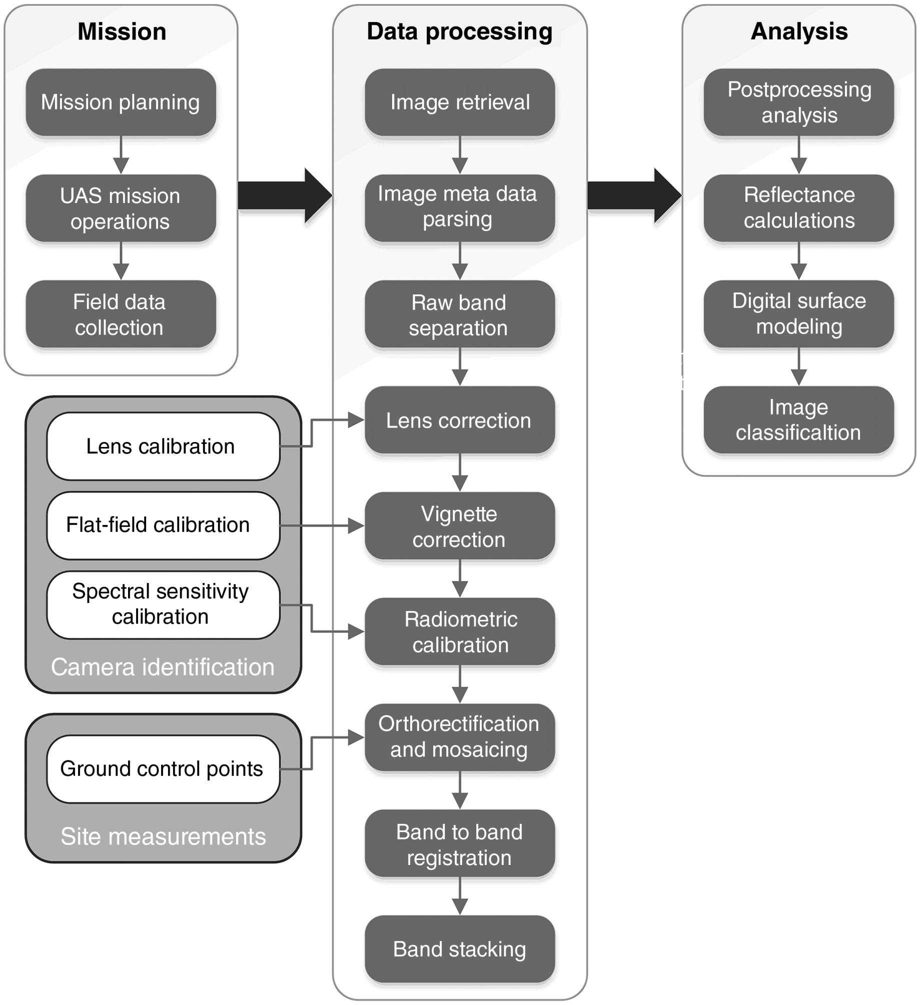

Figure 4. UAS analysis workflow for converted digital cameras.

MicaSense (MicaSense Inc., www.micasense.com). For applications that rely on spectral signatures of targets, often these systems are a necessity. A variety of agricultural applications such as crop water stress (Zarco-Tejada *et al.*, 2013) and identifying citrus greening disease (Garcia-Ruiz *et al.*, 2013) have demonstrated the effectiveness of these systems for both multispectral and hyperspectral imaging.

Many of the implementation strategies of calibrated digital cameras can be similarly applied to these calibrated imagers. As with other optical systems, corrections such as background noise, radial distortion, and vignetting are required for accurate radiometric measurements (Del Pozo *et al.*, 2014). Multispectral sensors, based on CMOS or CCD sensors, utilize a wide range of spectral sensitivity of sensors and optical bandpass filters such as those commercially sold by Androver (Androver Inc., www.androver.com) or Edmund Optics (Edmund Optics Inc., www.edmundoptics.com). The advantage of these specialized sensors is the quality of the spectral measurements. While calibrated camera systems have broadband spectral responses, the specialized imagers are capable of measuring specific spectrum as described in the following section.

4.3.3 *Spectral sensitivity*

An understanding of spectral sensitivity is an important quality for proper measurement of reflected radiation. For optical imaging systems, a simplified model of the measured light radiation for each channel or band can be described as the integration of the camera's sensitivity, scene illumination, and the scene's reflectance over the spectral range as shown in the following equation:

$$I_{k,x} = \int_{\lambda_{\min}}^{\lambda_{\max}} C_k(\lambda)L(\lambda)R_x(\lambda)\,\mathrm{d}\lambda$$

where k is the channel, x is the spatial position, I is the measured intensity, $C_k(\lambda)$ is the imager sensitivity for band k, $L(\lambda)$ is the spectral power distribution of the illuminate, and $R_x(\lambda)$ is the spatial reflectance of point x. $C_k(\lambda)$ of the imager sensitivity can be measured or estimated through a variety of means (Jiang *et al.*, 2013). The illumination can be measured or estimated with existing solar models. The goal for most analysis application involves solving $R_x(\lambda)$ given $I_{k,x}$, which is a challenge due to the low intrinsic dimensionality. However, the solution for $R_x(\lambda)$ can be approximated when the camera sensitivity is sufficiently narrow, as with multispectral or hyperspectral imaging sensors.

When the channels or bands are not sufficiently narrow, a common solution utilizes colored panels or objects with a known spectral response. To calibrate scene illumination, *in situ* measurements either concurrently with the imagery or immediately prior or after are used (Clemens, 2012). The calibration of the imager with known reflectance values ensures an accurate ratio between bands rather than accurate radiation measurements.

Although the intended effect of calibrated imagers is to provide satellite-like measurements of particular wavelengths, in practice the differences in spectral sensitivity of the imagers pose a challenge for a unified data set. The following plots of the spectral sensitivity of a Canon 600D digital camera (Figure 5), Tetracam Mini-MCA6 (Figure 6), and the Landsat 8 Satellite (Figure 7) depict the significant variation. For common calculations such as NDVI, the differences in spectral sensitivities of the imaging systems can have significant differences in the final calculations even with satellite systems (Trishchenko, Cihlar, and Li, 2002). As these differences play a large role in the accuracy of the data, care should be taken in the proper selection of the sensor sensitivity to the desired data goal.

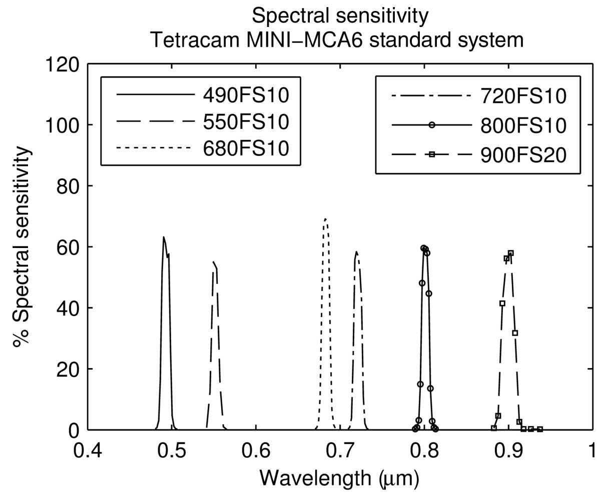

Figure 6. Spectral sensitivity of standard filters of a Tetracam Mini-MCA6 Standard System. (Reproduced with permission from Tetracam, 2016. © Tetracam Inc.)

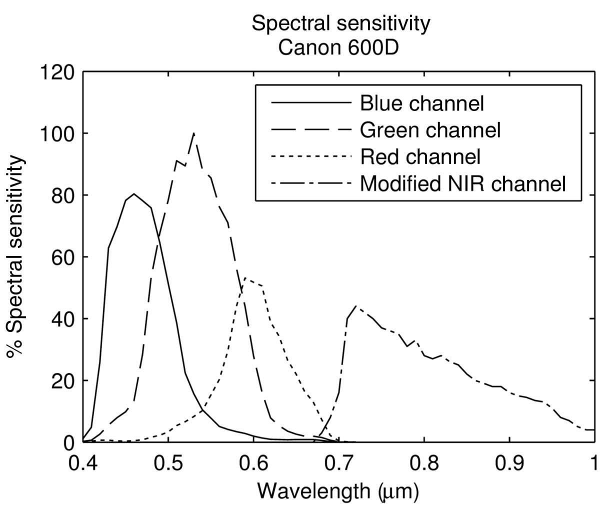

Figure 5. Spectral sensitivity for a Canon 600D camera. Modified NIR channel on a second camera (Jiang *et al.*, 2013).

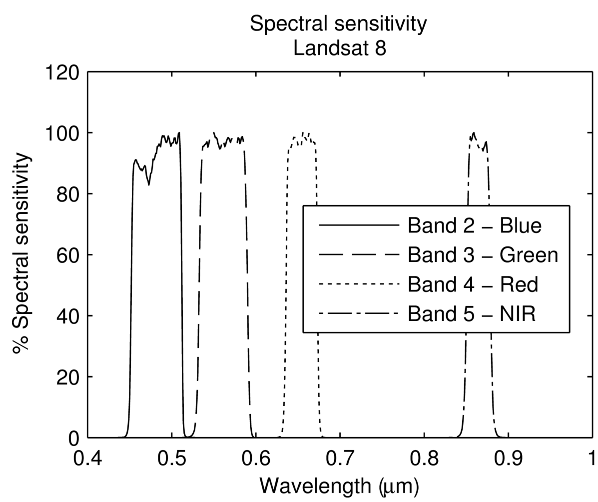

Figure 7. Spectral sensitivity of Landsat 8 (NASA, http://landsat.gsfc.nasa.gov/?page_id=7195).

5 CONCLUSION

The use of UASs as a remote sensing tool has a number of significant advantages to complement existing technology and methodology. However, as new capabilities are developed, there is a need for describing how to utilize and capitalize them efficiently. As more and more applications are developed and described, UAS methodology will mature and effective projects will be the norm. For many applications, such as those based around detection or identification applications, existing technology is capable. While it is tempting to use UASs as a direct replacement for satellites for analysis applications, there are additional challenges that need to be addressed, especially toward accurate spectral measurements. However, the future is bright for UAS remote sensing applications, and sooner than later the use of UASs will become regular and mature.

REFERENCES

Ambrosia, V.G., Wegener, S.S., Sullivan, D.V., Buechel, S.W., Dunagan, S.E., Brass, J.A., Stoneburner, J., and Schoenung, S.M. (2003) Demonstrating UAV-acquired real-time thermal data over fires. *Photogramm. Eng. Remote Sensing*, **69**(4), 391–402.

Baldridge, A., Hook, S., Grove, C., and Rivera, G. (2009) The ASTER spectral library version 2.0. *Remote Sens. Environ.*, **113**(4), 711–715.

Berni, J., Zarco-Tejada, P.J., Suárez, L., and Fereres, E. (2009) Thermal and narrowband multispectral remote sensing for vegetation monitoring from an unmanned aerial vehicle. *IEEE Trans. Geosci. Remote Sens.*, **47**(3), 722–738.

Bhatta, B. (2013) *Research Methods in Remote Sensing*, Springer.

Cavoukian, A. (2009) *Privacy by Design: The 7 Foundational Principles*, Information and Privacy Commissioner of Ontario, Ontario, Canada.

Chabot, D. and Bird, D.M. (2012) Evaluation of an off-the-shelf unmanned aircraft system for surveying flocks of geese. *Waterbirds*, **35**(1), 170–174.

Chao, H. and Chen, Y. (2012) *Remote Sensing and Actuation Using Unmanned Vehicles*, John Wiley & Sons, Inc., Hoboken

Clemens, S.R. (2012) Procedures for correcting digital camera imagery acquired by the AggieAir Remote Sensing Platform. Masters thesis. Utah State University.

Del Pozo, S., Rodríguez-Gonzálvez, P., Hernández-López, D. and Felipe-García, B. (2014) Vicarious radiometric calibration of a multispectral camera on board an unmanned aerial system. *Remote Sens.*, **6**(3), 1918–1937.

Doherty, P. and Rudol, P. (2007) A UAV search and rescue scenario with human body detection and geolocalization. *AI 2007: Advances in Artificial Intelligence*, Springer, Berlin, pp. 1–13.

Freed, M., Harris, R., and Shafto, M. (2004) Human-interaction challenges in UAV-based autonomous surveillance. *Proceedings of the 2004 Spring Symposium on Interactions between Humans and Autonomous Systems Over Extended Operations*.

Garcia-Ruiz, F., Sankaran, S., Maja, J.M., Lee, W.S., Rasmussen, J., and Ehsani, R. (2013) Comparison of two aerial imaging platforms for identification of Huanglongbing-infected citrus trees. *Comput. Electron. Agric.*, **91**, 106–115.

Hinkley, E.A. and Zajkowski, T. (2011) USDA forest service – NASA: unmanned aerial systems demonstrations – pushing the leading edge in fire mapping. *Geocarto Int.*, **26**(2), 103–111.

Hirsch, J. 2013 *Hunting wild pigs with drones*. April 18, 2013. Available at http://modernfarmer.com/2013/04/hunting-pigs-with-drones/ (accessed September 23, 2014).

Jang, S. and Kim, J. (2008) Survey of electro-optical infrared sensor for UAV. *Aerospace Technol. Trends*, **6**(1), 124–134.

Javernick, L., Brasington, J., and Caruso, B. (2014) Modeling the topography of shallow braided rivers using structure-from-motion photogrammetry. *Geomorphology*, **213**, 166–182.

Jensen, A.M., Baumann, M., and Chen, Y.Q. (2008) Low-cost multispectral aerial imaging using autonomous runway-free small flying wing vehicles. *2008 IEEE International Geoscience and Remote Sensing Symposium (IGRASS 2008)*, IEEE, pp. V-506–V-509.

Jiang, J., Liu, D., Gu, J., and Susstrunk, S. (2013) What is the space of spectral sensitivity functions for digital color cameras? *2013 IEEE Workshop on Applications of Computer Vision (WACV 2013)*, IEEE,pp. 168–179.

Jones, H.G. and Vaughan, R.A. (2010) *Remote Sensing of Vegetation: Principles, Techniques, and Applications*, Oxford University Press.

Laliberte, A.S., Herrick, J.E., Rango, A., and Winters, C. (2010) Acquisition, orthorectification, and object-based classification of unmanned aerial vehicle (UAV) imagery for rangeland monitoring. *Photogramm. Eng. Remote Sensing*, **76**(6), 661–672.

Murphy, R.R. (2004) Human–robot interaction in rescue robotics. *IEEE Trans. Syst. Man. Cybern. C Appl. Rev.* **34**(2), 138–153.

Peschel, J.M. and Murphy, R.R. (2013) On the human–machine interaction of unmanned aerial system mission specialists. *IEEE Trans. Hum. Mach. Syst.*, **43**(1), 53–62.

Rasmussen, J., Nielsen, J., Garcia-Ruiz, F., Christensen, S. and Streibig, J.C. (2013) Potential uses of small unmanned aircraft systems (UAS) in weed research. *Weed Res.*, **53**(4), 242–248.

Ren, W. and Beard, R. (2004) Trajectory tracking for unmanned air vehicles with velocity and heading rate constraints. *IEEE Trans. Control Syst. Technol.*, **12**(5), 706–716.

Rock, G., Ries, J. and Udelhoven, T. (2011) Sensitivity analysis of UAV-photogrammetry for creating digital elevation models (DEM). *Proceedings of Conference on Unmanned Aerial Vehicle in Geomatics*.

Stark, B., Smith, B., and Chen, Y.Q. (2013) A guide for selecting small unmanned aerial systems for research-centric applications. *Proceedings of Research, Education and Development of Unmanned Aerial Systems (RED-UAS2013)*.

Stark, B., Smith, B., and Chen, Y.Q. (2014) Survey of thermal infrared remote sensing for unmanned aerial systems. *Proceedings of the International Conference on Unmanned Aerial Systems (ICUAS)*, pp. 1294–1299.

Trishchenko, A.P., Cihlar, J., and Li, Z. (2002) Effects of spectral response function on surface reflectance and NDVI measured with moderate resolution satellite sensors. *Remote Sens. Environ.*, **81**(1), 1–18.

Whitehead, K., Moorman, B. and Hugenholtz, C. (2013) Brief communication: low-cost, on-demand aerial photogrammetry for glaciological measurement. *Cryosphere*, **7**(6), 1879–1884.

Woods, D.D., Tittle, J., Feil, M., and Roesler, A. (2004) Envisioning human–robot coordination in future operations. *IEEE Trans. Syst. Man Cybern. C Appl. Rev.*, **34**(2), 210–218.

Zarco-Tejada, P.J., Gonzalez-Dugo, V., Williams, L., Suarez, L., Berni, J.A., Goldhamer, D. and Fereres, E. (2013) A PRI-based water stress index combining structural and chlorophyll effects: assessment using diurnal narrow-band airborne imagery and the CWSI thermal index. *Remote Sens. Environ.*, **138**, 38–50.

Chapter 3

Autonomous Parachute-Based Precision Delivery Systems

Oleg A. Yakimenko

Graduate School of Engineering and Applied Science, Naval Postgraduate School, Monterey, CA, USA

1 INTRODUCTION

Aerial cargo delivery using conventional uncontrolled round canopies has been around for quite a while. It has been and still is a major method for delivering a variety of payloads to the areas that are otherwise hard to get to. For various reasons, an aircraft that carries cargo in its cargo bay may need to fly high forcing a high-altitude deployment of parachute systems. Canopy opening usually occurs right after a cargo parachute system release. The inevitable consequence of this high-altitude deployment/high-altitude opening approach is that uncontrolled parachute system remains at the mercy of the winds all way down resulting in large misses of the intended point of impact (IPI). Introduction of controlled gliding parachutes, ram-air parafoils, to skydivers in the late 1960s (Jalbert, 1966) immediately suggested their use for cargo delivery as well. While earlier systems could only rely on the ground-based radio navigational aids (beacons), traditionally used in aviation, availability of the satellite-based Global Positioning System (GPS) eliminated the last barrier toward full autonomy of aerial payload delivery systems and resulted in the development of the family of different-weight systems capable of delivering and accurately placing payload with very little prior knowledge of the winds. The recently published monograph (Yakimenko, 2015) describes the current state of precise aerial delivery from the standpoint of modeling and design of control algorithms and this chapter represents a quintessence of this work providing the overall look at the problem and making some key points.

Unmanned Aircraft Systems. Edited by Ella Atkins, Aníbal Ollero, Antonios Tsourdos, Richard Blockley and Wei Shyy.
 ISBN: 978-1-118-86645-0.

2 CONCEPT OF OPERATIONS AND KEY REQUIREMENTS

Figure 1a shows a typical precision aerial delivery system (PADS) rigged with a cargo bag. It consists of parachute system sitting atop the airborne guidance unit (AGU), which in turn sits atop a cargo bag. Figure 1a also features a paper honeycomb beneath a cargo bag to attenuate impact and plywood skidboard. In rigged PADS, a paper honeycomb also separates AGU from a cargo. Shown in Figure 1a is the A-22-type container delivery system (CDS) consisting of a sling assembly, cargo cover, and four suspension webs connecting the container to the parachute. Other CDS may utilize pallets or an adjustable nylon cloth and webbing

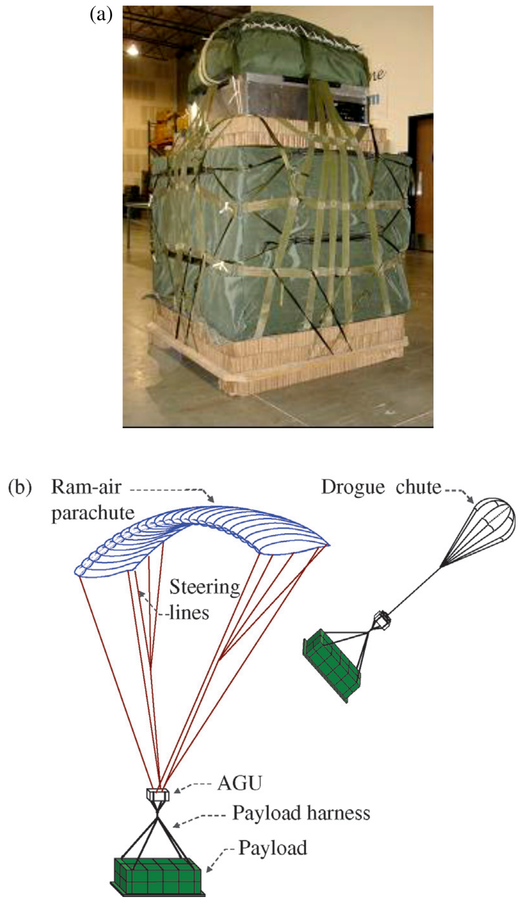

Figure 1. Rigged (a) and deployed (b) PADS. (Reproduced with permission from AIAA, 2016.)

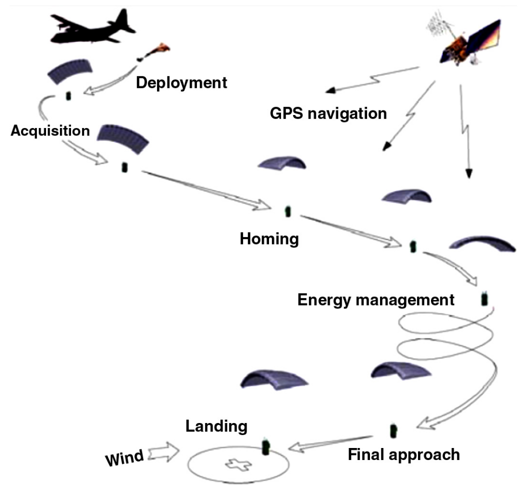

Figure 2. General representation of a sequence of events from PADS deployment till soft landing. (Reproduced with permission from AIAA, 2016).

container. These CDS may have different dimensions to accommodate bundles of food, water, medicine, ammunition, and so on. CDS can also accommodate carrying rigid inflatable and foldable boats, motorcycles, snowmobiles, wheeled vehicles, and other bulky equipment.

Upon release of PADS at the so-called computer air release point (CARP), computed based on the best knowledge of the winds, and a short freefall phase, a parachute canopy fully opens (Figure 1b) (Lingard, 1995). The release from an airplane may involve arming AGU manually/remotely or using a static line. As shown in Figure 1b, extraction of the heavier PADS out of an air carrier is done using a drogue chute. It also helps stabilizing the system before a main canopy deploys. A fully deployed PADS consists of the canopy, suspension lines, payload harness, and AGU. Different PADS designs may also include the slider, risers, and other auxiliary equipment such as reefing, drogue, and brake release cutters (Lingard, 1995). AGU includes sensors, computer, and electrically driven actuators (motors) to pull the steering lines down.

Figure 2 shows a schematic diagram of a typical airdrop mission (Wegereef and Jentink, 2003). Once the GPS signal is received and PADS position relative to IPI determined (navigation task), AGU computes the best course of actions (guidance task) and produces and executes the servos control commands (control tasks). Directional control of a typical parafoil-based PADS (aka steering) is realized by pulling down the control lines attached to the outer portion (spanwise) of the trailing edge (TE) differentially (asymmetrically). First, PADS steers toward a desired landing zone (aka drop zone (DZ)). When DZ is reached, energy management (EM) phase is commenced. Lastly, the final approach maneuver (also referred to as a terminal guidance phase) is conducted to land at IPI, preferably against the winds, using a flare maneuver (simultaneous symmetric pull down of the steering lines) to reduce the sink rate ensuring soft landing. If DZ is reached with enough altitude excess, the touchdown precision depends on the terminal guidance algorithm. That is where the constantly varying surface winds take a toll. As such AGU tries to constantly estimate the current altitude winds and propagate this prediction to the lower altitudes.

Some PADS utilize a two-stage architecture. In this case, a high-speed parafoil, the first stage, with a good wind penetration capability brings PADS to some point above IPI (or slightly upwind IPI if the surface winds are known) where a standard uncontrollable round canopy, the second stage, is deployed.

These days a majority of PADS use a ram-air parafoil (Figure 3a). However, the earlier research also involved other concepts (Figure 3b–f) (Eilertson, 1969). Even though these

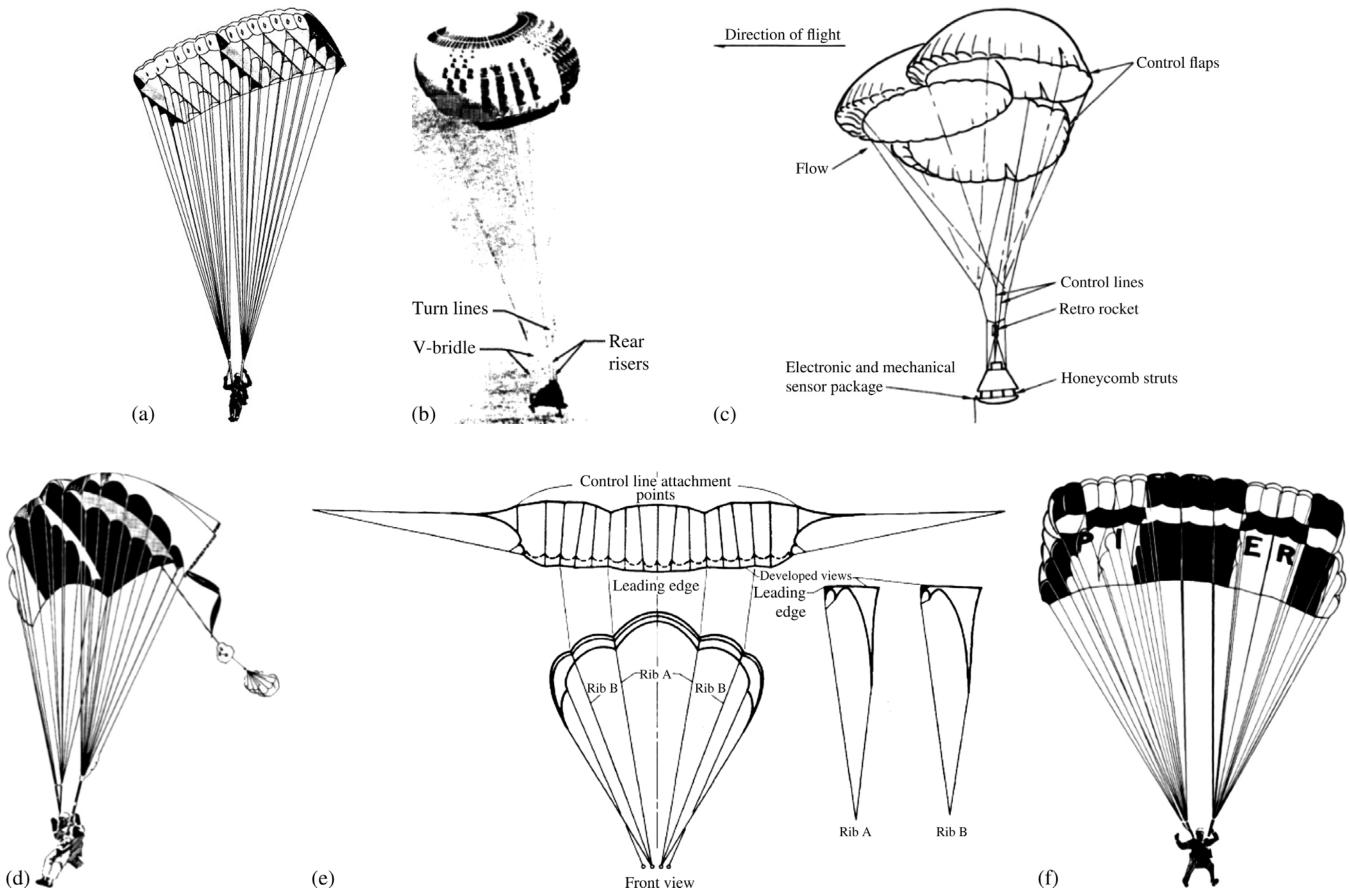

Figure 3. Steerable parachute concepts. (a) Parafoil. (b) Parasail. (c) Cloverleaf. (d) Parawing. (e) Sailwing. (f) Volplane. (Reproduced with permission from AIAA, 2016.)

other solutions exhibit lesser glide ratio (GR), some of them are still considered as a viable option in a variety of applications.

Based on the success of the earlier research using ram-air parafoils, a joint US Army/US Air Force program, Joint Precision Airdrop System (JPADS), was established in 1997 to explore the way to cardinally improve accuracy of aerial cargo delivery. The Air Force was responsible for developing the mission planning computer (JPADS-MP) that would forecast winds over DZ based on all wind data available in the vicinity of DZ in the recent past and then produce a CARP that would minimize the landing error for conventional nongliding payload delivery systems. The Army was responsible for developing different-weight PADS and common-architecture AGU to support a variety of parachute sizes and designs and ensure a flare maneuver prior to impact. As of 2011, the five JPADS categories were defined as microlight (ML) (~5–70 kg), ultralight (UL) (~100–300 kg), extralight (XL) (~300 kg to 1.1 tons), light (L) (~2.3–4.5 tons), and medium (M) (~4.5–19 tons) (JPADS, 2014).

One of the major requirements to JPADS is to have a substantial standoff range from which PADS can still reach IPI. This range is obviously proportional to the product of lift-to-drag ratio (L/D) (equal to GR in no-wind conditions) and deployment altitude. Winds aloft can either extend this range or shrink it. The slower the rate of descent, the greater the effect. Typically, PADS has at least 2.5:1 GR, and therefore, if deployed from 11 km altitude above the surface level, may reach IPI from a standoff distance of up to about 25 km. (The X:1 format for GR shows explicitly how much horizontal displacement X can be obtained per unit of vertical displacement.)

Another major requirement is to have a touchdown accuracy (IPI miss distance) less than 100 m circular error probable (CEP). These days the smaller PADS are capable of achieving 10 m CEP, while the larger PADS are only able to deliver payloads with about 300 m CEP.

Speaking of touchdown accuracy, it should be noted that it has two dimensions. The first dimension is a system accuracy e_{sys}, which is computed as the touchdown error for all PADS released from an air carrier. The second dimension is a terminal accuracy, e_{term}, which is computed for only those systems that reached the DZ area and had enough altitude to execute the terminal guidance phase (Brown and Benney, 2005). While the latter one is defined entirely by perfection of guidance, navigation, and control (GNC) system, its ability to mitigate the effect of the unknown surface winds and perform a flare maneuver if appropriate, the first one may be affected by inability to reach the DZ area or reaching it with no altitude excess because of one of the following factors: launch acceptability region (LAR) being computed with major errors or CARP being missed by air carrier, parachute opening failure, damaged or twisted control lines, and inoperable or malfunctioning AGU. The difference between system accuracy and terminal accuracy can also be cast as PADS reliability expressed as a probability of PADS reaching the DZ area from which a guided approach and landing can successfully be completed, P_{DZ}. If $P_{\mathrm{DZ}} = 1$, then $e_{\mathrm{sys}} = e_{\mathrm{term}}$. In most of the cases however, $P_{\mathrm{DZ}} < 1$ and as a result $e_{\mathrm{sys}} > e_{\mathrm{term}}$.

Distinguishing between two accuracies (or assessing P_{DZ}) is a tricky thing. The desire to limit the number of successful airdrops to improve terminal guidance leads to a degraded value of PADS reliability. Statistical analysis performed on the results of massive PADS airdrops allows revealing P_{DZ} in a more systematic way. As an example, Figure 4 shows a typical distribution of PADS touchdown error measured in the units of median radial error (MRE). Compared to the circular normal distribution (CND), distributions for three same-weight-category PADS shown in Figure 4 feature a "heavy tail," so that the chance of PADS landing beyond a three-MRE circle around IPI is about two orders of magnitude higher compared to what would be in the case of CND. Situation shown in Figure 4 is typical for any guided system

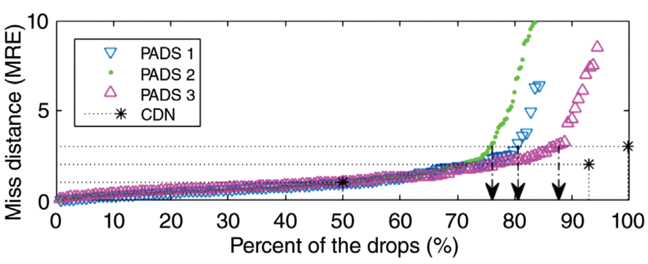

Figure 4. Typical miss distance distribution for the same-weight JPADS category. (Reproduced with permission from AIAA, 2016.)

in general – While improving the MRE (or CEP) drastically compared to an unguided analogous one, the error distribution does not follow CND anymore.

For three different PADS shown in Figure 4, MRE is different (not shown here) and the system accuracy would be judged based upon its values. System reliability could be judged upon the number of "outliers" (the number of data points greater than three MREs). For three PADS shown in Figure 4, P_{DZ} could be estimated as 0.81, 0.76, and 0.88, respectively. Throwing outliers away and reassessing MRE for the remaining data points yield terminal accuracy for each PADS.

Finally, one more major requirement to JPADS is that airdrop equipment should be recovered and reused unless cost per drop unit is negligible. The desired relative cost for PADS was set to \$6 per pound of payload delivered (\$13.22 per kilogram). This requirement has a major effect on the range of applications PADS can be used in because recovering them is not always practical or possible at all. Hence, decreasing the cost of PADS but ensuring the same or even better accuracy is the main stream in the development of next-generation PADS.

3 PADS FAMILY AND STEADY-STATE PERFORMANCE

The Orion PADS developed in the early 1990s by SSE Inc. of Pennsauken, NJ was the first commercially available system with high-GR parafoils supplied by Pioneer Aerospace of Melbourne, FL (Allen, 1995). It was capable of utilizing different ram-air parafoils from 30 to 680 m^2 and delivering 90 kg to 16 tons payload. Upon exiting, a drogue chute was deployed to stabilize attitude and velocity. As the drogue deploys, AGU separates from the payload. After a preset time, or at a preset altitude, the main canopy opens, and AGU takes control. Orion's AGU had all functionality the later PADS had. The GS-750 parafoil-based Orion (with the 14 m wingspan and 70 m^2 surface area) demonstrated the desired 100 m CEP accuracy and was the first PADS fielded to the US Department of Defense. The larger 45 m wingspan version of Orion PADS capable of steering a 16 metric tons payload was adapted by NASA as the recovery system for the International Space Station X-38 experimental Crew Return Vehicle (CRV) and was demonstrated at Precision Airdrop Technology Conference and Demonstration (PATCAD) event held in Yuma, AZ, in 2001.

Later on, within the JPADS program, several different-weight self-guided PADS were developed. They were demonstrated during five PATCAD in the United States and two Precision Airdrop Capability Demonstration events conducted in France. Overall almost 700 airdrops, primarily

Table 1. PADS representatives by JPADS weight categories.

Microlight	Ultralight	Extralight	Light	Medium
		2 K Screamer	10 K Screamer	
200 CADS	500 Panther	2 K Panther	10 K CADS	
160 Snowbird	500 Pegasus	2 K Sherpa Ranger	10 K Sherpa Provider	
150 Mosquito	500 MicroFly	2 K FireFly	10 K DragonFly	30 K MegaFly
				42 K Gigafly
Onyx ML	Onyx UL		5 K Para-Flite	
5 Mosquito	300 SPADeS	1 K SPADeS	1 K SPADeS	
5 Snowflake	500 AGAS	2 K AGAS	5 K AGAS	

using a Lockheed C-130 Hercules air carrier, were executed. Among other payload delivery systems, the self-guided PADS included Affordable Guided Airdrop System (AGAS) developed by Natick, Vertigo Incorporated, and Capewell Components LLC; Buckeye PADS developed by Southwest Research Incorporated; CADS PADS developed by Cobham Public Ltd., UK; MegaFly, DragonFly, FireFly, and MicroFly PADS developed by Airborne Systems; Onyx PADS developed by Atair Aerospace Inc.; Panther PADS developed by Pioneer Aerospace Corporation/Aerazur; Para-Flite PADS developed by Para-Flite Inc.; ParaLander PADS developed by European Aeronautic Defence and Space Company, Pegasus PADS developed by FXC Corporation, Inc., Screamer PADS developed by Strong Enterprises; Sherpa, SnowGoose, and Snowbird PADS developed by Mist Mobility Integrated Systems Technology Inc. (MMIST), Canada; SNCA PADS developed by NAVOCAP, France; Snowflake PADS developed by the University of Alabama in Huntsville/Naval Postgraduate School/Arcturus UAV; SPADeS PADS developed by Dutch Space, The Netherlands; and Mosquito PADS developed by STARA Technologies Inc. Table 1 shows a distribution of these self-guided PADS among different JPADS weight categories with a number in front of the name specifying maximum weight in pounds.

Four of 27 aforementioned systems are shown in Figures 5 and 6 as representative examples of the ML, UL, EL, and M JPADS weight categories (PATCAD, 2005; Sego, 2001; JPADS, 2014).

One unique design, AGAS, mentioned in Table 1, was conceived to bridge the gap between expensive high-GR PADS and relatively inexpensive uncontrolled (ballistic) round parachutes. Slight modification of rigging system for a standard round-canopy-based payload delivery system and addition of AGU allowed achieving a limited steering authority casting this system as PADS. More specifics on this system will be given in the last section of this chapter.

Also demonstrated at PATCAD events were two powered PADS that might be cast as an unmanned aerial vehicles

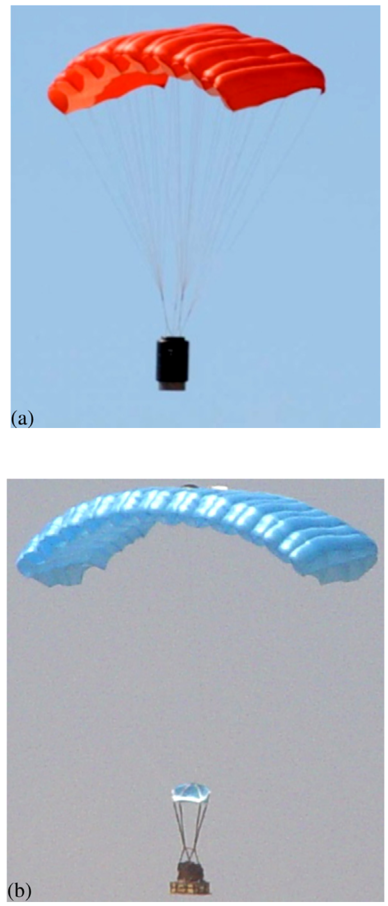

Figure 5. Mosquito (a) and Pegasus (b) PADS. (Reproduced with permission from AIAA, 2016.)

(UAVs). The first one was the SnowGoose PADS by MMIST, which is now fielded and used by the US Special Operations Command (Figure 7a). The second one was a Buckeye powered paraglider (PPG). These days PPG is commonly used in university research because it allows gaining easily some altitude as a powered UAV (Figure 7b) and then shutting its engine down to emulate the behavior of PADS.

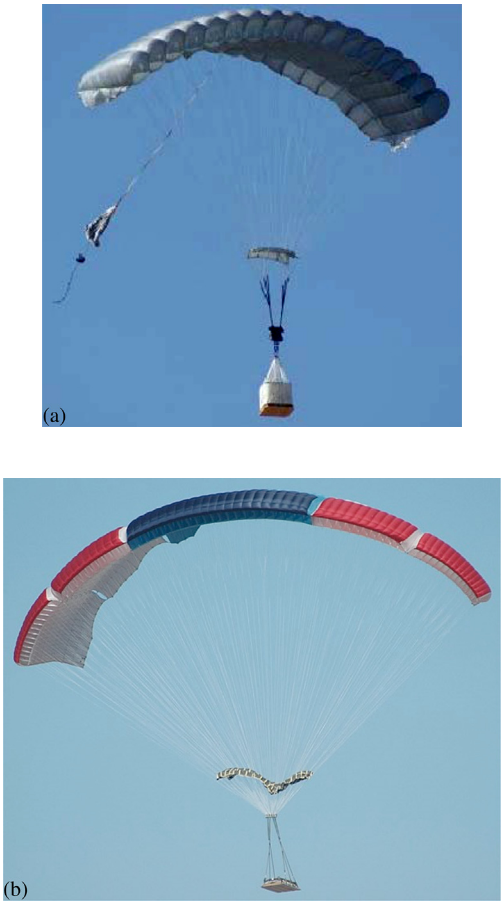

Figure 6. Sherpa (a) and GigaFly (b) PADS. (Reproduced with permission from AIAA, 2016.)

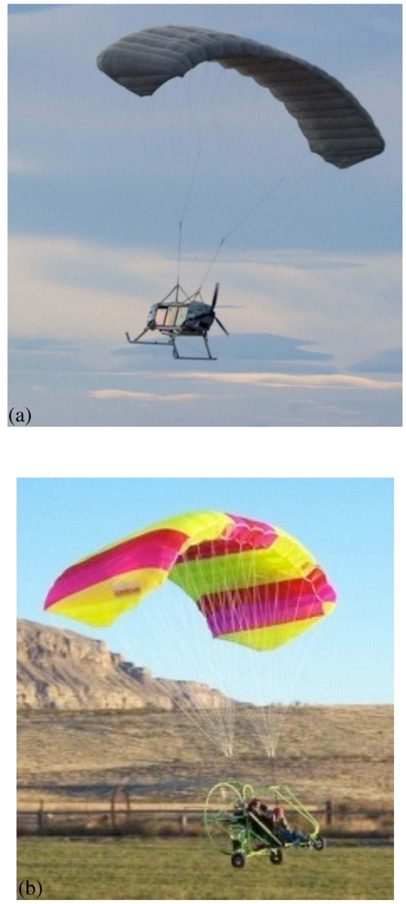

Figure 7. SnowGoose UAV (a) and an example of PPG (b). (Reproduced with permission from AIAA, 2016.)

Table 2. Reported and computed properties of representative different-weight PADS.

PADS	m (ton)	S (m^2)	c (m)	b (m)	AR	m/S (kg m^{-2})	GR, X:1	V_h (m s^{-1})	V_v (m s^{-1})	TR (° s^{-1})
SPADeS	0.16	34	4	8.6	2.2	5	3.3	11.7	3.6	47
DragonFly	4.5	325	11	30	2.7	14	3.9	18.0	4.6	10
MegaFly	11.8	836	16	52	3.3	14	3.6	21.0	5.9	5

Table 2 presents some parameters of three different-weight PADS to show their spread. It shows a nominal payload mass m, canopy area S, chord c, span b, aspect ratio (AR), wing loading (WL), GR, maximum turn rate (TR), horizontal V_h and vertical V_v components of airspeed in a steady gliding flight. The TR corresponds to the maximum safe differential (asymmetric) TE deflection affecting about a quarter of the aft part of a chord.

To supplement this table, Figure 8 shows TR versus canopy area as a log–log graph superimposed on prediction for different-size canopies obtained for WL of 4.9 kg m^{-2} in

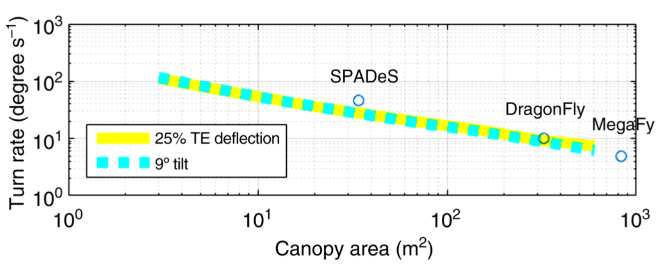

Figure 8. Control authority versus canopy area. (Reproduced with permission from AIAA, 2016.)

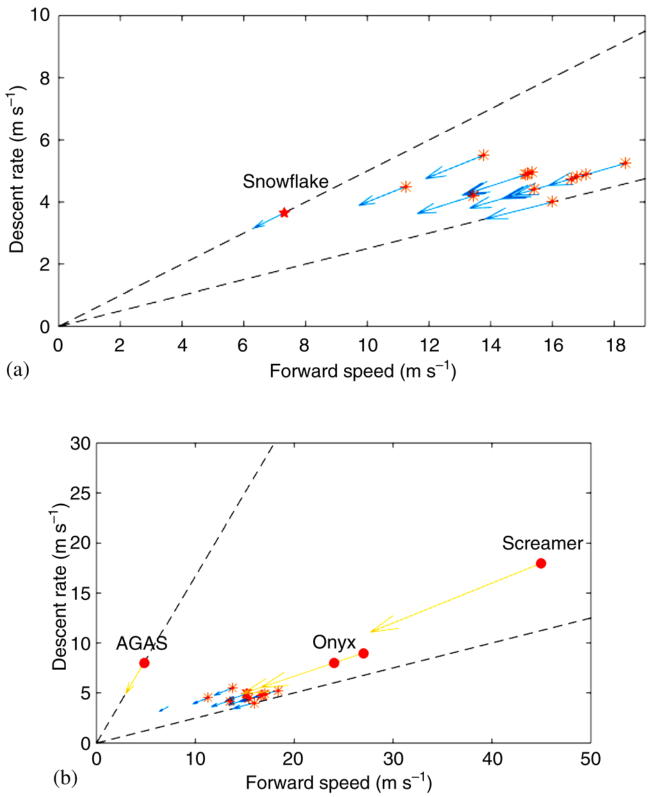

Figure 9. Rate of descent versus forward speed for one-stage PADS (a), and for all PADS (b). (Reproduced with permission from AIAA, 2016.)

(Goodrick, 1984). Figure 8 also shows TR that would be achieved using another method for a directional control, alternative to that of TE deflection. This alternative would involve tilting the resultant aerodynamic force vector into the turn by slightly deflecting the inboard tip and thus producing a net lateral pressure differential across the span. Data in Figure 8 correspond to 9° tilt for canopies of all sizes.

Figure 9a shows a spread of gliding performance (in no-wind conditions) for the most parafoil-based one-stage systems listed in Table 1 graphically. For comparison, Figure 9b adds some unique systems, specifically the round-canopy-based AGAS and the two two-stage PADS, Onyx and Screamer, featuring a higher WL, which results in a higher airspeed, but still about the same GR as all one-stage systems.

To better understand the relationship between the GR and airspeed components, we should write down two equations for the forces acting on PADS horizontally and vertically:

$$L\sin(\gamma) - D\cos(\gamma) = 0, \quad mg - L\cos(\gamma) - D\sin(\gamma) = 0 \tag{1}$$

Here γ is the glide angle (negative to the flight path angle), $L = L_c + L_l + L_s$ and $D = D_c + D_l + D_s$ are the total system lift and drag with contributions from canopy, suspension lines, and payload (also referred to as store), $m = m_s + m_c + m_e$ is the total mass of the system composed of the mass of store, canopy with suspension lines, and air entrapped inside ram-air canopy, and g is the acceleration due to gravity. The first equation further yields

$$\tan(\gamma) = (L/D)^{-1} = (C_L/C_D)^{-1} = \mathrm{GR}^{-1} \tag{2}$$

where $C_L = L/(QS)$ is the lift coefficient and $C_D = D/(QS)$ is the drag coefficient ($Q = 0.5\rho V^2$ is the dynamic pressure determined by the air density ρ and the airspeed V). The higher the GR, the smaller the glide angle and therefore the greater the gliding range for a given height loss.

Substituting Equation 2 in Equation 1 allows defining the airspeed of PADS in a steady gliding flight as

$$V = \left(\frac{2g}{\rho}\frac{m}{S}\frac{1}{\sqrt{C_L^2 + C_D^2}}\right)^{0.5} = \left(\frac{2g}{\rho}\frac{m}{S}\frac{1}{C_L\sqrt{1+\mathrm{GR}^{-2}}}\right)^{0.5}$$

$$\approx \left(\frac{2gm}{\rho S C_L}\right)^{0.5}(1 - 0.25\,\mathrm{GR}^{-2}) \tag{3}$$

This equation shows that the airspeed is dependent on air density, WL, and aerodynamic characteristics of parachute (which implicitly depends on the trim angle of attack). An airspeed down along the glide path defined by Equation 2 will increase with increasing altitude, WL, and GR.

The horizontal and vertical components of the airspeed vector are

$$V_h = V\cos(\gamma), \quad V_v = V\sin(\gamma) \tag{4}$$

Substitution of Equations 2 and 3 in Equation 4 yields

$$\begin{aligned} V_h &\approx \left(\frac{2gm}{\rho S C_L}\right)^{0.5}(1 - 0.75\mathrm{GR}^{-2}), \\ V_v &\approx \left(\frac{2gm}{\rho S C_L}\right)^{0.5}(1 - 0.75\mathrm{GR}^{-2})\mathrm{GR}^{-1} \end{aligned} \tag{5}$$

which means that under the same conditions, the increase of GR results in a slight increase of horizontal component of airspeed and decrease of its vertical component. Equation 5 computed for the design C_L of 0.5 and GR of 2–4 for varying WL at sea level are shown graphically in Figure 10. Vertical arrows show the direction of parameter variation while increasing GR (decreasing glide angle). As seen, data of Figure 10 correlate with that of Figure 9.

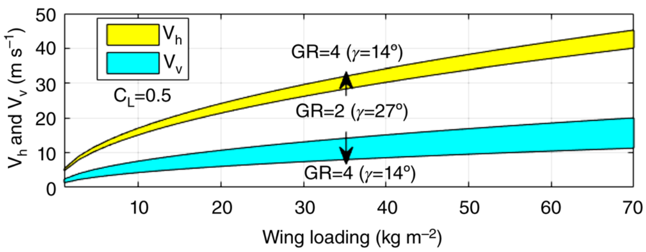

Figure 10. Ram-air parachute airspeed vector components versus WL.

4 MODELING

4.1 Governing equations

For the purpose of mission planning and trajectory optimization, the PADS model can be represented by its kinematic equations:

$$\begin{bmatrix} \dot{x} \\ \dot{y} \\ \dot{z} \end{bmatrix} = \begin{bmatrix} V_\mathrm{h}\cos(\chi_\mathrm{a}) \\ V_\mathrm{h}\sin(\chi_\mathrm{a}) \\ V_\mathrm{v} \end{bmatrix} + \begin{bmatrix} w_x \\ w_y \\ w_z \end{bmatrix} \tag{6}$$

In these equations, x, y, and z represent the PADS coordinates in the local tangent plane $\{n\}$, w_x, w_y, and w_z are the components of the wind vector $\mathbf{W}$, and χ_a is the heading angle, that is, the angle from North to the projection of airspeed vector $\mathbf{V}_\mathrm{a}$ onto a horizontal plane. In practice, for the simple models, the sideslip angle β is usually neglected, so χ_a is considered to be the same as the yaw angle ψ, which defines an orientation of the longitudinal axis of the body coordinate frame $\{b\}$ with respect to North, i.e. $\chi_\mathrm{a} \approx \psi$.

Obviously, assuming PADS model described by Equation 6, the horizontal and vertical motion can be decoupled. In this case, the first two equations

$$\begin{bmatrix} \dot{x} \\ \dot{y} \end{bmatrix} = \begin{bmatrix} V_\mathrm{h}\cos(\psi) \\ V_\mathrm{h}\sin(\psi) \end{bmatrix} + \begin{bmatrix} w_x \\ w_y \end{bmatrix} \tag{7}$$

represent a three degree-of-freedom (DoF) model with x and y being the states and yaw angle, serving as a control input. To account for yaw angle dynamics, we can write

$$\dot{\psi} = K_\psi \delta_\mathrm{a} \tag{8}$$

where δ_a represents an asymmetric TE deflection, and K_ψ is the gain. More sophisticated model may assume second-order dynamics:

$$\begin{bmatrix} \dot{\psi} \\ \ddot{\psi} \end{bmatrix} = \begin{bmatrix} 0 & 1 \\ 0 & T_\psi^{-1} \end{bmatrix} \begin{bmatrix} \psi \\ \dot{\psi} \end{bmatrix} + T_\psi^{-1} \begin{bmatrix} 0 \\ K_\psi \end{bmatrix} \delta_\mathrm{a} \tag{9}$$

where T_ψ is the time constant.

The last equation in Equation 6 can be augmented with an additional term increasing the descent rate while turning compared to that of a straight gliding flight:

$$\dot{z} = V_\mathrm{v} + w_z + k_{\mathrm{v}\dot{\psi}}|\dot{\psi}| \tag{10}$$

Here, $k_{\mathrm{v}\dot{\psi}}$ is the weighting coefficient that can be determined from flight data. This equation ties maneuvering in the horizontal plane with the total altitude loss and should definitely be accounted for during the EM and terminal guidance phases.

For the purpose of trajectory optimization, Equation 7 should be rewritten to exclude time:

$$\begin{bmatrix} x'_\mathrm{h} \\ y'_\mathrm{h} \end{bmatrix} = \frac{-V_\mathrm{h}}{V_\mathrm{v} + w_z} \begin{bmatrix} \cos(\chi_\mathrm{a}) \\ \sin(\chi_\mathrm{a}) \end{bmatrix} - \frac{1}{V_\mathrm{v} + w_z} \begin{bmatrix} w_x \\ w_y \end{bmatrix} \tag{11}$$

Here x'_h and y'_h are derivatives with respect to altitude h ($h = -z$). Equations 8 and 9 then take the following form:

$$\psi'_\mathrm{h} = \frac{-1}{V_\mathrm{v} + w_z} u_\mathrm{c} \tag{12}$$

$$\begin{bmatrix} \psi'_\mathrm{h} \\ \dot{\psi}'_\mathrm{h} \end{bmatrix} = \frac{-1}{V_\mathrm{v} + w_z} \begin{bmatrix} 0 & 1 \\ 0 & T_\psi^{-1} \end{bmatrix} \begin{bmatrix} \psi \\ \dot{\psi} \end{bmatrix} - \frac{T_\psi^{-1}}{V_\mathrm{v} + w_z} \begin{bmatrix} 0 \\ K_\psi \end{bmatrix} \delta_\mathrm{a} \tag{13}$$

While this model captures all features important from the standpoint of mission planning, it might be necessary to involve one more state, the roll angle ϕ, and account for effect of the angle of attack (AoA) α. In this case, the 4DoF model can be written as follows (Jann, 2004):

$$\begin{bmatrix} \dot{u} \\ \dot{\psi} \\ \dot{w} \end{bmatrix} = \begin{bmatrix} m^{-1}(L(\alpha)\sin(\alpha) - D(\alpha)\cos(\alpha)) - w\dot{\psi}\sin(\phi) \\ u^{-1}(g\sin(\phi) + w\dot{\phi})\cos^{-1}(\phi) \\ m^{-1}(-L(\alpha)\cos(\alpha) - D(\alpha)\sin(\alpha)) + g\cos(\phi) + u\dot{\psi}\sin(\phi) \end{bmatrix} \tag{14}$$

In this equation, u and w are the components of the groundspeed vector $\mathbf{V}$ ($\mathbf{V} = \mathbf{V}_\mathrm{a} + \mathbf{W}$) expressed in $\{b\}$. The kinematic equations then take the following form:

$$\begin{bmatrix} \dot{x} \\ \dot{y} \\ \dot{z} \end{bmatrix} = {}^n_b\mathbf{R} \begin{bmatrix} u \\ 0 \\ w \end{bmatrix} \tag{15}$$

where ${}^n_b\mathbf{R}$ is the rotation matrix (from $\{b\}$ to $\{n\}$). Roll angle dynamics due to asymmetric TE deflection can be either modeled as a first-order system

$$T_\phi \dot{\phi} + \phi = K_\phi \delta_a \quad (16)$$

or neglected

$$\phi = K_\phi \delta_a \quad (17)$$

The 6DoF model accounts for three translational and three rotational degrees of freedom, and includes the angular velocity vector $\boldsymbol{\omega} = [p, q, r]^T$ (defined in $\{b\}$) and the v component of the groundspeed vector $\mathbf{V}$. Translational and rotational kinematics are described as

$$\begin{bmatrix} \dot{x} \\ \dot{y} \\ \dot{z} \end{bmatrix} = {}^n_b\mathbf{R}\mathbf{V}, \quad \begin{bmatrix} \dot{\phi} \\ \dot{\theta} \\ \dot{\psi} \end{bmatrix} = \begin{bmatrix} 1 & \sin(\phi)\tan(\theta) & \cos(\phi)\tan(\theta) \\ 0 & \cos(\phi) & -\sin(\phi) \\ 0 & \sin(\phi)\sec(\theta) & \cos(\phi)\sec(\theta) \end{bmatrix} \boldsymbol{\omega} \quad (18)$$

The dynamic equations are cumbersome, but may be presented in a compact form as

$$\dot{\mathbf{V}}^* = \mathbf{A}^{-1}\left(\mathbf{B}(\boldsymbol{\omega}, \phi, \theta, \psi, \mathbf{W})\mathbf{V}^* + \begin{bmatrix} \mathbf{F}_a + \mathbf{F}_g \\ \mathbf{M}_a \end{bmatrix}\right) \quad (19)$$

where $\mathbf{V}^* = [u, v, w, p, q, r]^T$, $\mathbf{F}_a$ and $\mathbf{M}_a$ are the aerodynamic force and moment vectors, $\mathbf{F}_g$ is the gravitational force vector (all in $\{b\}$). Apart from the matrix $\mathbf{B}$ depending on the states and the wind vector, both matrices $\mathbf{A}$ and $\mathbf{B}$ depend on geometric and mass properties of PADS (the distance between the origin of $\{b\}$ and canopy-fixed coordinate frame $\{p\}$, rigging angle μ defining a rotation of $\{p\}$ with respect to $\{b\}$, and PADS total mass), apparent mass tensor $\mathbf{I}_{am}$ and apparent inertia tensor $\mathbf{I}_{ai}$ (to be considered next).

While the 6DoF model includes three inertial position components of some point in the body frame $\{b\}$ and three Euler orientation angles of $\{b\}$ with respect to $\{n\}$, the higher fidelity models also include additional Euler angles defining orientation of payload (coordinate frame $\{s\}$) relative to $\{b\}$. The number of DoF depends on payload rigging geometry. The 7DoF might be needed in the case the canopy harness is attached to payload using four risers, as shown in Figure 5a. The extra DoF in this case describes payload yaw angle relative to $\{b\}$. A two-riser scheme (Figures 5b, 6b, and 7) would call for adding the payload yaw and pitch angles (8DoF). To fully describe a single-riser (swivel) scheme (Figure 6a) allowing all three Euler angles (including a bank angle of payload relative to $\{b\}$) to have their own dynamics, a 9DoF model would be required (Gorman and Slegers, 2011).

4.2 Apparent mass and inertia

While Equation 19 explicitly includes aerodynamic and gravity forces and moments driving translational and rotational dynamics, there is one more force that should be taken into account. When PADS glides in the air, it sets the air around it into a motion. In turn, this motion introduces pressure forces on PADS that are called the apparent mass pressures. The magnitude (effect) of these pressures is inversely proportional to the mass ratio representing the ratio of a mass of PADS to an air mass displaced or associated with it, $M_r = m\rho^{-1}S^{-1.5}$. For a large PADS, M_r can fall as low as about 0.5 and therefore must be accounted for.

The apparent mass force

$$\tilde{\mathbf{F}}_{am} = -\left(\mathbf{I}_{am}\begin{bmatrix} \dot{\tilde{v}}_x \\ \dot{\tilde{v}}_y \\ \dot{\tilde{v}}_z \end{bmatrix} + \mathbf{S}(\tilde{\boldsymbol{\omega}})\mathbf{I}_{am}\begin{bmatrix} \tilde{v}_x \\ \tilde{v}_y \\ \tilde{v}_z \end{bmatrix}\right) \quad (20)$$

and apparent inertia moment

$$\tilde{\mathbf{M}}_{ai} = -\left(\mathbf{I}_{ai}\begin{bmatrix} \dot{\tilde{p}} \\ \dot{\tilde{q}} \\ \dot{\tilde{r}} \end{bmatrix} + \mathbf{S}(\tilde{\boldsymbol{\omega}})\mathbf{I}_{ai}\begin{bmatrix} \tilde{p} \\ \tilde{q} \\ \tilde{r} \end{bmatrix} + \mathbf{S}(\tilde{\mathbf{V}}_a)\mathbf{I}_{am}\begin{bmatrix} \tilde{v}_x \\ \tilde{v}_y \\ \tilde{v}_z \end{bmatrix}\right) \quad (21)$$

act at the centroid of PADS apparent mass. For ellipsoidal canopy shape, this centroid roughly coincides with a volumetric canopy centroid. Equations 20 and 21 expressed in the rotating parafoil coordinate frame $\{p\}$ involve the canopy airspeed angular velocity vectors $\tilde{\mathbf{V}}_a = [\tilde{v}_x, \tilde{v}_y, \tilde{v}_z]^T$ and $\tilde{\omega} = [\tilde{p}, \tilde{q}, \tilde{r}]^T$. In Equations 20 and 21, $\mathbf{S}$ is a skew symmetric matrix and apparent mass and inertia matrices, $\mathbf{I}_{am}$ and $\mathbf{I}_{ai}$, assume the diagonal form:

$$\mathbf{I}_{am} = \mathrm{diag}([A, B, C]), \quad \mathbf{I}_{ai} = \mathrm{diag}([I_A, I_B, I_C]) \quad (22)$$

For a typical arched wing with elliptical, noncambered cross section in potential flow with t and a being the thickness and arc, respectively, the basic expressions for six apparent mass terms in Equation 22 can be written as

$$A = k_A\rho\frac{\pi}{4}t^2 b, \quad B = k_B\rho\frac{\pi}{4}(t^2 + 2a^2)c, \quad C = k_C\rho\frac{\pi}{4}c^2 b \quad (23)$$

$$I_A = k_A^*\rho\frac{\pi}{48}c^2 b^3, \quad I_B = k_B^*\rho\frac{4}{48\pi}c^4 b, \quad I_C = k_C^*\rho\frac{\pi}{48}t^2 b^3 \quad (24)$$

For a typical PADS with $AR = bc^{-1} = 3$, arc-to-span ratio $a^* = ab^{-1} = 0.15$, and relative thickness $t^* = tc^{-1} = tb^{-1}AR = 0.15$, the coefficients in Equations 23 and 24 were estimated in Lissaman and Brown (1993) as

$$k_A = 0.899, \quad k_B = 0.34, \quad k_C = 0.766, \quad k_A^* = 0.630,$$
$$k_B^* = 0.961, \quad k_C^* = 1 \tag{25}$$

Utilizing the computational fluid dynamics (CFD) code for the same wing and accounting for the shape of the wing tips, these coefficients were corrected in Barrows (2002) as

$$k_A = 0.945, \quad k_B = 0.614, \quad k_C = 0.806, \quad k_A^* = 0.589,$$
$$k_B^* = 0.784, \quad k_C^* = 0.953 \tag{26}$$

Both sets of coefficients are relatively close to each other (the difference in k_B is most likely caused by the tip geometry) and are used in Equations 23 and 24 to model apparent mass forces and moments in Equations 20 and 21.

4.3 PADS aerodynamics

When fully inflated, the ram-air parachute resembles a low-AR wing. The airfoil-shaped ribs are sewn chordwise between the low-permeability upper and lower surfaces at a number of spanwise intervals to form a series of cells. While most early parafoil wings used the modified Clark YM-18 airfoil with a maximum thickness of $0.18c$, nowadays other low-speed airfoils, like NASA LS1-0417, are used as well. The wing shape is maintained by ram-air pressure entering through the opening over the entire length of parafoil leading edge (Jalbert, 1966).

Suspension lines are attached to alternate ribs and connect the parachute to payload. To reduce the number of suspension lines (and consequently reduce the drag) but still maintain the chordwise profile of the lower surface suspension lines are usually cascaded. All lines in the spanwise direction have the same length $R = [0.6; 1]b$ chosen to ensure stability). This results in arc-anhedral shape.

The earlier theoretical studies on ram-air parachute aerodynamics were undertaken in the early 1970s. A comprehensive bibliography on this subject up to the late 1990s is given in Goodrick (1975) and Lingard (1995). Some of the latest developments, including application of extended lifting-line theory, CFD, and coupled CFD-FSI (fluid–structure interaction), are highlighted in Yakimenko (2015).

Comprehensive wind tunnel testing of ram-air parafoils was conducted by Nicolaides (1971) and Ware and Hassell (1969) at the University of Notre Dame 2 ft × 2 ft and

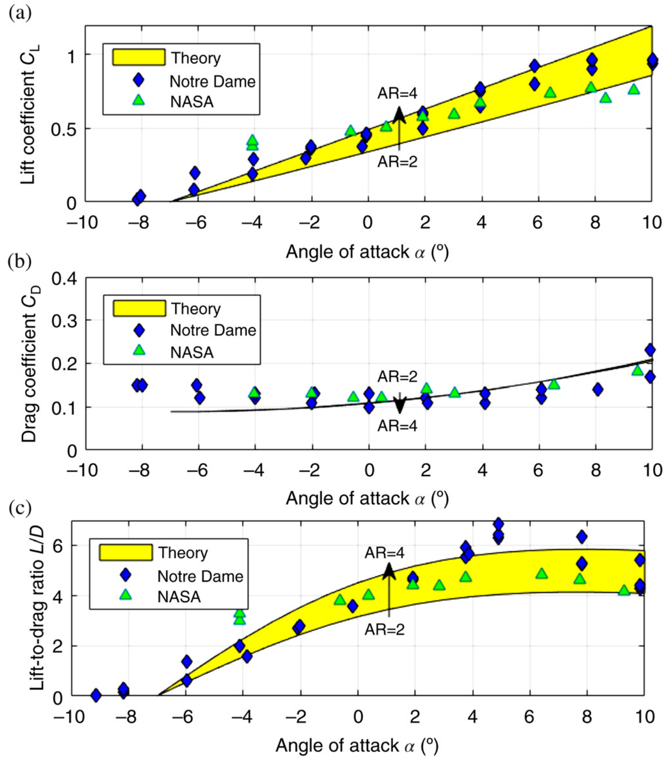

Figure 11. Theoretical lift (a) and drag (b) coefficients along with their ratio (c) for ram-air wings with AR = 2–4.

Langley 30 ft × 60 ft low-speed wind tunnels. Parafoil model sizes ranged from 84 cm^2 to 14 m^2 and AR ranged from 0.5 to 3. Figure 11a and b represents some of the data obtained in these experiments with an AR = 3 parafoil overlaid over theoretical lift and drag coefficients, C_L^c and C_D^c, obtained for parafoils with AR = 2–4 with the zero-lift AoA α_0 of $-7°$ and stall AoA of about 10° (Lingard, 1995). The vertical arrow in these figures represents the direction of parameter change while increasing AR (the lift curve slope increased while the drag curve did not vary much). As seen from these figures, theoretical data match experimental data fairly well. Figure 11c represents a comparison between the theoretical and experimental values of GR.

Arc anhedral, described by the anhedral angle $\varepsilon = 0.25/(R/b) \neq 0$ (spanwise downward angle from horizontal to a parafoil tip), causes the reduction of the total wing lift proportional to $\cos^2(\varepsilon)$, while wing's drag is not affected explicitly. However, other elements of PADS introduce an additional drag so that the overall drag coefficient of PADS is considerably larger than that of Figure 11b resulting in about 40–50% decrease of GR. Among the largest contributors of that additional drag are the suspension lines. Figure 12 shows

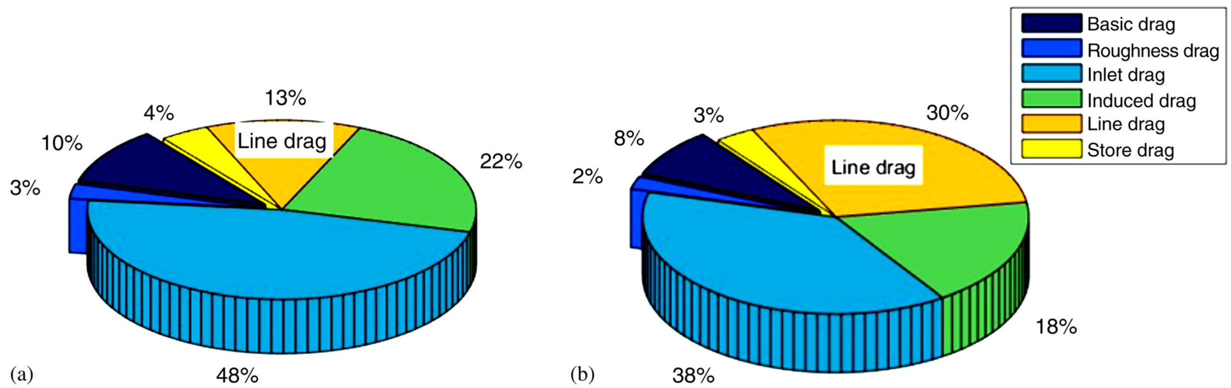

Figure 12. Typical drag contributions for a $30\,\mathrm{m}^2$ (a) and $300\,\mathrm{m}^2$ (b) ram-air parachutes. (Reproduced with permission from AIAA, 2016.)

examples of total drag contributions for the small and large ram-air parafoils (Lingard, 1995).

Figure 12 shows that open airfoil nose, inlet, contributes the most. Specifically, its contribution is on the order of $0.5\overline{h}$, where $\overline{h} = h_{\mathrm{in}}/c$ is the relative inlet height. Contribution of basic airfoil drag is about 0.015 and contribution of surface irregularities and fabric roughness is on the order of 0.004 (Ware and Hassell, 1969).

Assuming a drag coefficient for a line related to its lengthwise area (perpendicular to the flow) being 1, the drag coefficient for n suspension lines almost perpendicular to the airspeed vector and having an average length R and a diameter d is proportional to the ratio of the lines area and canopy area, $C_{\mathrm{D}}^{\mathrm{l}} = nRd/S$. Increasing the size of PADS and keeping the same n/S ratio makes C_{D}^{l} being proportional to R, which in turn is proportional to b (to keep the R/b ratio the same). That is why Figure 12 features an increase of relative contribution of suspension lines drag with the size of PADS. In practice, increase of the canopy size leads to increase of the volume of trapped air inside it, and results in PADS center of gravity shifting toward canopy. Hence, larger PADS require an increase of R/b ratio compared to that of smaller PADS.

The lift, drag, and pitch moment coefficients of payload (store) depend of its geometry. For a rectangular parallelepiped and small AoA, they can roughly be represented as

$$C_D^s \approx C_{\mathrm{D}}^{*}(k + (1-k)\alpha^2)\overline{S}^{\mathrm{s}}, \quad C_L^s \approx \alpha\overline{S}^{\mathrm{s}}, \quad C_m^s \approx 0.2\alpha\overline{S}^{\mathrm{s}} \tag{27}$$

where $k = S_{\mathrm{fr}}S_{\mathrm{bot}}^{-1}$ is the ratio of the front and bottom areas of payload, $\overline{S}^{\mathrm{s}} = S^{\mathrm{bot}}S^{-1}$ is the relative bottom area, and AoA is in radians. For cubic solid payload, a drag coefficient C_{D}^{*} is 1.05. For parallelepiped geometries other than cube, it may vary from 0.9 to 1.8 depending on payload's cross-sectional (front) AR. Dependencies of $C_{\mathrm{D}}(\beta)$, $C_Y(\beta)$, and $C_n(\beta)$ are described by similar equations with S^{bottom} replaced with S^{side} and the values of coefficients for $C_Y(\beta)$ and $C_n(\beta)$ decreased.

Compared to the rigid wings, the theoretical studies (including CFD) can only produce some rough estimates of aerodynamic parameters. The use of suspension lines and the flexible nature of parafoils make it difficult to handle them in the wind tunnel and almost impossible to introduce the sideslip angles. That is why employing combined CFD–FSI simulations to account for a canopy deformation might be the most reliable resource of aerodynamic data. Canopy deformation occurs both spanwise and chordwise, affects anhedral arc radius and projected planform in flight, and also causes spanwise negative twist (because of uneven aerodynamic loading). Deflecting TE causes even more changes of planform. Figure 13 shows what happens to a low-AR double-cell rectangular planform parafoil in a brake regime with both TE down (see more details in Yakimenko (2015)). For these canopies, such deformations may cause up to about 15% reduction in span and 5% reduction in root chord, which results in about 20% reduction in a projected planform area and 10% reduction in AR. Simultaneous (up to 20%) change of the lift and drag coefficients, however, leaves GR unaffected.

Ultimately, PADS system identification (SID) can be conducted using the flight tests results. However, compared to other aerial vehicles, SID of PADS is a real challenge. Flight test instrumentation includes the GPS receiver, which records its 3D position and velocity vector components in $\{n\}$ at 1–5 Hz, and inertial measurement unit (IMU), which adds measurements of accelerations, Euler angles and angular rates at up to 100 Hz. It may also include air data sensors to record surrounding air parameters along with components of an airspeed vector. AGU records actuator positions. More

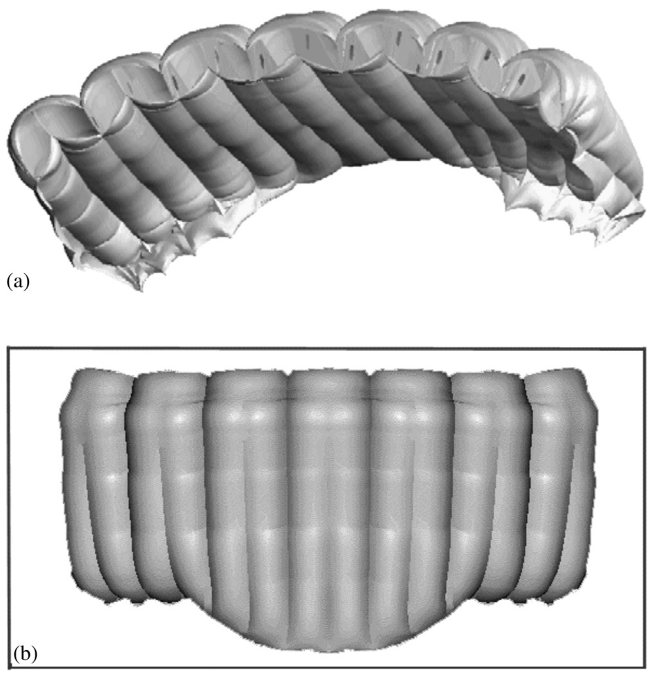

Figure 13. Parawing shape in a brake regime (a) as compared to the nominal constructed shape (b). (Reproduced with permission from AIAA, 2016.)

or less recent wind data are usually provided by dropsondes. Otherwise, airspeed and components of the wind vector must be estimated as well.

However, in most PADS configurations, all these data describe the motion of AGU only. If AGU resides atop payload, these data describe the motion of payload. Developing a high-fidelity model additionally requires information about relative motion of payload with respect to parachute canopy. To address this issue, onboard instrumentation package may include uplooking camera installed atop payload. After a proper calibration, image processing algorithms allow estimating both relative position and relative orientation of parachute with respect to payload (camera). In addition to this, these days a miniature IMU can be sewn into canopy at multiple locations to measure a variety of parameters of various canopy parts at the same time. If the airdrop is recorded using multiple ground cameras, spread apart around DZ, post-flight image processing may also allow estimating positions of both canopy and payload.

As a result, while flight test data are routinely used to validate the low-fidelity and linear models, not many attempts were made to date to perform SID on the high-fidelity PADS models. The most comprehensive ones were based on a single-criterion error method used to validate a 6DoF model of the ALEX PADS featuring 19 varied parameters (mostly coefficients of aerodynamic and control derivatives), multicriteria identification technique to investigate an 8DoF model of the Pegasus PADS that included 33 varied parameters and eight adequacy criteria, and the Extended Kalman filter approach applied in attempt to estimate 55 parameters of the 6DoF model of the prototype of X-38 Crew Return Vehicle (CRV) (Yakimenko, 2015).

4.4 Effect of the control inputs

So far, no consideration was given to the effect of symmetric, δ_s, and asymmetric, δ_a, control inputs on horizontal and vertical components of airspeed vector (excluding Equation 10). Turn dynamics assumed a symmetric linear dependence of a steady-state yaw rate $\dot{\psi}_{ss}$ versus δ_a. That is where SID using flight test data becomes useful.

Assuming normalized inputs, so that $\delta_s \in [0;1]$ and $\delta_a \in [-1;1]$, the regression analysis performed on several PADS reveals that the dependence of V_h, V_v, and GR on the control inputs can accurately be described by the same-form quadratic relationship:

$$\xi = \xi_0(1 - p_\delta \overline{\delta}^2_{s;a}) \tag{28}$$

In this equation ξ_0 is the value at $\overline{\delta} = 0$ and parameter p_δ shows the decrease in the value at full actuator deflection ($\overline{\delta} = 1$). Depending on the size of PADS and trimming conditions (parafoil rigging), these parameters vary as follows: For GR $\xi_0 \in [3;4]$ and $p_\delta \in [0.2;0.4]$, for V_h $\xi_0 \in [11;23]\,\mathrm{m\,s^{-1}}$ and $p_\delta \in [0.24;0.43]$, and for V_v $\xi_0 \in [3.6;6.8]\,\mathrm{m\,s^{-1}}$ and $p_\delta \in [-0.8;0.24]$. The spread of the decrease factor p_δ for these parameters is shown graphically in Figures 14 and 15.

As seen, a full symmetric TE deflection causes about 20% decrease of V_v and about a doubled decrease of V_h. As a result, a full symmetric TE deflection usually leads to about 20–40% decrease of GR. This decrease is gradual, so at $\overline{\delta}_s \approx 0.3$ it is only 1/10 of it, meaning that for the relatively small $\overline{\delta}_s$ the effect may be considered negligible. An asymmetric TE deflection happens to have a much stronger effect. While having almost no effect on V_h, because of banking it has a strong effect on V_v causing its increase. This increase can be quite substantial (up to 80%).

The effect of asymmetric TE deflection on $\dot{\psi}_{ss}$ can essentially be modeled with the quadratic regression as well. Slightly modified to allow for the asymmetry and nonzero TR at $\overline{\delta}_a = 0$, it takes the following form (Figure 16):

$$\dot{\psi}_{ss} = K_\psi \operatorname{sign}(\overline{\delta}_a)\overline{\delta}^2_a + \dot{\psi}_0 \tag{29}$$

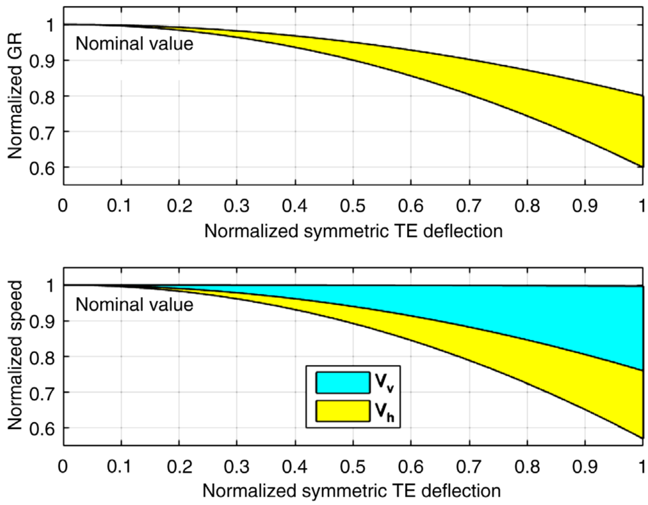

Figure 14. Variation of GR, V_{v}, and V_{h} versus $\bar{\delta}_{\mathrm{s}}$.

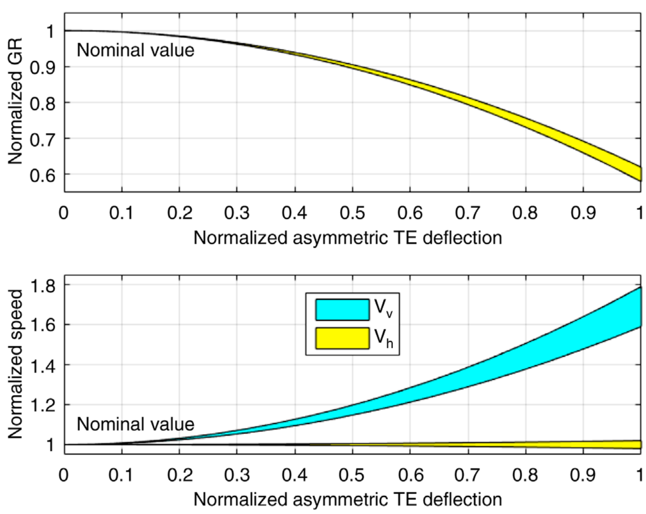

Figure 15. Variation of GR, V_{v}, and V_{h} versus $\bar{\delta}_{\mathrm{a}}$.

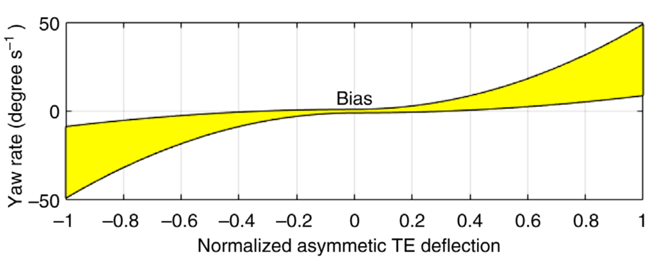

Figure 16. Variation of $\dot{\psi}_{\mathrm{ss}}$ versus $\bar{\delta}_{\mathrm{a}}$.

Introduction of nonlinear control efficiency compensates for some canopy deformation effects while deflecting TE as described earlier. The values of K_{ψ} vary from 10 to 50° s^{-1} (the smaller the PADS, the more the agility), which matches data of Figure 8. Due to canopy asymmetry and errors in a nominal control lines setting, Equation 29 allows for a bias. Usually, it is on the order of a couple of degrees per second. As seen from Figure 16, small deflections lead to a sluggish response. Moreover, if their steering lines have a sag, then PADS may exhibit inverse reaction in response to small δ_{a}. That is why the nominal control lines setting usually assumes some tension, that is, $\delta_{\mathrm{s0}} > 0$. That also brings PADS to the range of a higher sensitivity to control inputs, so that the linear control models can be used. (The negative effect however is that because of this tension in the control lines, pulling them down takes a little longer time than releasing.)

4.5 Linearized models and stability

Linearized models are used to study PADS stability and develop controllers. These models have the standard form:

$$\delta \underline{x} = \mathbf{A}\delta\mathbf{x} + \mathbf{B}\delta\mathbf{u} \tag{30}$$

where **A** and **B** are the state and input matrices, and $\delta\mathbf{x}$ and $\delta\mathbf{u}$ are variations of state and control vectors with respect to a nominal flight. Usually, longitudinal and lateral–directional states are decoupled. Depending on application, the state and the control vector could be as simple as

$$\mathbf{x}^{\mathrm{lon}} = [u, w, q, \theta]^T, \quad \mathbf{x}^{\mathrm{lat}} = [v, p, r, \phi, \psi]^T \tag{31}$$

(to study stability of a 6DoF model), all way up to

$$\mathbf{x}^{\mathrm{lon}} = [u, w, q, \theta, q_{\mathrm{s}}, \theta_{\mathrm{s}}]^T \quad \text{and}$$
$$\mathbf{x}^{\mathrm{lat}} = [v, p, r, \phi, \psi, p_{\mathrm{s}}, r_{\mathrm{s}}, \phi_{\mathrm{s}}, \psi_{\mathrm{s}}]^T \tag{32}$$

(to capture a payload motion in the 9DoF model). (In Equation 32, additional parameters with subindex *s* describe relative dynamics of a store.) The corresponding control vectors are

$$\mathbf{u}^{\mathrm{lon}} = \delta_{\mathrm{s}} \quad \text{and} \quad \mathbf{u}^{\mathrm{lat}} = \delta_{\mathrm{a}} \tag{33}$$

For a powered PADS, the control vector for the longitudinal channel would also include an engine throttle setting:

$$\mathbf{u}^{\mathrm{lon}} = [\delta_{\mathrm{T}}; \delta_{\mathrm{s}}]^T \tag{34}$$

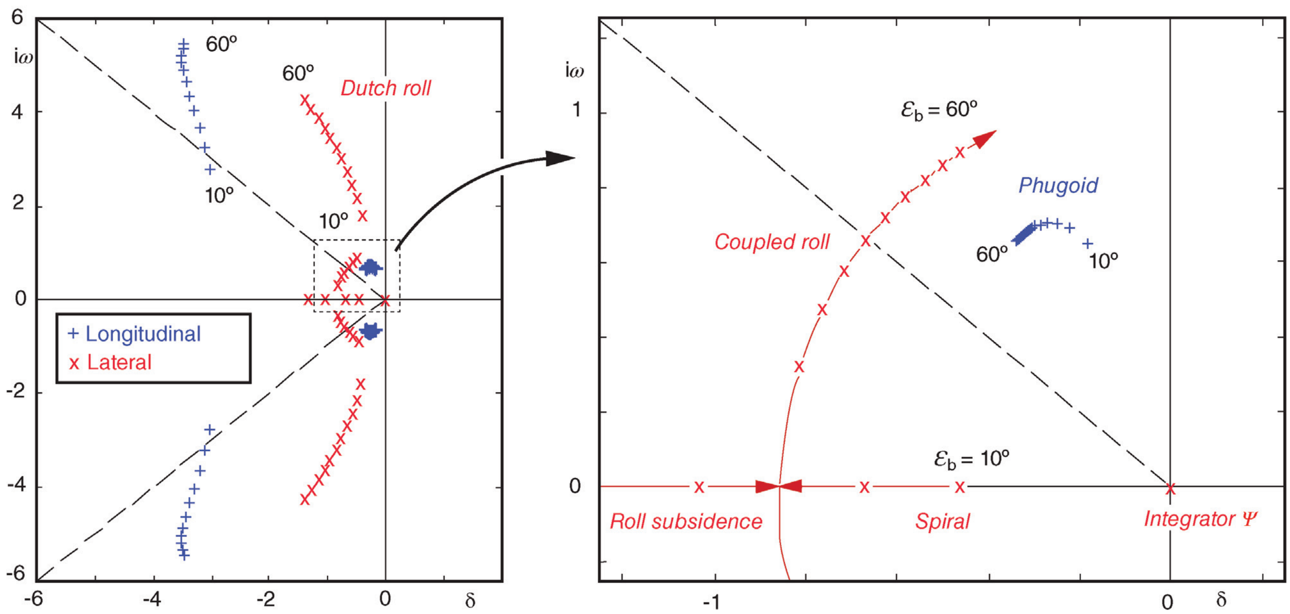

Figure 17. PADS model root locus while varying $\varepsilon_b = 10-60°$. (Reproduced with permission from AIAA, 2016.)

Varying PADS parameters and using a standard root locus technique applied to the state matrix **A** of a linearized model allows exploring system dynamics graphically. For example, Figure 17 shows root loci while varying the angle $\varepsilon_b = 2\varepsilon$ (double anhedral angle), which changes the R/b ratio from 2.9 to 0.5 (Jann, 2004). As seen, increasing canopy's curvature (shortening suspension line length) results in increase of the frequency of oscillations of AoA (short-period mode) and sideslip angle (Dutch-roll mode). It also leads to a decrease of damping of these two modes as well as a coupled roll-spiral mode (roll angle). Hence, increasing canopy's curvature (decreasing line length R) has a destabilizing effect. A very small canopy curvature (anhedral angle) results in the coupled roll-spiral mode split into two aperiodic modes, roll subsidence mode and spiral mode, traditional for an aircraft.

5 PADS GNC

All self-guided PADS rely on AGU GNC software to gather information about current PADS position relative to IPI, estimate PADS parameters and winds, and develop and continuously adjust guidance strategy generating the corresponding control inputs to follow this strategy. Hence, as in the case of any autonomous vehicle, AGU software consists of the navigation, guidance, and control blocks. For most of modern PADS, AGU's sensor suite includes GPS receiver and barometric altimeter only; some AGUs may also include IMU. Larger PADS also employ ultrasound or laser altimeters to sense the height above the ground to execute a flare maneuver. Future AGU may include optical sensors enabling navigation in the GNP-denied environment.

Compared to an aircraft, PADS are unpowered, much slower, and underactuated. Landing PADS would be similar to executing an engine-off maneuver using a rudder only. Also, compared to an aircraft PADS are very vulnerable to the wind. Hence, along with the traditional task of understanding current PADS position with respect to IPI, determining the current wind as long as the current values of V_h, V_v, and TR (which in general are not known upfront because ideally PADS should be able to use different parafoils/rigging schemes and different loads) is the primary goal of the navigation block.

Guidance block accepts this information to provide with the best possible solution allowing getting from the current PADS position to IPI. The control block ensures stable flight behavior, satisfactory tracking of the trajectory generated by the guidance block, and timely implementation of the flare maneuver for the soft landing. The outer loop of the control block generates its commands in terms of a desired yaw rate $\dot{\psi}_c$, and the inner loop then converts these commands into the desired inputs to two motors.

In PADS utilizing a one-point swivel attachment, AGU is suspended above the confluence point (like in Figure 6a). Some other PADS utilize a two-point attachment scheme and may have AGU suspended above the confluence point

(Figure 6b) or sitting atop a payload (Figure 5b). Using a four-point attachment, like in Figure 5a, allows having AGU atop a payload as well. Having AGU atop a payload seems to be a simpler solution, while AGU suspended between the canopy and payload provides a very flexible attachment point for a variety of payload sizes and shapes and, what is probably even more important, simplifies interface between AGU and canopy as well as feedback control by measuring the states of canopy rather than payload.

5.1 Maneuver-based guidance

The first detailed GPS-based guidance strategy was published for the NASA Spacewedge PADS (Figure 18a) (Sim *et al.*, 1994). The transitions between phases were controlled by onboard barometric altimeter measuring altitude above IPI. The surface wind direction and speed as well as IPI barometric altimeter settings were provided upfront. Upon approaching the DZ area with a certain altitude excess, which completes the homing phase, PADS enters a standard holding pattern aligned with the surface wind. The length of this pattern was chosen to produce about 150 m altitude loss per one pattern loop. When altitude falls below 90 m, PADS continues with the landing pattern gliding along the downwind leg passing IPI and then proceeding with the base and final approach legs. The initiation of a base turn starts at 45–60 m based on the surface wind. The flare maneuver is initiated when onboard height sensor (ultrasonic or laser) senses a height of 8 m above ground.

The major pitfall of this approach was in determining a relative PADS position based on a GPS signal only. Back then (before the accuracy-degrading selective availability "jitter" was removed), it could only provide an accuracy of ±100 m (against today's ±10 m). Hence, further refinement of this scheme involved development of an integrated GPS/IMU navigation system. Control algorithms included online estimate of the current winds.

For the subsequent PADS, guidance strategy was refined to substitute a rectangular EM pattern with the circular one (Figure 18b). In this latter approach, the turn radius while in the EM pattern was initially fixed. Later, however, it was made adjustable (resulting in a different altitude loss per one loop) to be able to enter the final approach phase at the correct altitude and direction (as shown in Figure 18b) (Jann, 2004). Alternative versions of this guidance scheme included shifting the holding pattern downwind to allow more time for possible final corrections (Figure 18c).

These days, many PADS in different weight categories still use the circular pattern of Figure 18b. Specifically, this guidance strategy was employed by single-stage ML and UL

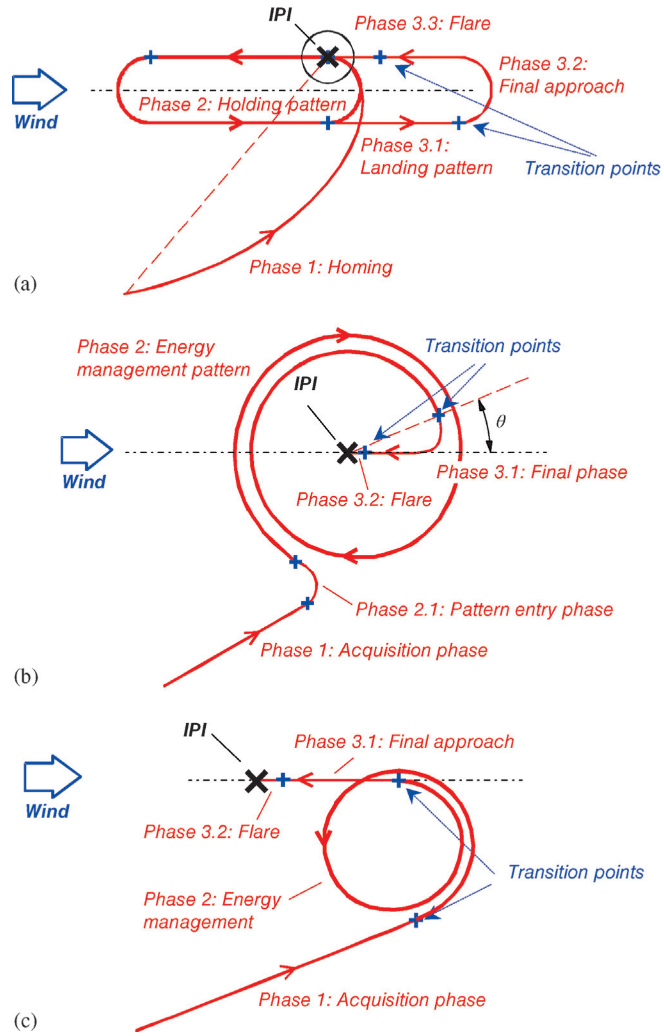

Figure 18. Rectangular (a) and circular (b and c) EM strategies. (Reproduced with permission from AIAA, 2016.)

Mosquito and Onyx PADS. It is also used by the first stage of the two-stage EL and L Screamer PADS with a following deployment of the second stage on the final approach phase elevated to accommodate the altitude loss while deploying and dereefing the second-stage round canopy.

Instead of a circular EM pattern, many other PADS utilize a figure-8 (lemniscate) pattern (Figure 19) oriented transverse to the desired landing direction. Compared to a circular pattern downwind of IPI (Figure 18c), figure-8 pattern is more stable and ensures a simpler exit because most of the time PADS flies either perpendicular to the wind direction or upwind (while the circular EM pattern has a substantial downwind portion). Most figure-8-based algorithms utilize a maneuver-based EM, that is, a sequence of a predefined control inputs while in the pattern, others establish this

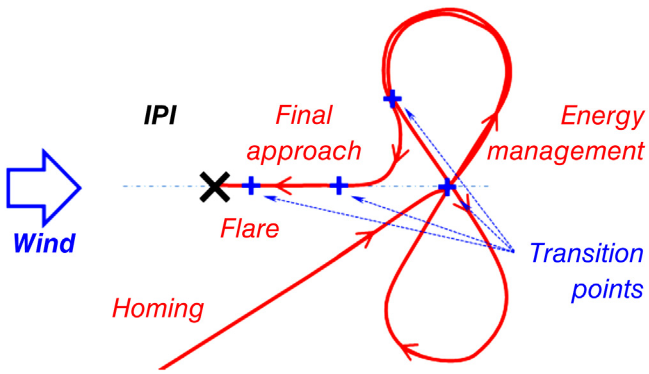

Figure 19. Figure-8 EM strategy.

maneuver in $\{n\}$ using a set of four way points (WPs) (Jann, 2004). The location of these WPs is varied based on the current 3D position relative to IPI and wind estimates.

5.2 Accounting for the variable winds

Obviously, variable winds aloft and surface winds play a crucial role in both system accuracy and terminal accuracy. Some preliminary knowledge of the winds aloft is necessary to generate a proper LAR and assign a reliable CARP within it; some knowledge of the surface winds is essential for the terminal guidance phase.

As an illustration, Figure 20 shows the winds at the same location collected hourly, starting from 6 a.m. in the morning. By looking at these data, there is no doubt that atmospheric data change throughout a day drastically, so even an hour difference could result in a completely different wind profile. Actual temperature, pressure, and density (versus altitude) change throughout the day as well, and for sure differ from parameters of the standard atmosphere model, especially near the surface.

As mentioned in Section 2, JPADS-MP was developed to have a better wind forecast around the DZ area. It uses all available data, including NOAA's national operational weather forecasts, wind sounding balloons, wind data derived by the airdrop aircraft and on-scene *in situ*, wind and weather data observations from hand-launched dropsondes, and produces a high-fidelity, high-resolution 3D grid of winds, pressure, and density valid at the intended drop time. It also utilizes the local topographic data since it drives the atmospheric flow in the lower layers of the atmosphere, especially in complex, rugged terrain (Wright, Benney, and McHugh, 2005). Knowing these winds, $\hat{\mathbf{W}}(h)$, allows offsetting CARP computed for a release altitude h^* for a specific

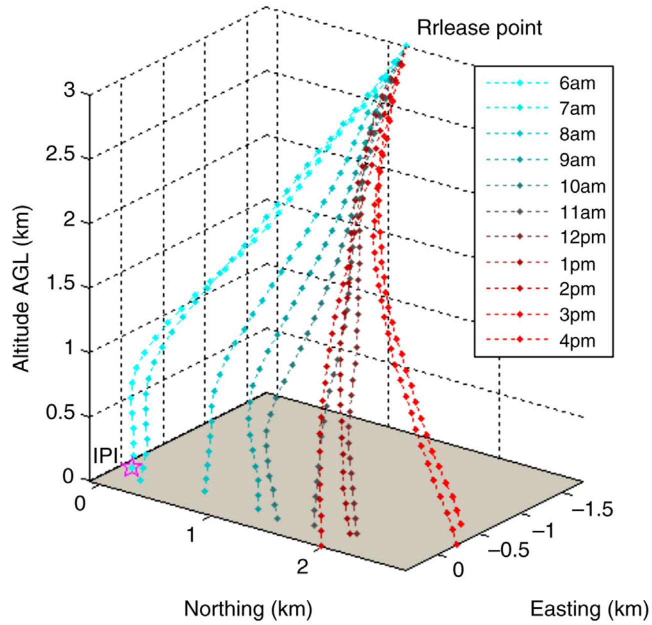

Figure 20. Uncontrolled trajectories with the different wind profiles. (Reproduced with permission from AIAA, 2016.)

PADS (characterized by an estimate $\hat{V}_{\mathrm{v}}(h)$) in no-wind conditions by a horizontal vector $\mathbf{d}_{\mathrm{W}}^*$:

$$\mathbf{d}_{\mathrm{W}}^* = \int_{h_{\mathrm{IPI}}}^{h^*} \frac{\hat{\mathbf{W}}(h)}{\hat{V}_{\mathrm{v}}(h)} \mathrm{d}h \tag{35}$$

During the actual descent, AGU attempts to estimate the current winds and adjust guidance strategy based on these most recent estimates.

Decisions made during the terminal guidance phase are made upon some knowledge of the surface-layer winds. These decisions explicitly affect the PADS terminal accuracy and that is why knowing surface-layer winds is very important. Modeling the near-surface winds in GNC algorithms may be based on different assumptions:

$$W^{\mathrm{cons}}(h) = \mathrm{const}\,(h), \quad W^{\mathrm{lin}}(h) = (\hat{W}_{\mathrm{H}} - \hat{W}_{\mathrm{surf}})H^{-1}h + \hat{W}_{\mathrm{surf}},$$

$$W^{\log}(h) = \frac{\hat{W}_{\mathrm{H}} - \hat{W}_{\mathrm{surf}}}{\ln (H+1)} \ln (h+1) + \hat{W}_{\mathrm{surf}} \tag{36}$$

In these models, $\hat{W}_{\mathrm{H}}$ is the wind estimate available at altitude H and $\hat{W}_{\mathrm{surf}}$ is the wind estimate at IPI (if available).

Figure 21 shows two examples of the wind profiles from the ground up to 750 m above IPI. They are split into

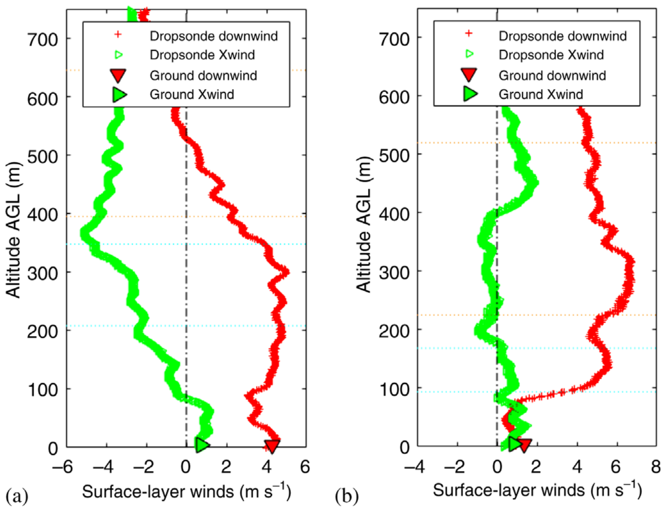

Figure 21. Examples of the surface-layer winds. (Reproduced with permission from AIAA, 2016.)

downwind and crosswind components relative to the desired direction of landing. Shown with a triangle marker are measurements provided by the surface winds measurement device and collected several minutes after the entire $W(h)$ profile was obtained (using a dropsonde). Horizontal lines depict decision-making altitudes. These two profiles show all kinds of problems associated with the wind modeling. The wind profile of Figure 21a demonstrates that at $h \approx 550$ m wind changes its direction, so whatever assumptions were made above this altitude became obsolete. It also shows the crosswind component dying toward the ground. Starting from $h \approx 300$ m all way down, the downwind component can be modeled as a constant. If surface wind data were available to PADS when it was at $h \approx 300$ m, it would definitely add confidence to the validity of this model. On the contrary, the wind profile of Figure 21b exhibits no major changes down to $h \approx 100$ m, when the winds suddenly die. If the constant model were assumed, it would result in a huge overshot. Again, knowing the surface winds and assuming a linear model could probably help in this case as well.

Figure 22 features a miniature portable IPI station based on the Kestrel pocket weather tracker paired wirelessly with a Blackberry cell phone (via Bluetooth interface) to allow transmitting the IPI coordinates and real-time ground atmospheric data to a descending PADS (in this case, Snowflake PADS AGU also used a cell phone paired to autopilot). If GSM network is not available, a common RF-based station could be used (Bourakov, Yakimenko, and Slegers, 2009). Figure 22a features a situation when the landing direction is determined by a portable IPI station orientation. Alternatively, the weather station may be mounted on a vane to broadcast a current surface wind direction as well. That would allow PADS to land exactly into the wind. Introduction of this weather station alone allowed Snowflake PADS to mitigate situations as shown in Figure 21b when the winds estimated right before the final base turn to IPI and happened to be way too different compared to the current surface winds. Mounting this miniature portable IPI station onto a moving platform enabled a novel capability of landing onto a

Figure 22. Miniature surface weather station (a), landing onto a moving platform (b), and miniature MAXMS dropsonde (c). (Reproduced with permission from AIAA, 2016.)

nonstationary IPI. Experimenting with the Snowflake PADS also demonstrated a capability to deploy a miniature dropsonde shown in Figure 22b allowing measuring the entire $W(h)$ profile rather than just a surface wind and incorporating this profile into terminal guidance decisions.

5.3 Optimal precision placement guidance

Most of guidance algorithms accommodate the best-known wind profile by planning a trajectory in the wind-fixed coordinate system with the IPI position shifted according to Equation 35. In this case, while executing a terminal guidance maneuver, these algorithms have to somehow accommodate the changes in the surface-layer wind. The only remedy in this case is to start a final approach leg a little bit high and execute a side-wave maneuver if actual winds happen to be weaker than predicted.

Ideally, mitigation of a constantly changing situation (discrepancy between the actual and desired positions caused by unmodeled winds and variations in PADS dynamics) could be accomplished by continuously solving the two-point boundary value problem with a fixed time. PADS kinematics in the horizontal plane with a yaw rate being a bounded control input can be described with as little as three differential equations (Equations 7 and 8). The initial condition of PADS at some point "A" right after exiting the EM pattern would be described by $\mathbf{x}(0) = [x_0, y_0, \psi_0]^T$, and the final condition, point "B", by some point on the final approach leg close to the flare initiation point $\mathbf{x}(t_\mathrm{f}) = [x_\mathrm{f}, y_\mathrm{f}, \psi_\mathrm{f}]^T$.

One attempt to address this problem using a classical calculus of variations resulted in a creation of bank of solutions computed off-line that was stored on a memory card and then used in AGU. This bank of optimal trajectories, lookup table, allowed choosing a specific terminal flight path (a sequence of TR commands) while entering a terminal area based on the current conditions defined by altitude, along-track and cross-track positions with respect to IPI and heading. Each of lookup table trajectories either hits the target or, if that is not possible from the given initial state, minimizes a function of position and heading error at impact (Carter *et al.*, 2007).

Direct methods of calculus of variations that search for the optimal solution within a set of parametrized candidate solutions represent much more robust choice allowing to conduct a real-time trajectory optimization/correction. To date, two different approaches were implemented and published. One approach was developed by Draper Laboratory and tested for the FireFly, DragonFly, and MegaFly PADS. Another approach was developed and tested for the Snowflake PADS. Both approaches are schematically shown in Figure 23 and proved to be very effective.

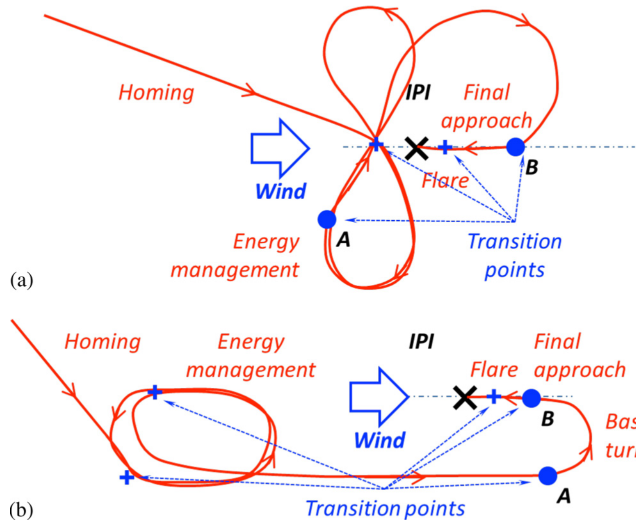

Figure 23. Examples of quasi-optimal terminal guidance.

The Draper Lab approach assumes homing toward IPI and executing the figure-8 EM upwind of IPI. When PADS descents low enough (in Figure 23a, it corresponds to some point A), the terminal phase J-hook maneuver is commenced. During this maneuver, the band-limited guidance (BLG) method is used to compute the commanded heading rate as a function of current relative position, heading, and heading rate with the goal of reaching a prescribed final position, heading, and heading rate at point B.

BLG relies on parametrization of a candidate heading rate profile:

$$\psi'_\mathrm{h}(h) = \sum_{k=0}^{M} \psi'_k \sin(\xi_k)/\xi_k \tag{37}$$

with $\xi_k = \pi(h - k\Delta h)/\Delta h$. Varied parameters ψ'_k represent TR at consecutive multiples of Δh and ensure that the control system will be able to track the heading rate command profile accurately (i.e., where specific PADS dynamics is incorporated). This form allows explicitly restricting the heading rate profiles by the frequency that is significantly less than the bandwidth of closed-loop system (Carter *et al.*, 2009). The trajectory is obtained by integrating Equation 37 and substituting results back to Equation 7. The optimized performance index consists of a weighted sum of the squared miss distance and heading error at point B (Figure 23a). Utilizing a finite-horizon control, a new optimal solution is generated from the current point to the same final point B every several seconds.

Another direct-method-based approach is based on the inverse dynamics in the virtual domain (IDVD) method (Figure 23b). In this case, after homing to a rectangular EM pattern upwind of IPI and executing at least two full EM pattern loops allowing to accurately estimate the current winds, PADS follows a standard aircraft landing pattern (Slegers and Yakimenko, 2011). The base turn initiation point (point A in Figure 23b) is based on the wind estimates continued throughout the downwind leg. Using the IDVD method, AGU constantly updates the TR command based on the optimal solution sought among parametrizations of the PADS coordinates that use some scaled abstract argument $\bar{\tau} = \tau/\tau_f \in [0; 1]$:

$$\begin{aligned} x(\bar{\tau}) &= P_1(\bar{\tau}) = a_0^1 + a_1^1\bar{\tau} + a_2^1\bar{\tau}^2 + a_3^1\bar{\tau}^3 + b_1^1 \sin(\pi\bar{\tau}) + b_2^1 \sin(2\pi\bar{\tau}) \\ y(\bar{\tau}) &= P_2(\bar{\tau}) = a_0^2 + a_1^2\bar{\tau} + a_2^2\bar{\tau}^2 + a_3^2\bar{\tau}^3 + b_1^2 \sin(\pi\bar{\tau}) + b_2^2 \sin(2\pi\bar{\tau}) \end{aligned} \tag{38}$$

The coefficients a_i^η and b_i^η ($\eta = 1, 2$) in Equation 38 are defined by the boundary conditions set for up to the second-order derivative at $\tau = 0$ and $\bar{\tau} = 1$. The yaw angle ψ is then found from Equation 7, which using Equation 38 becomes

$$\psi(\bar{\tau}) = \tan^{-1}\left(\frac{\lambda(\bar{\tau})y'_{\bar{\tau}}(\bar{\tau}) - \hat{w}_y}{\lambda(\bar{\tau})x'_{\bar{\tau}}(\bar{\tau}) - \hat{w}_x}\right) \tag{39}$$

Equation 39 uses the speed factor $\lambda(\bar{\tau})$ allowing mapping the virtual domain of parameter $\bar{\tau}$ to the physical time domain to ensure a constant forward speed. In this scheme, parameter τ_f then is the only varied parameter; however, for more flexibility, the list of varied parameters could easily be extended to include some or all final states as long as they belong to the glide path leading to IPI.

6 OTHER DEVELOPMENTS

6.1 Glide slope angle control

Improving touchdown performance for large PADS featuring higher V_h and slower TR compared to those of smaller PADS is still a challenge. One solution to this problem might be to control V_v to be able to increase it during the final approach, right before touchdown. In this case, PADS would always arrive to the DZ area a little high and then follow the common strategy employed by human jumpers. This approach is also referred to as a glide slope (angle) control.

One technique includes augmenting a parafoil-based PADS with a drogue using a two-point drogue bridle attachment at AGU and payload swivel as shown in Figure 24a (Moore, 2012). This concept assumes a one-time step decrease of the overall GR at an accurately determined deployment point on the final approach. Another scheme includes continuous control of GR via changing PADS rigging angle and therefore AoA using a variable AoA

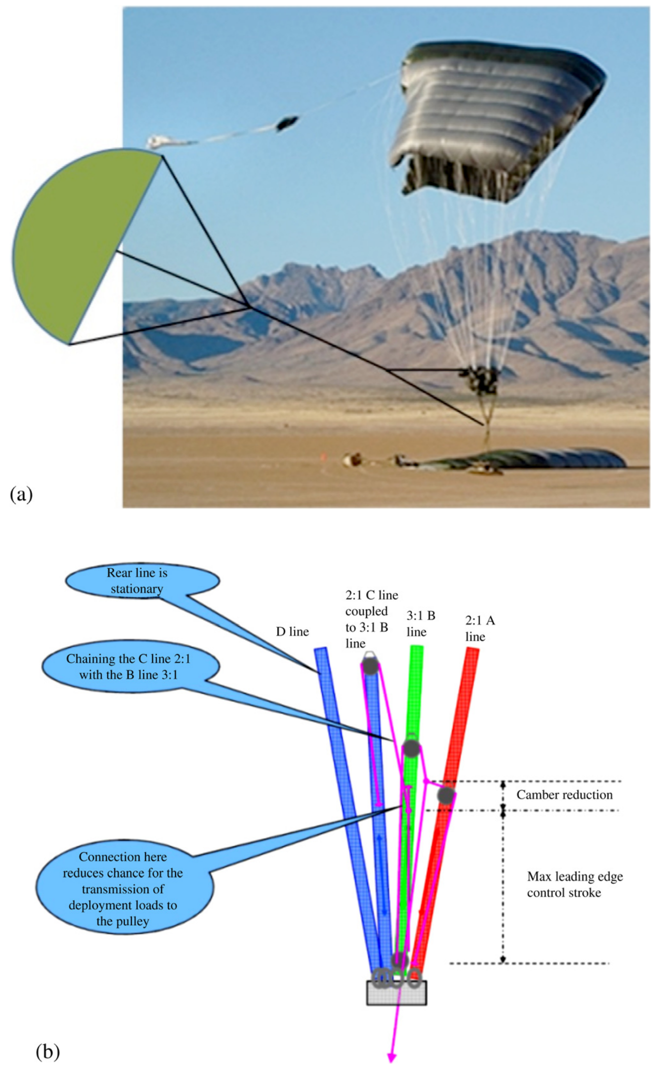

Figure 24. Drogue add-on (a) and VACS concepts (b). (Reproduced with permission from AIAA, 2016.)

control system (VACS) (Figure 24b). The entire pulley riser system would be removed from the deployment load path during canopy opening by a slackened control line. Figure 24b shows an example of varying the length of three out of four line groups (Moore, 2012). A differential AoA change in this case could induce differential lift (Figure 8). Hence, while paraglider operators (where this scheme originally came from) typically employ this so-called speed system in combination with the TE control, VACS needs no TE deflection control at all.

Another technical solution to control the glide slope angle is to use the upper surface aerodynamic spoilers. To enable it, a spanwise slit should be introduced across a number of cells in the center section of the upper surface of the canopy

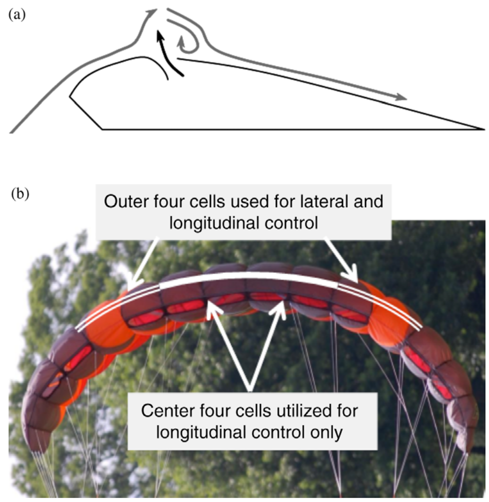

Figure 25. Airflow bubble acting like a spoiler (a) and slit spoilers locations (b). (Reproduced with permission from AIAA, 2016.)

(Figure 25a) (Higgins, 1979). The cells that contain a slit have a control line attached to the leading edge of the slit. These lines pass through the bottom skin of parafoil and run down to AGU. The same type of aerodynamic controllers spread farther apart from midsections along the upper surface of parafoil that can produce a sufficient TR control (when actuated differentially) and therefore eliminate the need for the TE deflection control as well (Figure 25b) (Ward and Costello, 2013).

6.2 Reduced cost PADS

To this end, Figure 26 shows an achieved relative cost for the different-weight PADS presented in Section 3 against the desired $6 per pound value. As seen, currently the objective value can only be met by L (and M) systems. However, UL and XL systems, that have much broader usage, are far away from meeting it. The ratio of the AGU and parafoil costs is about the same, 6 to 4, for all JPADS weight categories

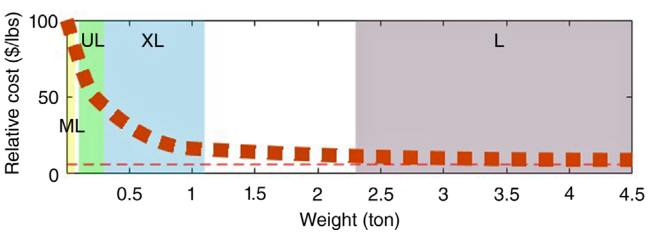

Figure 26. Relative cost of the current different-weight PADS-compared to the required objective value.

(because larger systems require larger motors and batteries). Hence, there are developments to bring down the cost of both PADS components. While the alternative approaches to steer a parafoil without using TE, discussed in the previous section, contribute to reducing the size (cost) of AGU, this section explores alternative methods of aerial payload delivery using modified round and cross canopy systems, even at the cost of slightly degraded precision performance compared to that of PADS. That is because traditional flat canopies, like G-14, G-12, and G-11, are 3-4 times cheaper compared to the same-weight-category ram-air parafoils and cruciform parachutes are about 20 times cheaper.

One of the first successful attempts of this kind was the development of AGAS in the late 1990s (Dellicker, Benney, and Brown, 2001). The idea was to use a standard G-12 type canopy and utilize four variable-length risers to disturb the shape of parachute canopy and therefore provide a limited horizontal control authority. The canopy disturbance was achieved by lengthening one or two adjacent risers from the nominal 6 to 8 m (30% lengthening). Both CFD analysis and flight tests proved that lengthening a single riser leads to about 0.5:1 GR, while lengthening two adjacent risers results in up to 0.8:1 GR. These modest (compared to those of PADS) values allowed developing a robust GNC that ensured very good touchdown accuracy given that AGAS is deployed within LAR computed based on the relatively accurate winds profile (that is, when the development of the JPADS-MP had begun). Released at CARP somewhere within LAR, AGAS was capable of steering toward some nominal trajectory, defined in $\{n\}$ and originated at IPI, compensating for wind variations and unmodeled dynamics. Figure 27a shows an example of such a nominal trajectory (the thick central curve) and a set of Monte Carlo simulations originating within LAR and employing the high-fidelity AGAS model with the developed control algorithm. In practice, during the very first tests, three AGAS deployed from 3 km above IPI level exceeded the threshold requirement of 100 m CEP landing 56, 76, and 78 m away from IPI, while two standard (uncontrolled) G-12-based systems, released at the same time as AGAS, were blown for more than 1 km away from IPI. Figure 27b features two AGAS with the two adjacent and single riser lengthened, which gives an idea about canopy shape disturbance.

Further development of this idea may involve even cheaper cruciform-type canopies, featuring good drag to canopy area ratio and good static and dynamic stability characteristics. These parachutes are composed of two identical cloth rectangles, crossed and joined to each other at the square intersection to form a flat surface having four equal arms. Suspension lines are attached to the outer edges of the four arms (Figure 28a).

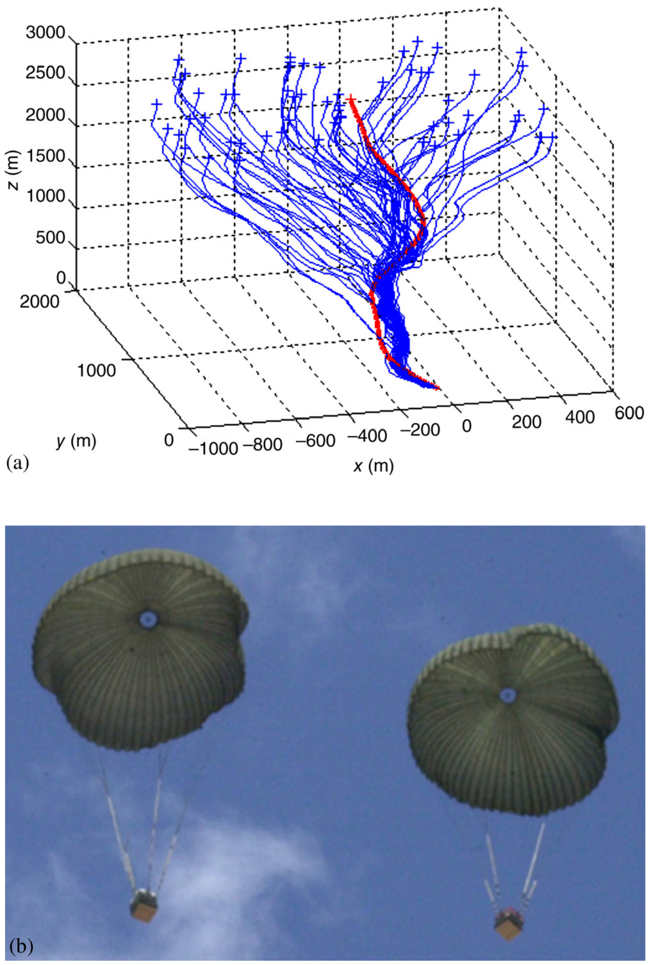

Figure 27. Monte Carlo simulation for GNC algorithm verification (a), and two AGAS steering toward the same nominal trajectory (b). (Reproduced with permission from AIAA, 2016.)

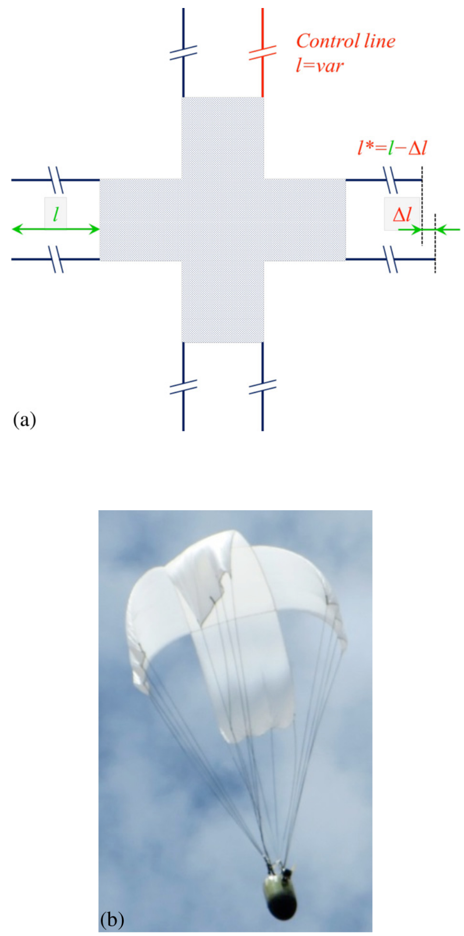

Figure 28. Layout of a controlled cruciform parachute (a) and subscale tests (b). (Reproduced with permission from AIAA, 2016.)

Fixed shortening or lengthening of one of the suspension lines by Δl (Figure 28a) puts parachute to spin (Figure 28b). Deflecting the adjacent line allows controlling this spin (Figure 29). Deflecting both lines evenly creates a horizontal force that can be used in a manner similar to that of AGAS. Preliminary tests on a small prototype exhibited a 0.4:1 GR. Compared to AGAS, this scheme utilizes a single (as opposed to four) control and allows a directional control (while AGAS may only steer in one of eight directions).

Partially connecting two- and three-canopy assemblies at the skirt, as shown in Figure 30, and pulling one side of the skirt down allow steering a cluster of canopies. Figure 30a and b shows two snapshots of a flight test of the prototype two-canopy assembly composed of one-quarter-scale G-12 canopies featuring a steady-state glide and turn, respectively (Lee and Buckley, 2004). In these initial tests, the encouraging values of up to 0.9:1 GR and a 2.5° s^{-1} TR were achieved.

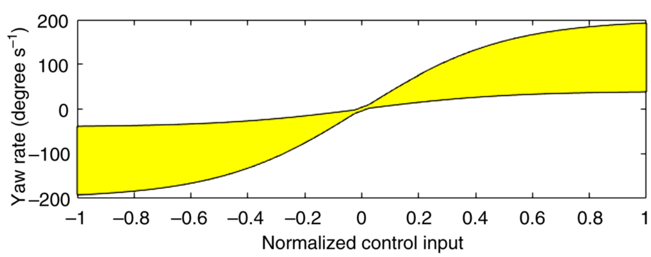

Figure 29. Yaw rate control authority for a cruciform parachute.

One more seemingly inexpensive approach includes varying the descent rate of circular parachutes. It can be done continuously, by reefing and disreefing of the skirt resulting in changes to the effective drag area (which might be more appropriate for small canopies due to the power demands of the actuation system), or in a one-time action, by delayed canopy deployment. Figure 31 presents a general idea of

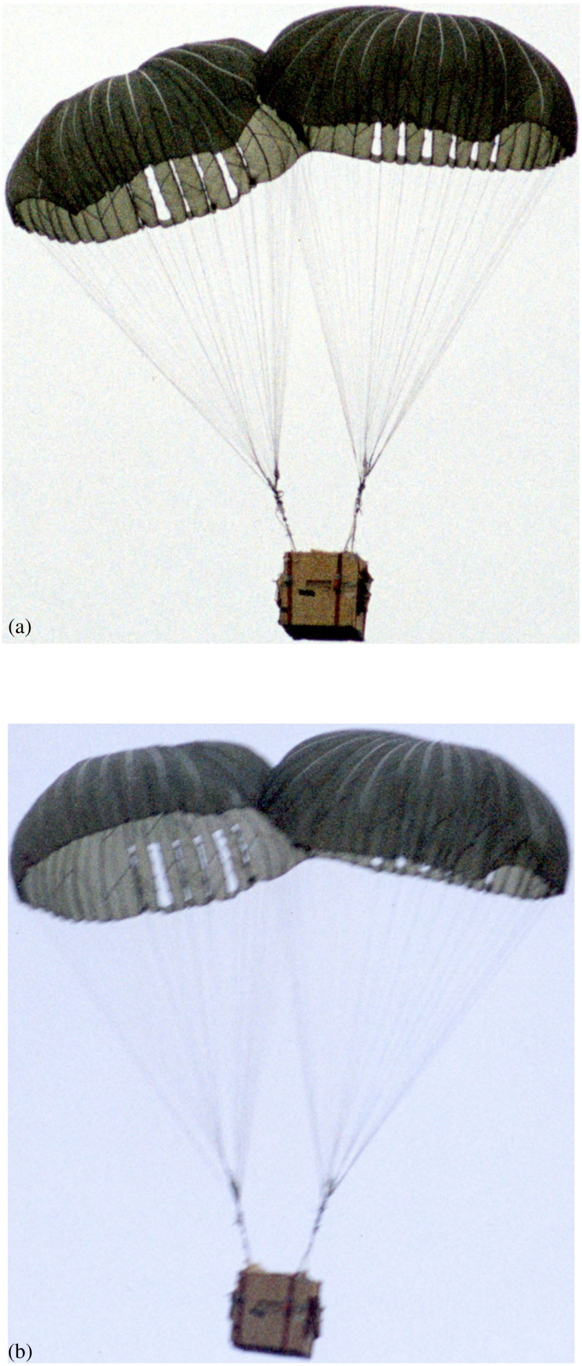

Figure 30. Steady glide (a) and turn (b) of a steerable cluster of two parachutes. (Reproduced with permission from AIAA, 2016.)

using a variable reefing (Fields, 2013). With a canopy fully opened (reefing control line fully extended), PADS has a slowest descent rate and therefore glides with the winds for a longer time. As the reefing control line is reeled in, the effective canopy drag area is reduced and the descent rate increases. This results in a shorter gliding distance. By

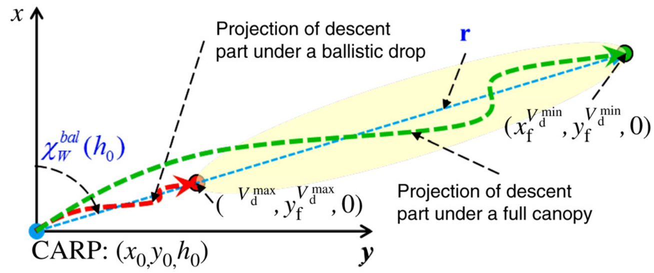

Figure 31. Reachability area using a canopy reefing control.

varying reefing level, PADS has some range it can land within (shown as a shaded area). A projection of all possible touchdown points initiated from the current 3D point with a constant descent rate V_d is represented by the line

$$x_f(V_d) = x_0 + \frac{h_0}{V_d} W^{bal}(h_0) \cos\left(\chi_W^{bal}(h_0)\right),$$

$$y_f(V_d) = y_0 + \frac{h_0}{V_d} W^{bal}(h_0) \sin\left(\chi_W^{bal}(h_0)\right) \tag{40}$$

where $W^{bal}(h_0)$ and $\chi_W^{bal}(h_0)$ are the magnitude and direction of the so-called ballistic winds computed for an altitude h_0. The technical implementation of a reversible reefing system for circular canopies can vary. To this end, several reefing techniques were investigated (Fields and Basore, 2015). These techniques included the four reefing strategies stemmed from a single control line approach, in which a single control line can manipulate the parachute size/shape directly while carrying only a small portion of the suspension line load. This way the descent rate is inversely proportional to the control line length (linearly proportional to the level of reefing).

7 CONCLUSION

The touchdown accuracy of uncontrolled round parachutes deployed from high altitudes depends entirely on some knowledge of underlying air column characteristics. They include the vertical profiles of air density defining the height above DZ and winds. Since neither of these parameters is known precisely, a touchdown error for these systems is measured in hundreds of meters. Introduction of a gliding parachutes and capability to use GPS as a major sensor for controlling them resulted in reducing a touchdown error of aerial payload delivery by an order of magnitude. A variety of GNC algorithms developed in the past two decades made these PADS fully autonomous with a very little interface required only to set up an upcoming mission. The efforts on improving PADS performance, including extending standoff distances, further reducing a miss distance even in the GPS-denied environment and reducing overall costs of PADS operations, still continue. The latest developments incorporate using terrain maps to be able to deliver payloads to a complex rugged-terrain DZ, and networking between multiple PADS, which enables using massive airdrop with collision avoidance. Other research is conducted in the area of precise aerial placement of a remote sensor grid or delivering payloads in the urban environment. Started as a program to improve precision of aerial payload delivery, JPAD program developed a new type of unmanned aerial vehicle equipped to address the challenges of traditional and new applications.

REFERENCES

Allen, R.F. (1995) Orion advanced precision airborne delivery system. *Proceeding of the 13th AIAA Aerodynamic Decelerator Systems Technology Conference and Seminar*, AIAA-1995-1539-CP, Clearwater Beach, FL.

Barrows, T.M. (2002) Apparent mass of parafoils with spanwise camber. *J. Aircr.*, **39**(3), 445–451. (Also available as Barrows, T.M. (2001) Apparent mass of parafoils with spanwise camber. *Proceeding of the 16th AIAA Aerodynamic Decelerator Systems Technology Conference and Seminar*, Boston, MA, May 21–24.)

Bourakov, E.A., Yakimenko, O.A., and Slegers, N.J. (2009) Exploiting a GSM network for precise payload delivery. *Proceedings of the 20th AIAA Aerodynamic Decelerator Systems Technology Conference*, AIAA, Reston, VA.

Brown, G. and Benney, R. (2005) Precision aerial delivery systems in a tactical environment. *Proceedings of the 18th AIAA Aerodynamic Decelerator Systems Technology Conference and Seminar*, AIAA, Reston, VA.

Carter, D., George, S., Hattis, P., McConley, M., Rasmussen, S., Singh, L., and Tavan, S. (2007) Autonomous large parafoil guidance, navigation, and control system design status. *Proceedings of the 19th AIAA Aerodynamic Decelerator Systems Technology Conference and Seminar*, AIAA-2007-2514, Williamsburg, VA.

Carter, D., Singh, L., Wholey, L., Rasmussen, S., Barrows, T., George, S., McConley, M., Gibson, C., Tavan, S., and Bagdonovich, B. (2009) Band-limited guidance and control of large parafoils. *Proceedings of the 20th AIAA Aerodynamic Decelerator Systems Technology Conference and Seminar*, AIAA-2009-2981, Seattle, WA.

Dellicker, S., Benney, R., and Brown, G. (2001) Guidance and control for flat-circular parachutes. *J. Aircr.*, **38**(5), 809–817.

Eilertson, W.H. (1969) *Gliding Parachutes for Land Recovery of Space Vehicles: Case 730, NASA-CR-108990*, Bellcomm Inc., Washington. DC.

Fields, T. (2013) A descent rate control approach to developing an autonomous descent vehicle, PhD thesis, University of Nevada, Reno, NV.

Fields, T. and Basore, N. (2015) Reversible control line reefing system for circular parachutes. *Proceeding of the 23rd AIAA Aerodynamic Decelerator Systems Technology Conference and Seminar*, Daytona Beach, FL.

Goodrick, T. (1975) Theoretical study of the longitudinal stability of high performance gliding airdrop systems. *Proceedings of the 5th AIAA Aerodynamic Decelerator Systems Conference*, AIAA-1975-1394, Albuquerque, NM.

Goodrick, T. (1984) Scale effects on performance of ram air wings. *Proceedings of the 8th AIAA Aerodynamic Decelerator and Balloon Technology Conference*, AIAA 84–0783, Hyannis, MA.

Gorman, C.M. and Slegers, N.J. (2011) Comparison and analysis of multi-body parafoil models with varying degrees of freedom. *Proceeding of the 21st AIAA Aerodynamic Decelerator Systems Technology Conference and Seminar*, Dublin, Ireland.

Higgins, M.W. (1979) Control system for ram air gliding parachute. U.S. Patent 4,175,722.

Jalbert, D. (1966) Multi-cell wing type aerial device. U.S. Patent 3,285,546.

Jann, T. (2004) *Modellierung, Identifizierung und Autonomes Fliegen eines Gleitfallschirm-Last-Systems*, PhD dissertation, DLR-FB-2004-33, Institute of Flight Mechanics, DLR Braunschweig, Germany.

JPADS (2014) JPADS: making precision airdrop a reality. *Defense Industry Daily*. www.defenseindustrydaily.com/jpads-making-precision-airdrop-a-reality-0678/

Lee, C.K. and Buckley, J. (2004) Method for steerable clustered round parachutes. *J. Aircr.*, **41**(5), 1191–1195.

Lingard, J.S. (1995) Precision aerial delivery/ram-air parachute system design. *Proceeding of the 13th AIAA ADS Conference and Seminar*, Clearwater Beach, FL.

Lissaman, P.B.S. and Brown, G.J. (1993) Apparent mass effects on parafoil dynamics. *Proceedings of the 12th RAeS/AIAA Aerodynamic Decelerator Systems Technology Conference and Seminar*, AIAA-1993-1236, London, England.

Moore, J. (2012) White Paper: Variable Angle of Attack Control System (VACS) for Gliding Aerial Delivery, Response to Request for Information prepared for InSitech by JM Technologies Inc.

Nicolaides, J.D. (1971) *Parafoil wind tunnel tests*. AFFDL-TR-70-146, U.S. Air Force Flight Dynamics Lab, Wright-Patterson Air Force Base, Ohio.

PATCAD (2005) Precision Airdrop Technology Conference and Demonstration, Final Report, U.S. Army RDECOM, Natick, MA.

Sego, K., Jr. (2001) Development of a high glide, autonomous aerial delivery system – Pegasus 500 (APADS). *Proceedings of the 16th AIAA Aerodynamic Decelerator Systems Technology Conference*, AIAA-2001-2073, Boston, MA.

Sim, A.G., Murray, J.E., Neufeld, D.C., and Reed, R.D. (1994) Development and flight testing of a deployable precision landing system. *J. Aircr.*, **31**(5), 1101–1108.

Slegers, N. and Yakimenko, O. (2011) Terminal guidance of autonomous parafoils in high wind-to-airspeed ratios. *Proc. Inst. Mech. Eng. G J. Aerosp. Eng.*, **225**(3), 336–346.

Ward, M. and Costello, M. (2013) Autonomous control of parafoils using upper surface spoilers. *Proceedings of the 22nd AIAA Aerodynamic Decelerator Systems Technology Conference*, AIAA, Reston, VA.

Ware, G.M. and Hassell, J.L., Jr. (1969) *Wind Tunnel Investigation of Ram Air Inflated All-Flexible Wings of Aspect Ratio 1.0 to 3.0*, NASA TM SX-1923.

Wegereef, J. and Jentink, H. (2003) SPADES: a parafoil delivery system for payloads until 200 kg. *Proceedings of the 17th AIAA Aerodynamic Decelerator Systems Technology Conference and Seminar*, Monterey, CA.

Wright, R., Benney, R., and McHugh, J. (2005) Precision airdrop system. *Proceedings of the 18th AIAA Aerodynamic Decelerator Systems Technology Conference and Seminar*, AIAA, Reston, VA.

Yakimenko, O. (Ed.) (2015) *Precision Aerial Delivery Systems: Modeling, Dynamics, and Control*, Progress in Astronautics and Aeronautics, AIAA, Arlington, VA. ISBN: 978-1-62410-195-3.

Chapter 4
Networked Multiple UAS

Philip B. Charlesworth
Airbus Group Innovations, Newport, UK

1 INTRODUCTION

Unmanned aerial systems (UAS) are widely percieved as a key emerging technology. Many applications have emerged for single UAS (1):

- Land management, including forestry and agriculture, vegetation, and livestock monitoring
- Commercial, including crop dusting, surveying, and broadcasting
- Earth science, including cloud and aerosol measurements, meteorology, contaminant measurement, glacier and ice-sheet monitoring, extreme weather monitoring, and wildlife census
- Homeland security including coastal patrol, forest fire mapping, and emergency communications

Networks of multiple UAS may be required for many reasons. The most common reason is to form UAS sensor networks with the aim of collaborating on a common task. Another reason for networking UAS is to use one or more platforms as an intermediate data relay to overcome terrain or other obstructions. There is a growing desire to use UAS as elements in ad hoc communications networks.

Such networks are conceptually similar to terrestrial networks; however, there are some significant differences. A key benefit of multi UAS networks is the mobility of the nodes, allowing the network to physically reconfigure itself in response to changing demand. Changes in location and attitude of each platform can obstruct the radio path between platforms, resulting in changes to the network topology. The main performance parameters for UAS networks are similar to terrestrial networks: available bandwidth, range, availability, latency and other quality of service (QoS) metrics.

Flight paths can be planned to optimise against these QoS metrics, avoid threats or forbidden regions, or make best use of available onboard resources such as fuel or stored electrical power. This dynamic behavior makes UAS networks different to their terrestrial equivalents. The mobility of UAS may be constrained by other limitations such as the physical performance of the platforms or the airspace regulatory environment in which they operate.

The design of multi-UAS networks requires an understanding of basic radio principles. This chapter starts with a short introduction to radio link modelling. It then considers some common topologies for line-of-sight (LOS) and beyond line-of-sight (BLOS) communications with aircraft. Selection of the appropriate antenna, and correctly locating it on

Unmanned Aircraft Systems. Edited by Ella Atkins, Aníbal Ollero, Antonios Tsourdos, Richard Blockley and Wei Shyy.
 ISBN: 978-1-118-86645-0.

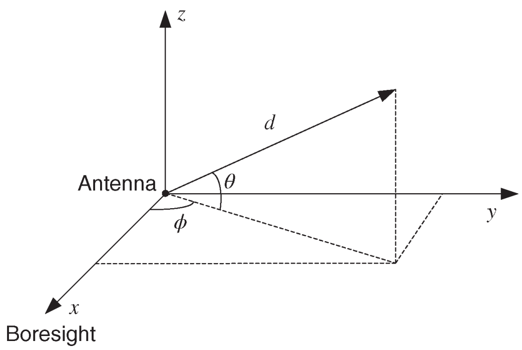

Figure 1. Coordinate system for antennae.

the airframe, is a key decision so this area is explored in greater depth. Finally, the chapter describes the state of the art in multi-UAS networks.

2 PRINCIPLES OF RADIO LINKS

A transmitter that radiates a power P_t equally in all directions at a frequency f Hz will generate a finite amount of power at a distance d m. The received power P_{r} can be calculated by using the well-known Friis Equation 2. In this equation, c is the speed of light.

$$P_{\mathrm{r}} = P_{\mathrm{t}}\left(\frac{c}{4\pi fd}\right)^2 \tag{1}$$

Sometimes Equation 1 is presented in terms of the wavelength $\lambda = \frac{c}{f}$ rather than the frequency f. Equation 1 can be rearranged to show the amount of loss that occurs between the transmitter and receiver antenna as the signal passes through the free space. This loss, known as the free space path loss L_{fs}, is simply the ratio of the received and transmitted powers.

$$L_{\mathrm{fs}} = \frac{P_{\mathrm{t}}}{P_{\mathrm{r}}} = \left(\frac{4\pi fd}{c}\right)^2 \tag{2}$$

Practical antennae do not transmit and receive equally in all directions but tend to favor some directions, either by design or as a consequence of their location. This preference for transmission and reception in certain directions is referred to as the gain of the antenna and is defined as the ratio of the power in a particular direction over the power that would occur if the antenna was isotropic.

Figure 1 shows the coordinate system that is commonly used for specifying antenna gain. An antenna reference direction known as the boresight is aligned with the x-axis.

The boresight is often the direction of maximum gain and is generally aligned with the x-axis. The direction of an object from the boresight can be defined in terms of the two angles, ϕ and θ. The antenna radiation pattern is commonly annotated $G\ (\phi, \theta)$ to indicate that gain changes with direction. It is common for antenna manufacturers to specify radiation pattern in two orthogonal planes, usually the $x{-}y$ plane and the $x{-}z$ plane.

Equation 1 can be modified to include the use of directional transmitter and receiver antennae whose gains are denoted $G_t\ (\phi_t, \theta_t)$ and $G_r\ (\phi_r, \theta_r)$, respectively:

$$P_{\mathrm{r}} = P_{\mathrm{t}}G_{\mathrm{t}}(\phi_{\mathrm{t}}, \theta_{\mathrm{t}})G_{\mathrm{r}}(\phi_{\mathrm{r}}, \theta_{\mathrm{r}})\left(\frac{c}{4\pi fd}\right)^2 \tag{3}$$

For links that are modulated with data, the required link quality can be expressed in one of several forms. Most commonly it is expressed as a minimum receiver power P_{r} that will satisfy a specific signal-to-noise ratio (SNR) at the receiver input. Sometimes, it is specified as a required SNR that is normalized to provide a measure of independence from the choice of modulation scheme. When normalized to 1 Hz of bandwidth and 1 bit s^{-1}, it is expressed as the ratio of the energy in one bit E_{b} to the noise power in 1 Hz N_0. Equation 3 can be modified to calculate the ratio E_{b}/N_0 as follows:

$$\frac{E_{\mathrm{b}}}{N_0} = \frac{P_{\mathrm{t}}G_{\mathrm{t}}(\phi_{\mathrm{t}}, \theta_{\mathrm{t}})G_{\mathrm{r}}(\phi_{\mathrm{r}}, \theta_{\mathrm{r}})}{T_{\mathrm{sys}}R_{\mathrm{b}}K}\left(\frac{c}{4\pi fd}\right)^2 \tag{4}$$

In Equation 4, T_{sys} is the equivalent nose temperature of the receiver in Kelvin, R_{b} is the data rate in bits s^{-1}, and K is Boltzmann's constant 1.38×10^{-23} (J K^{-1}).

The boresight gain of an antenna with an effective area A_{eff} and efficiency η can be calculated from Equation 5. In Equation 5, the effective area A_{eff} is related to the physical area of a reflector or other aperture antenna. Further details on the design and theory of antennae can be found in Ref. 3.

$$G = \frac{4\pi A_{\mathrm{eff}}}{\lambda^2}\eta \tag{5}$$

The main frequency bands for UAV communications networks are VHF, UHF and SHF. The limits of these frequency bands are defined by Article 2 of the ITU Radio Regulations (4) and summarized in Table 1.

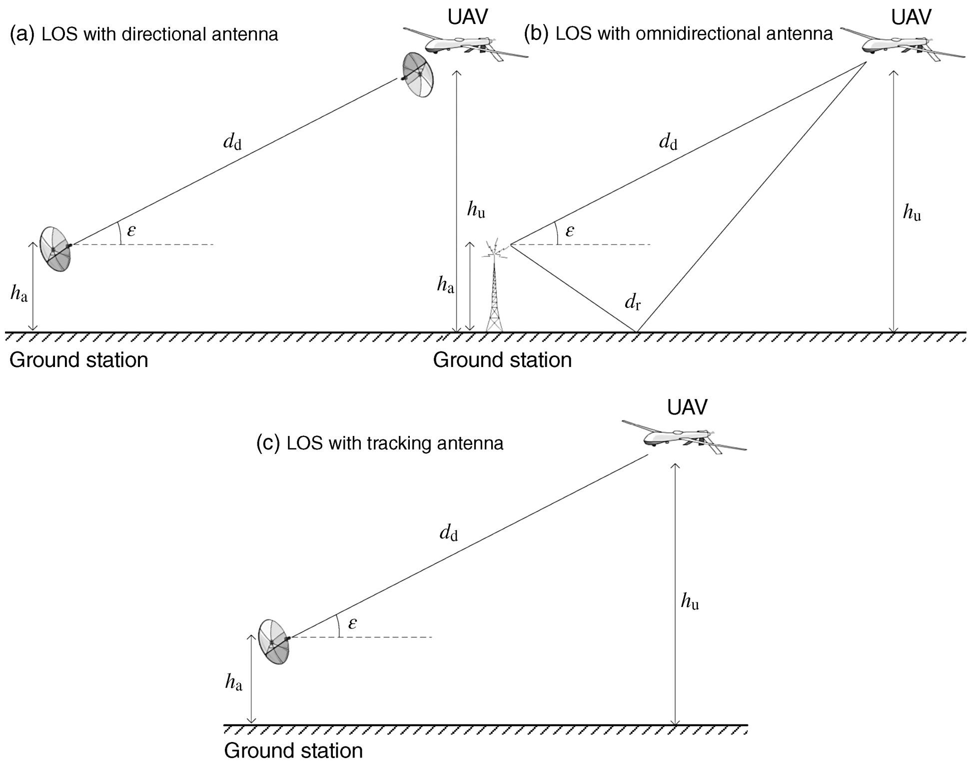

Figure 2. Line-of-sight radio links.

Table 1. Radio frequency bands.

Frequency band	Frequency limits	ITU band number
VHF	30–300 MHz	8
UHF	300–3000 MHz	9
SHF	3–30 GHz	10

3 AIR-TO-GROUND COMMUNICATIONS

Air-to-ground communications can be categorized as line-of-sight (LOS) or beyond line of sight (BLOS). LOS communications require exist when the UAV is above the radio horizon of the ground terminal. This does not always imply visibility of the UAV as the refraction and diffraction of radio waves can facilitate communications beyond the optical horizon, particularly in UHF and SHF bands.

The most effective communications system has directional antennae at both ends of the link as shown in Figure 2a. If the product $G_t(\phi_t, \theta_t)\, G_r(\phi_r, \theta_r) > 1$, it enables a corresponding reduction in power P_t or increase in data rate R_b, both of which are desirable. As the gain of either antenna increased more of the RF power is focused into a narrower beam. This generates a need for a tracking system to accurately point the antennae. On a small UAV, a tracking system can require significant amounts of internal space and electrical power.

The simplest case of a LOS path is a connection between a ground station with omnidirectional antennae at the ground station and on the UAV, as shown in Figure 2b. The performance of a system with omnidirectional antennae is relatively independent of the attitude or location of the aircraft, so no tracking or antenna pointing is required. This comes at the cost of reduced antenna gain so power must be increased or data rate reduced to satisfy the link budget. Furthermore, it opens the possibility of multiple RF paths and destructive interference of signals, inter-symbol interference, and other significant problems.

Between these two extremes is a compromise in which the UAV has an omnidirectional antenna and the ground station has a tracking antenna. In this system, the product $G_t(\phi_t, \theta_t)\, G_r(\phi_r, \theta_r) > 1$ so the power and data rate are better than the system with omnidirectional antennae. The omnidirectional antenna on the UAV allows changes in aircraft attitude without affecting link availability. Using a directional ground antenna introduces a tracking requirement; however, there are fewer constraints on space and power on ground than on the aircraft.